Aus der
Klinik und Poliklinik für Dermatologie und Allergologie
Klinikum der Ludwig-Maximilians-Universität München

In-vivo Evaluation von Hauttumoren und inflammatorischen Dermatosen mittels nicht invasiver Bildgebung

Dissertation
zum Erwerb des Doktorgrades der Medizin
an der Medizinischen Fakultät
der Ludwig-Maximilians-Universität zu München

vorgelegt von
Charlotte Louise Gust

aus
St. Louis, MO (USA)
2024

Aus der
Klinik und Poliklinik für Dermatologie und Allergologie
Klinikum der Ludwig-Maximilians-Universität München

In-vivo Evaluation of skin tumors and inflammatory dermatoses with non-invasive imaging modalities

Dissertation
zum Erwerb des Doktorgrades der Medizin
an der Medizinischen Fakultät
der Ludwig-Maximilians-Universität zu München

vorgelegt von
Charlotte Louise Gust

aus
St. Louis, MO (USA)
2024

Mit Genehmigung der Medizinischen Fakultät
der Universität München

Erstes Gutachten:	Prof. Dr. Elke Sattler
Zweites Gutachten:	Prof. Dr. Wolfgang Zink
Drittes Gutachten:	Prof. Dr. Tanja von Braunmühl
weitere Gutachten:	

Dekan: Prof. Dr. med. Thomas Gudermann

Tag der mündlichen Prüfung: 19.09.2024

Contents

List of Abbreviations

AK	actinic keratosis
BCC	basal cell carcinoma
BD	bowens disease
BZK	Basalzellkarzinom (Deutsch)
DEJ	dermo epidermal junction
H&E	haematoxylin and eosin
LC-OCT	line-field confocal optical coherence tomography
MM	malignant melanoma
OCT	optical coherence tomography
RCM	reflectance confocal microscopy
SCC	squamous cell carcinoma
µm	micrometer

Zusammenfassung (German Summary)

Diese kumulative Dissertation befasst sich mit verschiedenen Anwendungsmöglichkeiten nicht-invasiver Diagnostik in der Dermatologie. Sie soll zu einem besseren Verständnis der unterschiedlichen Methoden der nicht-invasiven Diagnostik verhelfen und ihre verschiedenen Einsatzmöglichkeiten aufzeigen. Neben den bereits etablierteren Methoden wie der Dermatoskopie, der optischen Kohärenztomographie und der konfokalen Laserscanmikroskopie liegt der Fokus dieser Arbeit insbesondere auf der neuen Imaging Methode LC-OCT. Die bisher wenig erforschte Technik wurde unter anderem im Bereich der Frühdiagnostik von Hautkrebsvorstufen und Hauttumoren angewendet mit dem Ziel der Etablierung diagnostischer Kriterien. Diese wurden mit Korrelaten von bereits bekannten OCT, KLSM und Histologie Kriterien verglichen und im späteren zeitlichen Verlauf auf Anwendbarkeit bei dermatoskopisch unklaren Läsionen geprüft.

Liegt nach visueller Inspektion und Dermatoskopie der Verdacht auf eine Hautkrankheit vor, wird häufig eine Gewebeprobe entnommen, um diesen zu bestätigen. Diese Vorgehensweise ist kostspielig, zeitaufwendig und nicht immer zielführend, insbesondere, wenn es sich um größere oder multilokuläre Läsionen handelt. Für die Diagnose von Hauttumoren und vielen anderen Hautkrankheiten ist die konventionelle Histologie der Goldstandard. Es wird nach potenziellen Methoden gesucht, die eine vergleichbare diagnostische Genauigkeit bieten und deren Einsatz kostengünstiger und zeitsparender als die feingewebliche Untersuchung ist.

Im Rahmen des Forschungsprojektes wurden mithilfe der bisher wenig erforschten LC-OCT Technik Aufnahmen von Hauttumoren gemacht und diese mit den korrespondierenden H&E Schnitten verglichen. Hieraus wurden charakteristische Merkmale für die jeweiligen Hautkrankheiten herausgearbeitet und mit bereits bekannten Merkmalen aus der OCT und KLSM verglichen. Die LC-OCT zeigte hierbei eine höhere diagnostische Sicherheit bei der Diagnostik und Subtypisierung von Basalzellkarzinomen im Vergleich zu den anderen Techniken.

Betrachtet man klinisch nicht sicher einordbare, BZK-verdächtige Läsionen mittels LC-OCT, lässt sich eine sehr gute diagnostische Sicherheit und „Performance“ bei der Unterscheidung von BZKs von anderen BZK-verdächtigen Läsionen im Vergleich zur Dermatoskopie und der Histologie als Goldstandard erreichen. LC-OCT kann den

Kliniker bei der Diagnose und Subtypisierung von Basalzellkarzinomen unterstützen und sowohl den diagnostischen Ansatz als auch das Behandlungsprocedere optimieren. Neben der Vermeidung der Entnahme von unnötigen Hautproben, hätte dies zudem Auswirkungen auf die Therapie. Während noduläre oder sklerodermiforme Tumore operativ behandelt werden sollten, können bei oberflächlichen Basalzellkarzinomen auch konservative Therapien zum Einsatz kommen.

Erweitert man das Anwendungsspektrum der LC-OCT auf weitere keratinozytäre Tumore, wie das Spinozelluläre Karzinom oder seine Vorstufe die aktinische Keratose, eröffnen sich neue Möglichkeiten zur Einstufung der Feldkanzerisierung. Anhand der Analyse von Keratinozytenmorphologie und Architektur der dermoepidermalen Junktion können verlässlich verschiedene Stadien von keratinozytären Karzinomen unterschieden werden und diese histologisch korreliert werden.

Zudem zeigte sich, dass die LC-OCT aktinische Keratosen basierend auf des basalen Wachstumsmuster der Keratinozyten einstufen konnte und so die Möglichkeit eröffnet, die PRO-Klassifizierung in-vivo abzubilden. Mit dieser Klassifikation lässt sich das maligne Entartungspotential von AKs anhand der Keratinozytenverlagerung in die papilläre Dermis einschätzen und mittels LC-OCT wäre dies in Zukunft auch nicht-invasiv möglich.

Die Untersuchung von melanozytären Läsionen mittels LC-OCT zeigte keine Unterschiede in der „Performance“ im Vergleich zur konfokalen Laserscanmikroskopie, somit ist mit Hilfe der LC-OCT die Unterscheidung von Nävi und Melanomen gut möglich.

Zukünftige Projekte sehen eine Erweiterung der Anwendungsmöglichkeiten von nichtinvasiver Diagnostik in der Dermatologie vor. In einer kürzlich publizierten prospektiven Studie wurde die Anwendbarkeit besagter Techniken in der Diagnostik der Onychomykose getestet. Weitere potenzielle Zukunftsprojekte könnten im Anwendungsbereich von entzündlichen Dermatosen, zum Beispiel die Psoriasis oder das atopischen Ekzems, umfassen. Darüber hinaus könnte der Einfluss der Künstlichen Intelligenz in diesem schnell fortschreitendem Forschungsfeld weiter untersucht werden. Ein erster Ansatz wurde mit der Anwendung von Künstlicher Intelligenz bei der PRO-Klassifizierung von aktinischen Keratosen gemacht. In Zukunft könnten weitere potenzielle Anwendungsgebiete von Künstlicher Intelligenz in einem kontinuierlich weiterentwickelnden Feld der Dermatologie geprüft werden.

Abstract

This cumulative dissertation focusses on various applications of non-invasive imaging modalities in Dermatology. It aims to contribute to a better understanding of different non-invasive diagnostic methods and demonstrates their various applications. In addition to already established methods such as Dermoscopy, optical coherence tomography (OCT) and reflectance confocal microscopy (RCM), this work particularly addresses the new imaging method LC-OCT. This relatively unexplored technique has been applied in the early diagnosis of precancerous skin lesions and skin tumors with the intention of establishing diagnostic criteria. These were compared to correlates of already known OCT, RCM and histology criteria and tested for applicability in cases of dermatoscopically unclear lesions.

When suspicion of a skin disease arises after clinical inspection and Dermoscopy, a tissue sample is taken to confirm diagnosis. This approach is costly, time-consuming and not always conclusive, especially in larger or multilocular lesions. Conventional histology is the gold standard for diagnosing skin tumors and many other skin diseases. Efforts are being made to find methods that provide comparable diagnostic accuracy whilst being more cost-effective and timesaving than histological examination. In the context of this research project, images of skin tumors were taken using the LC-OCT technique and compared with corresponding H&E sections. Characteristic features for the respective skin diseases were identified and compared to already known features from OCT and RCM. LC-OCT showed higher diagnostic confidence in the diagnosis and subtyping of BCC compared to other techniques.

When considering lesions clinically not confidently classifiable as BCC but suspicious for BCC, very good diagnostic confidence and performance were achieved with LC-OCT to distinguish these lesions, compared to Dermoscopy and histology as the gold standard. Pitfalls, lesions misdiagnosed as BCC, occurred in 14 out of 182 lesions and consisted of sebaceous hyperplasia, molluscum contagiosum, pyogenic granuloma and actinic keratosis. Nevertheless, LC-OCT can assist clinicians in the diagnosis and subtyping of BCC and optimize both the diagnostic approach and the treatment procedure. In addition to avoiding unnecessary skin biopsies, this would have implications for therapy as well. While nodular and fibrosing BCCs should be treated surgically, conservative therapy options can be considered for superficial BCC.

Expanding the application spectrum of LC-OCT to other keratinocytic tumors, such as squamous cell carcinoma or its precursor actinic keratosis, showed new possibilities for the classification of field cancerization. By analyzing keratinocyte morphology and the architecture of the dermoepidermal junction, various stages of keratinocytic carcinomas can reliably be distinguished and correlated histologically.

Furthermore, LC-OCT was able to classify actinic keratoses based on the basal growth pattern of keratinocytes, providing the possibility to depict the PRO classification in vivo. The classification estimates the malignant transformation potential of AK by the displacement of keratinocytes into the papillary dermis, which could be achieved noninvasively with LC-OCT in the future.

Examining melanocytic lesions with LC-OCT showed no difference in performance in comparison to RCM, making LC-OCT a useful tool to discriminate between nevi and melanomas.

There has been a tremendous development in the field of non-invasive in vivo imaging in Dermatology. From early detection of skin cancer to staging or diagnosing skin diseases, non-invasive imaging methods support clinicians in their daily practice and decision making.

For the future an expansion of application to the inflammatory field of Dermatology is intended. In a prospective study we recently analyzed the applicability of non-invasive imaging tools in the diagnosis of onychomycosis. Further research in this field is necessary and potential new applications could entail inflammatory dermatoses like psoriasis and atopic dermatitis. Moreover, the influence of artificial intelligence in this fast-evolving research field could be further investigated. A first approach was made with artificial intelligence-based PRO score assessment in actinic keratosis. Whilst this was a first step towards a new chapter of non-invasive imaging, there will be numerous potential applications of artificial intelligence to be investigated in the future in this continuously advancing field of Dermatology.

1 Publications

1.1 Cumulative Dissertation Publications

1.1.1 Paper 1

Gust C, Schuh S, Welzel J, Daxenberger F, Hartmann D, French LE, Ruini C, Sattler EC. Line-Field Confocal Optical Coherence Tomography Increases the Diagnostic Accuracy and Confidence for Basal Cell Carcinoma in Equivocal Lesions: A Prospective Study. Cancers (Basel). 2022 Feb 21;14(4):1082. doi: 10.3390/cancers14041082. PMID: 35205830; PMCID: PMC8870684.

1.1.2 Paper 2

Ruini C, Schuh S, Gust C, Kendziora B, Frommherz L, French LE, Hartmann D, Welzel J, Sattler E. Line-field optical coherence tomography: in vivo diagnosis of basal cell carcinoma subtypes compared with histopathology. Clin Exp Dermatol. 2021 Dec;46(8):1471-1481. doi: 10.1111/ced.14762. Epub 2021 Sep 24. PMID: 34047380.

1.1.3 Paper 3

Ruini C, Schuh S, Gust C, Kendziora B, Frommherz L, French LE, Hartmann D, Welzel J, Sattler EC. Line-field confocal optical coherence tomography for the in vivo real-time diagnosis of different stages of keratinocyte skin cancer: a preliminary study. J Eur Acad Dermatol Venereol. 2021 Dec;35(12):2388-2397. doi: 10.1111/jdv.17603. Epub 2021 Sep 24. PMID: 34415646.

1.1.4 Paper 4

Ruini C, Schuh S, Gust C, Hartmann D, French LE, Sattler EC, Welzel J. In-Vivo LC-OCT Evaluation of the Downward Proliferation Pattern of Keratinocytes in Actinic Keratosis in Comparison with Histology: First Impressions from a Pilot Study. Cancers (Basel). 2021 Jun 8;13(12):2856. doi: 10.3390/cancers13122856. PMID: 34201052; PMCID: PMC8228287.

1.1.5 Paper 5

Schuh S, Ruini C, Perwein MKE, Daxenberger F, Gust C, Sattler EC, Welzel J. Line-Field Confocal Optical Coherence Tomography: A New Tool for the Differentiation between Nevi and Melanomas? Cancers (Basel). 2022 Feb 23;14(5):1140. doi: 10.3390/cancers14051140. PMID: 35267448; PMCID: PMC8909859.

1.2 Published Publications

1.2.1 Paper A

Eijkenboom QL, Daxenberger F, Gust C, Hartmann D, Guertler A, Steckmeier S, Deussing M, French LE, Welzel J, Schuh S, Sattler EC. Line-field confocal optical coherence tomography, a novel non-invasive tool for the diagnosis of onychomycosis. J Dtsch Dermatol Ges. 2024 Jan 26. doi: 10.1111/ddg.15310. Epub ahead of print. PMID: 38279541.

1.2.2 Paper B

Thamm JR, Daxenberger F, Viel T, Gust C, Eijkenboom Q, French LE, Welzel J, Sattler EC, Schuh S. [KI-basierte Bestimmung des PRO-Scores in aktinischen Keratosen anhand von LC-OCT-Bilddatensätzen: Artificial intelligence-based PRO score assessment in actinic keratoses from LC-OCT imaging using Convolutional Neural Networks]. J Dtsch Dermatol Ges. 2023 Nov;21(11):1359-1368. German. doi: 10.1111/ddg.15194_g. PMID: 37946638.

1.2.3 Paper C

Daxenberger F, Deußing M, Eijkenboom Q, Gust C, Thamm J, Hartmann D, French LE, Welzel J, Schuh S, Sattler EC. Innovation in Actinic Keratosis Assessment: Artificial Intelligence-Based Approach to LC-OCT PRO Score Evaluation. Cancers (Basel). 2023 Sep 7;15(18):4457. doi: 10.3390/cancers15184457. PMID: 37760425.

1.2.4 Paper D

Ruini C, Kendziora B, Ergun EZ, Sattler E, Gust C, French LE, Bağcı IS, Hartmann D. In vivo examination of healthy human skin after short-time treatment with moisturizers using confocal Raman spectroscopy and optical coherence tomography: Preliminary

observations. Skin Res Technol. 2022 Jan;28(1):119-132. doi: 10.1111/srt.13101. Epub 2021 Sep 23. PMID: 34555219.

1.2.5 Paper E

Ruini C, Daxenberger F, Gust C, Schuh S, French LE, Welzel J, Sattler EC. Neues von der optischen Kohärenztomographie [Advances in optical coherence tomography]. Hautarzt. 2021 Dec;72(12):1048-1057. German. doi: 10.1007/s00105-021-04905-2. Epub 2021 Oct 26. PMID: 34698874.

2 Contribution to Publications

2.1 Contribution to Paper 1

My contribution to the paper “Line-Field Confocal Optical Coherence Tomography Increases the Diagnostic Accuracy and Confidence for Basal Cell Carcinoma in Equivocal Lesions: A Prospective Study” entailed formal analysis investigation, recruiting patients, data curation (Dermoscopy and LC-OCT imaging of the cases), histological analysis, preparing and writing the original draft of the paper and final reviewing and editing.

The paper can be found under 4.1 Paper 1 (page 13).

2.2 Contribution to Paper 2

My contribution to the paper “Line-Field Optical Coherence Tomography: In Vivo Diagnosis of Basal Cell Carcinoma Subtypes Compared with Histopathology” consisted of data curation (Dermoscopy, OCT, RCM and LC-OCT images), analysis of imaging results, comparison to histology and writing, reviewing and editing of the paper.

The paper can be found under 4.2 Paper 2 (page 31).

2.3 Contribution to Paper 3

My contribution to the paper “Line-Field Confocal Optical Coherence Tomography for the In Vivo Real-Time Diagnosis of Different Stages of Keratinocyte Skin Cancer: A Preliminary Study” were formal analysis, investigation, data curation, writing, reviewing, and editing of the final script.

The paper can be found under 5.1 Paper 3 (page 43).

2.4 Contribution to Paper 4

My contribution to the paper “In-Vivo LC-OCT Evaluation of the Downward Proliferation Pattern of Keratinocytes in Actinic Keratosis in Comparison with Histology: First Impressions from a Pilot Study” entailed data curation (LC-OCT), formal and histological analysis and reviewing and editing the script.

The paper can be found under 5.2 Paper 4 (page 54).

2.5 Contribution to Paper 5

My contribution to the paper “Line-Field Confocal Optical Coherence Tomography: A New Tool for the Differentiation between Nevi and Melanomas?” consisted of data curation (Dermoscopy, RCM, LC-OCT), data analysis and writing and editing of the publication.

The paper can be found under 5.3 Paper 5 (page 65).

3 Introduction

Non-invasive imaging modalities have become a valuable part of diagnosing and monitoring various skin conditions in the field of Dermatology. Over the past years the process of diagnosing skin cancer as well as inflammatory dermatoses has been evolving mountainously and new imaging methods have gained a foothold in the daily practice. Skin cancer has shown an increased incidence worldwide during the past decades and belongs to the most frequently occurring cancers in humans. Whilst skin cancer originating from keratinocytes like basal cell carcinoma (BCC) and squamous cell carcinoma occur more frequently, malignant melanomas (MM) have a higher mortality (Leiter, Keim, & Garbe, 2020).

En-vivo non-invasive imaging techniques allow a visualization of the skin without using invasive procedures like skin biopsies and aid in accurate diagnosing, treatment planning and monitoring of dermatological conditions. The capabilities of non-invasive imaging tools are extensive, however each tool differs in terms of penetration depth, resolution, sensitivity and specificity (Wassef & Rao, 2013). Clinical examination is usually followed by Dermoscopy, a diagnostic tool, that allows the visualization of skin structures not visible to the naked eye. Besides Dermoscopy more advanced imaging techniques as OCT, RCM and the newest technique LC-OCT are used.

Whereas OCT has a good penetration depth up to the dermis, it is at the expense of a lower resolution. In contrast RCM offers a resolution at cellular level, however with a smaller penetration depth than OCT, making it particularly suitable for the differential diagnosis of melanocytic lesions.

LC-OCT is a new, undoubtedly promising, imaging technique in Dermatology. Whilst offering exceptional cellular resolution, it furthermore allows a penetration depth down to the upper dermis, enabling an accurate assessment not just of the depth of invasion but also morphology of skin conditions. Preliminary studies suggest that LC-OCT has high potential, particularly when it comes to characterizing healthy skin as well as actinic keratoses, basal cell carcinomas, field cancerization, squamous cell carcinomas and mite infestations (Ruini, Schuh, Hartmann, et al., 2021). However, it is worth noting, that further research and studies are needed to refine and standardize LC-OCT criteria and techniques. In order to fully harness its potential in the field of Dermatology, a broader exploration of its application is necessary. The intention of

this research is standardized capture of diagnostic criteria and further validation of the efficacy and reliability of this new imaging technique whilst exploring possible new applications.

3.1 Non-invasive imaging

3.1.1 Dermoscopy

Dermoscopy involves examining skin lesions using skin surface or epiluminescence microscopes. Dermoscopes, handheld devices utilizing non-polarized and polarized light, enable visualization of specific features within skin lesions at up to 40x magnification, which assist in the differentiation of benign and malignant lesions. A Dermoscop is typically a handheld, portable device, which is relatively inexpensive and easily to be carried around. When conducting skin examinations with dermoscopy, a liquid is frequently used to reduce skin reflectivity. Identifying characteristic patterns with Dermoscopy can help distinguish benign from malignant skin lesions. Characteristics associated with BCC lesions are arborizing vessels, spoke wheel structures and blue-gray ovoid nests. Furthermore, features like ulceration, pigmentation, or shiny white streaks raise suspicion for BCC as well (Dinnes et al., 2018; Valdés-Morales, Peralta-Pedrero, Cruz, & Morales-Sánchez, 2020; Zalaudek et al., 2012).

3.1.2 Optical Coherence Tomography (OCT)

Optical Coherence Tomography, or OCT, is a well-established imaging technique initially used in ophthalmology and later adopted in the field of dermatology (Welzel, Lankenau, Birngruber, & Engelhardt, 1997). By operating on coherent light interferometry principles, light reflected from skin tissue is captured and a non-invasive, real-time cross-sectional imaging of the skin is possible. This imaging modality facilitates an imaging of skin layers up to a depth of 1.5-2mm with a lateral optical resolution of less than 7.5µm and an axial resolution ranging from 5 to 10µm (Wan et al., 2021). As a result, morphological features within the epidermis and dermis can be analyzed, however individual small cells cannot be portrayed. OCT produces both vertical and horizontal monochromatic images with a higher resolution but less penetration depth than conventional sonography. The dynamic mode enables the visualization of blood flow whilst displaying morphological features of skin tissue (Ulrich

et al., 2016). Furthermore, epidermal thickness and blood vessel depth can be evaluated (Olsen, Gaetti, Grandahl, & Jemec, 2022). An integrated camera enables real-time navigation of the skin lesions being examined. The commercially worldwide available OCT model is the VivoSight® device (Michelson Diagnostics Ltd., Maidstone, Kent, England). It is a multibeam Fourier domain device operating with a diode laser with a wavelength of 1305nm, offering a class 1 laser safety classification (Sinx et al., 2020). Its system entails a device cart, a PC with keyboard and monitor and a laser unit.

OCT is mainly used for diagnosing non-melanocytic skin tumors, notably basal cell carcinoma (BCC), actinic keratosis (AK) and squamous cell carcinoma (SCC) (Holmes et al., 2018). It plays an important role in the diagnosis and treatment of inflammatory and infectious diseases as well. Eczema, Rosacea, scaring and skin hydration are skin conditions where OCT can potentially be applicated (Manfredini et al., 2020).

3.1.3 Reflectance Confocal Microscopy (RCM)

Reflectance Confocal Microscopy is a non-invasive imaging technique, that provides high-resolution images of tissue structures down to the papillary dermis (around 200-300µm). RCM offers real-time, high-resolution imaging capabilities, helping clinicians make more accurate diagnoses and treatment decisions while minimizing patient discomfort and invasiveness.

In this research project the commercially available RCM Vivascope1500 and 3000, developed by MAVIG GmbH Munich, Germany were used. It utilizes a diode laser, emitting near-infrared light with 830nm wavelength, in order to illuminate biological tissue (Welzel & Schuh, 2017). A pinhole aperture selectively detects reflected light from a specific focal plane making imaging of cellular structures like keratinocytes, melanocytes, blood vessels and collagen fibers possible. By visualizing specific morphological features associated with melanocytic proliferation, such as cellular atypia, disorganization and pagetoid spread of melanocytes within the epidermis, RCM can help differentiating between benign and malignant lesions (Guitera et al., 2012).

Despite its many advantages, RCM also has limitations, for instance the limited penetration depth, which restricts the imaging of deeper, dermal skin structures. Additionally, curation and interpretation of RCM images requires specialized training and expertise.

Overall, RCM is a valuable imaging tool in dermatology. By providing detailed, high-resolution images of cellular structures it is particularly helpful in the diagnosis and management of melanoma and other skin cancers (Guitera et al., 2009; Pellacani et al., 2007).

3.1.4 Line-field confocal optical coherence tomography (LC-OCT)

Line-field confocal optical coherence tomography is a new non-invasive imaging method, that blends the principles of OCT interferometry and RCM's spatial filtering. The CE-marked LC-OCT deepLiveTM (DAMAE Medical, Paris, France) comprises a mobile central unit housing a monitor and a handheld probe (Ogien, Tavernier, Fischman, & Dubois, 2023). The device is non-invasive, painless and creates real time images.

The LC-OCT system consists of a two-beam interference microscope, a photodetector line camera and a class 1 supercontinuum laser, operating at a central wavelength of 800nm. While constantly adjusting its focus, multiple A-scans parallel to the skin surface up to a depth of 500nm are captured (Schuh, Ruini, Sattler, & Welzel, 2021). It has an axial resolution of 1.1µm and a lateral resolution of 1.3µm. Operating in real-time, LC-OCT offers three imaging modes portrayed in greyscale: vertical (en-coupe) akin to OCT and histology, horizontal (en-face) like RCM and 3D images. Short videos can be recorded at various frame rates and comprehensive 3D reconstruction is possible as well. Additionally, simultaneous capture of dermoscopic images facilitates precise positioning and lesion navigation.

3.2 Skin Cancer

Skin cancer is one of the most common malignant diseases in the population with skin types I-III. Its incidence is increasing from year to year at an alarming rate, resulting in a rising morbidity, mortality and increasing treatment costs (Lomas, Leonardi-Bee, & Bath-Hextall, 2012).

Skin cancer can be divided into two main classes: melanoma (black skin cancer) and non-melanoma skin cancer (basal cell carcinoma and squamous cell carcinoma).

3.2.1 Basal Cell Carcinoma

Basal cell carcinoma (BCC) is a semi-malignant, slow growing, locally destructive epithelial skin tumor. Metastasis is extremely rare, however local tissue invasion and destruction can affect morbidity. Whilst basal cell carcinoma is the most common form of skin cancer, its mortality rate is lower than melanoma (Ferrante di Ruffano et al., 2018). It is usually localized in the head and neck region and is predominantly seen in fair skin types. Treatment is based on clinical assessment, however the accurate estimation of the extent of the tumor in width and depth is not always possible. Therefore, a complete removal is often not achieved after the first excision. Therapy is based on the histological confirmation and depends on the subtype. Whilst most BCCs are surgically removed, superficial forms can be treated with topical medication, photodynamic therapy (PDT), cryosurgery or laser therapy (Suppa et al., 2023; Ulrich et al., 2015).

LC-OCT is able to identify BCC and its subtype non-invasively and in real time. In 52 histopathologically confirmed cases the following subtype criteria could be identified:

Superficial BCCs were characterized by a string of pearls pattern: tumor lobes connected to the DEJ resulting in a thickening of the epidermis. Infiltrative BCCs presented with a shoal of fish pattern: elongated hyporeflective tumor strands in between bright collagen strands. Keratinocyte Atypia, an altered DEJ, tumor nests in the dermis, dark clefting and vascularization were seen in nodular BCCs (Gust et al., 2022; Ruini, Schuh, Gust, et al., 2021).

3.2.2 Keratinocyte carcinoma

Squamous cell carcinoma (SCC) represents about 20% of non-melanoma skin cancer forms and are often located in sun-exposed areas of the body. Apart from sun exposure multiple factors like hair color, positive family history or degree of sunburns play a significant role in their development (Frost, Williams, & Green, 2000; Traianou et al., 2012). They are the second most common skin tumor after basal cell carcinomas and particularly seen on the face and scalp (Ruini, Witkowski, Cesinaro, Teixeira De Carvalho, & Pellacani, 2015).

Whereas actinic keratoses (AK) can be treated with local therapies such as topical agents like imiquimod and 5-fluorouracil or photodynamic therapy, advanced SCC often require surgical removal. Metastasis is less common than in melanoma and

closely associated with tumor size and depth of invasion. Therapy of metastatic or inoperable tumors entails radiotherapy, chemotherapeutics like cisplatin or 5-fluorouracil or immunotherapy such as anti-PD1 antibodies (Aggarwal, Puyana, Chandan, Jetter, & Tsoukas, 2024).

With the help of LC-OCT different stages of keratinocyte carcinoma, including AK, Bowen's disease (BD) and SCC can be diagnosed. Recognizing key features like keratinocyte morphology, architecture and the structure of the dermo epidermal junction (DEJ) and comparing them to histopathological correlations can aid in a better understanding of concurrent pre-cancerous and cancerous lesions in a tissue field, also known as field cancerization (Schmitz et al., 2016). Whereas a preserved DEJ was more common in AK and BD than SCC, increased epidermal thickness, acantholysis, bright particles, ulceration and an interrupted DEJ were seen in SCC. A Bowenoid pattern, entailing keratinocyte atypia in all epidermal layers, was found in BD. Overall the diagnostic confidence of different KC stages increased by 24.7% with the use of LC-OCT in comparison to Dermoscopy alone (Ruini, Schuh, Gust, et al., 2021).

LC-OCT has shown promise in reliably evaluating the basal keratinocyte growth pattern in vivo. Correlation with the histologic AK classification PRO model has shown a strong agreement between LC-OCT findings, different observers and histopathology. The PRO classification focuses on different stages of basal keratinocytes protruding downward into the dermis and correlates with the progression risk into invasive SCC (Pellacani et al., 2015). The potential ability to classify AKS non-invasively with LC-OCT based on the basal growth pattern of keratinocytes allows a clinical in-vivo reproduction of the PRO score (Ruini, Schuh, Gust, et al., 2021).

3.2.3 Melanoma

Melanoma originates from the uncontrolled proliferation of melanocytes. Manifesting in various organs containing said cells, occurrence ranges from mucosal surfaces to the spinal cord or the brain (Carr, Smith, & Wernberg, 2020). Cutaneous melanoma is the most common form and can present as superficial spreading, nodular, acral lentiginous or lentigo maligna melanoma (Mitsaki, Apalla, Lazaridou, Lallas, & Lallas, 2024). Melanoma staging relies on tumor thickness assessed via histology. The

Breslow Index correlates with prognosis, thicker lesions associate with lower survival rates (Wei et al., 2022).

In our study we evaluated 84 melanocytic lesions with LC-OCT and analyzed helpful parameter to discriminate between nevi and melanoma. Useful characteristics common in melanoma were: Irregular honeycombed patterns, presence of pagetoid spread in the epidermis and the absence of dermal nests. A 93% sensitivity and 95% specificity for diagnosing melanoma with LC-OCT was seen, therefore LC-OCT is a helpful tool to distinct between nevi and melanoma (Schuh et al., 2022).

4 Paper

4.1 Paper 1

Published in:

Gust, C.; Schuh, S.; Welzel, J.; Daxenberger, F.; Hartmann, D.; French, L.E.; Ruini, C.; Sattler, E.C. Line-Field Confocal Optical Coherence Tomography Increases the Diagnostic Accuracy and Confidence for Basal Cell Carcinoma in Equivocal Lesions: A Prospective Study. *Cancers* **2022**, *14*, 1082. https://doi.org/10.3390/cancers14041082

cancers

MDPI

Article

Line-Field Confocal Optical Coherence Tomography Increases the Diagnostic Accuracy and Confidence for Basal Cell Carcinoma in Equivocal Lesions: A Prospective Study

Charlotte Gust [1], Sandra Schuh [2], Julia Welzel [2], Fabia Daxenberger [1], Daniela Hartmann [1], Lars E. French [1,3], Cristel Ruini [1,4,*] and Elke C. Sattler [1,*]

1 Department of Dermatology and Allergy, University Hospital, LMU Munich, Frauenlobstr. 9-11, 80337 Munich, Germany; charlotte.gust@t-online.de (C.G.); fabiadaxenberger@gmail.com (F.D.); daniela.hartmann@med.uni-muenchen.de (D.H.); lars.french@med.uni-muenchen.de (L.E.F.)
2 Department of Dermatology and Allergy, University Hospital, 86179 Augsburg, Germany; sandra.schuh@uk-augsburg.de (S.S.); julia.welzel@uk-augburg.de (J.W.)
3 Dr. Phillip Frost Department of Dermatology and Cutaneous Surgery, Miller School of Medicine, University of Miami, Miami, FL 33125, USA
4 PhD School in Clinical and Experimental Medicine, University of Modena and Reggio Emilia, 41121 Modena, Italy
* Correspondence: cristelruini@gmail.com (C.R.); elke.sattler@med.uni-muenchen.de (E.C.S.); Tel.: +49-(0)89-4400-56010 (C.R.)

Simple Summary: Basal cell carcinoma is the most frequently occurring type of skin cancer. Its treatment can be either local or surgical depending on its subtype and extension, with early recognized and superficial cases being easier to treat. Some of them, however, display unspecific features, making diagnosis difficult. Non-invasive devices such as line-field confocal optical coherence tomography (LC-OCT) are able to recognize morphological features of different BCC subtypes with a good correlation to histopathology. We decided to study their application to clinically doubtful BCC cases.

Abstract: Diagnosing clinically unclear basal cell carcinomas (BCCs) can be challenging. Line-field confocal optical coherence tomography (LC-OCT) is able to display morphological features of BCC subtypes with good histological correlation. The aim of this study was to investigate the accuracy of LC-OCT in diagnosing clinically unsure cases of BCC compared to dermoscopy alone and in distinguishing between superficial BCCs and other BCC subtypes. Moreover, we addressed pitfalls in false positive cases. We prospectively enrolled 182 lesions of 154 patients, referred to our department to confirm or to rule out the diagnosis of BCC. Dermoscopy and LC-OCT images were evaluated by two experts independently. Image quality, LC-OCT patterns and criteria, diagnosis, BCC subtype, and diagnostic confidence were assessed. Sensitivity and specificity of additional LC-OCT were compared to dermoscopy alone for identifying BCC in clinically unclear lesions. In addition, key LC-OCT features to distinguish between BCCs and non-BCCs and to differentiate superficial BCCs from other BCC subtypes were determined by linear regressions. Diagnostic confidence was rated as "high" in only 48% of the lesions with dermoscopy alone compared to 70% with LC-OCT. LC-OCT showed a high sensitivity (98%) and specificity (80%) compared to histology, and these were even higher (100% sensitivity and 97% specificity) in the subgroup of lesions with high diagnostic confidence. Interobserver agreement was nearly perfect (95%). The combination of dermoscopy and LC-OCT reached a sensitivity of 100% and specificity of 81.2% in all cases and increased to sensitivity of 100% and specificity of 94.9% in cases with a high diagnostic confidence. The performance of LC-OCT was influenced by the image quality but not by the anatomical location of the lesion. The most specific morphological LC-OCT criteria in BCCs compared to non-BCCs were: less defined dermoepidermal junction (DEJ), hyporeflective tumor lobules, and dark rim. The most relevant features of the subgroup of superficial BCCs (sBCCs) were: string of pearls pattern and absence of epidermal thinning. Our diagnostic confidence, sensitivity, and specificity in detecting BCCs in the context of clinically equivocal lesions significantly improved using LC-OCT in comparison to dermoscopy only. Operator training for image acquisition is fundamental to achieve the best results.

check for updates

Citation: Gust, C.; Schuh, S.; Welzel, J.; Daxenberger, F.; Hartmann, D.; French, L.E.; Ruini, C.; Sattler, E.C. Line-Field Confocal Optical Coherence Tomography Increases the Diagnostic Accuracy and Confidence for Basal Cell Carcinoma in Equivocal Lesions: A Prospective Study. *Cancers* **2022**, *14*, 1082. https://doi.org/10.3390/cancers14041082

Academic Editor: Chyi-Chia Richard Lee

Received: 24 January 2022
Accepted: 16 February 2022
Published: 21 February 2022

Publisher's Note: MDPI stays neutral with regard to jurisdictional claims in published maps and institutional affiliations.

Not only the differential diagnosis of BCC, but also BCC subtyping can be performed at bedside with LC-OCT.

Keywords: basal cell carcinoma; dermoscopy; line-field confocal optical coherence tomography; bedside histology; skin imaging; non-invasive diagnostics in dermatology

1. Introduction

In recent decades, basal cell carcinoma (BCC) has progressed towards being the most frequently occurring type of skin cancer [1,2]. The diagnostic gold standard includes a biopsy or excision of the suspicious lesion and histopathological examination, resulting in a cost- and time-intensive process [3,4]. Treatment depends mainly on the histopathological subtype, with deep and nodular or infiltrating BCCs requiring a complete surgical excision, while superficial tumors can benefit from cryotherapy, lasers, or topical drugs such as imiquimod [2,3]. Therefore, the bedside diagnosis and subtyping of BCC are crucial for treatment planning. Clinical and dermoscopical examinations are commonly used in the daily clinical practice to diagnose BCCs, but non-invasive optical diagnostic methods, such as optical coherence tomography (OCT) and reflectance confocal microscopy (RCM), have shown a high potential in early detection of clinically unclear BCCs, with diagnostic sensitivity and specificity over 90% [5–7]. Additionally, the new line-field confocal OCT (LC-OCT), with higher penetration depth than RCM (500 µm compared to 250 µm) and higher resolution than OCT (1 µm compared to 7.5–10 µm) [8,9], has recently been used to detect BCCs non-invasively according to morphological criteria in preliminary studies [10–12]. However, there are no studies focused on clinically unclear lesions.

The aims of this study were: to verify in a real-life setting the diagnostic value of LC-OCT for clinically unclear BCC cases and to test for the ability to distinguish between superficial and other BCC subtypes, compared to dermoscopy and histopathology. Moreover, we reviewed morphological LC-OCT criteria for BCCs and provide an overview of the main diagnostic pitfalls.

2. Materials and Methods

This prospective study was performed at the Departments of Dermatology of the University of Munich and the University of Augsburg in Germany between November 2019 and February 2021. We prospectively recruited 182 clinically unclear lesions of 154 patients that were referred to our imaging departments from the general outpatient and inpatient departments and from external specialists in order to confirm or to rule out BCC prior to biopsy or excision. Clinical, dermoscopic (FotoFinder GmbH, Germany and Dermogenius-Dermoscan GmbH, Regensburg, Germany), and LC-OCT images of the cases were acquired and analyzed by two blinded imaging experts (CR, CG). Discordant cases were reviewed by a third expert (ES, SS, or JW). After the non-invasive imaging, surgical excision followed by histopathological examination was performed in all lesions.

For every case, the patient's age, sex, and the anatomical site of the lesion were registered. Afterwards, dermoscopy was performed and a dermoscopic diagnosis was registered together with a confidence level ranging from 1 = high (>75% confidence) to 2 = intermediate (>50% confidence) to 3 = low (<50% confidence). Finally, the lesions were scanned with the LC-OCT device (DAMAE Medical, Paris), which uses a class 1 supercontinuum laser with a central wavelength of 800 nm to create various A-scans up to a depth of approximately 500 µm. Three imaging modalities are available: vertical or en-coupe, horizontal or en-face, and a 3D reconstruction either in a vertical or horizontal field of view. Details are described elsewhere [8,9].

The following features were registered: LC-OCT diagnosis, confidence, image quality, and whether LC-OCT could rule out a BCC diagnosis or not. LC-OCT image quality was scored from 1 (high: perfect image, no artefacts) to 2 (low: lower resolution, minor artefacts)

to 3 (insufficient: major artefacts, unreadable). Confidence level was measured as described above for dermoscopy.

We calculated the frequency of the main descriptive morphological parameters used for the identification of BCCs in LC-OCT and their frequency as previously described in published studies [11] (Table 1). Key features useful for differentiating BCCs from non-BCCs and to differentiate between superficial BCC and other subtypes were identified by logistic regression.

To assess the LC-OCT performance, diagnostic accuracy, sensitivity, and specificity for BCCs compared to dermoscopy and to the gold standard histology were calculated using McNemar's tests. Calculation was performed for all lesions and additionally in the subgroup of cases with a confidence level rated as "high" by at least one of the observers.

The study was approved by the ethical committee of the LMU Munich (Protocol Number 17-699).

Table 1. LC-OCT parameters.

(**a**) Epidermal LC-OCT parameters vertical

EPIDERMAL LC-OCT PARAMETERS VERTICAL	Parameters used in logistic regression for:		Not-BCC (n = 69)	All BCC (n = 113)	Superficial BCC (n = 35)	Nodular BCC (n = 52)	Infiltrative BCC (n = 4)	Mixed BCC (n = 21)
	BCC vs. non BCC	Superficial BCC vs. other pure BCC subtypes (nodular, fibrosing)						
Hyperkeratoses	x		40 (58.0)	38 (33.6)	13 (37.1)	20 (38.5)	1 (25.0)	4 (19.0)
Thinning of the epidermis	x	x	5 (7.2)	48 (42.5)	7 (20.0)	34 (65.4)	1 (25.0)	6 (28.6)
Bowenoid morphology			14 (20.3)	5 (4.4)	3 (8.6)	2 (3.8)	0 (0)	0 (0)
Acanthosis, verrucous surface			11 (15.9)	4 (3.5)	1 (2.9)	2 (3.8)	0 (0)	1 (4.8)
Scales			39 (56.5)	34 (30.1)	12 (34.3)	14 (26.9)	2 (50.0)	6 (28.6)
Keratin plugs/horn cysts			17 (24.6)	0 (0)	0 (0)	0 (0)	0 (0)	0 (0)
Ulceration			15 (21.7)	35 (31)	9 (25.7)	17 (32.7)	2 (50.0)	7 (33.3)
Pagetoid cells			3 (4.3)	1 (0.9)	0 (0)	1 (1.9)	0 (0)	0 (0)
Ovoid concentric structures (sebaceous gland)			19 (27.5)	7 (6.2)	0 (0)	4 (7.7)	1 (25.0)	2 (9.5)
Atypical junctional nests			2 (2.9)	1 (0.9)	0 (0)	1 (1.9)	0 (0)	0 (0)
Tumour strands			6 (8.7)	2 (1.8)	0 (0)	2 (3.8)	0 (0)	0 (0)
Wave pattern/junctional nests			5 (7.2)	1 (0.9)	0 (0)	0 (0)	1 (25.0)	0 (0)
Dermal/deep nests			4 (5.8)	0 (0)	0 (0)	0 (0)	0 (0)	0 (0)
Atypical honeycombed pattern			49 (71.0)	74 (65.5)	19 (54.3)	39 (75.0)	3 (75.0)	13 (61.9)

Table 1. *Cont.*

(**b**) DEJ—dermal parameters vertical

DEJ-DERMAL PARAMETERS VERTICAL		Flattened rete ridges	Elongated rete ridges	Well defined DEJ	Less defined (disrupted) DEJ	Hyporefrecti ovoid structures/nests/lo	Dark rim/ clefting	Prominent vessels	Shoal of fish pattern of the lobules	String of pearls patterns of the lobules (connected to the DEJ)	White stromal reaction (vertical)	Black areas/hyporeflective cysts inside the nests
Parameters used in logistic regression for:	BCC vs. non BCC				X	X	X					
	Superficial BCC vs. other pure BCC subtypes (nodular, fibrosing)								X	X		
Not-BCC	(n = 69)	6 (8.7)	2 (2.9)	41 (59.4)	21 (30.4)	10 (14.5)	9 (13.0)	28 (40.6)	3 (4.3)	8 (11.6)	21 (30.4)	3 (4.3)
All BCC	(n = 113)	1 (0.9)	0 (0)	26 (23.0)	107 (94.7)	107 (94.7)	88 (77.9)	54 (47.8)	26 (23.0)	56 (49.6)	64 (56.6)	19 (16.8)
Superficial BCC	(n = 35)	0 (0)	0 (0)	10 (28.6)	34 (97.1)	32 (91.4)	29 (82.9)	14 (40.0)	13 (37.1)	28 (80.0)	16 (45.7)	1 (2.9)
Nodular BCC	(n = 52)	0 (0)	0 (0)	11 (21.2)	50 (96.2)	51 (98.1)	38 (73.1)	25 (48.1)	4 (7.7)	13 (25.0)	31 (59.6)	12 (23.1)
Infiltrative BCC	(n = 4)	1 (25.0)	0 (0)	1 (25.0)	3 (75.0)	2 (50.0)	1 (25.0)	4 (100)	4 (100)	0 (0)	3 (75)	0 (0)
Mixed BCC	(n = 21)	0 (0)	0 (0)	3 (14.3)	20 (95.2)	21 (100)	19 (90.5)	11 (52.4)	5 (23.8)	15 (71.4)	14 (66.7)	6 (28.6)

Table 1. *Cont.*

(**c**) LC-OCT parameters horizontal

PARAMETERS HORIZONTAL		Pagetoid cells in the epidermis-DEJ (horizontal)	Bright stromal reaction (horizontal)	Polarizatio of nuclei in the epidermis (horizontal)	Palisading (horizontal)	Clefting (horizontal)	Tumor nests/cords/silhouettes (horizontal)	Prominent vessels (horizontal)	Bright collagen alterations (elastosis)(horizontal)
Parameters used in logistic regression for:	BCC vs. non BCC			X	X	X	X		
	Superficial BCC vs. other pure BCC subtypes (nodular, fibrosing)								
Not-BCC	(n = 69)	4 (5.8)	17 (24.6)	2 (2.9)	1 (1.4)	3 (4.3)	10 (14.5)	9 (13.0)	30 (43.5)
All BCC	(n = 113)	28 (24.8)	70 (61.9)	58 (51.3)	40 (35.4)	38 (33.6)	78 (69.0)	42 (37.2)	79 (69.9)
Superficial BCC	(n = 35)	13 (37.1)	18 (51.4)	17 (48.6)	10 (28.6)	10 (28.6)	25 (71.4)	16 (45.7)	21 (60.0)
Nodular BCC	(n = 52)	11 (21.2)	34 (65.4)	28 (53.8)	23 (44.2)	23 (44.2)	37 (71.2)	16 (30.8)	43 (82.7)
Infiltrative BCC	(n = 4)	0 (0)	3 (75.0)	2 (50.0)	1 (25.0)	1 (25.0)	3 (75.0)	2 (50.0)	3 (75.0)
Mixed BCC	(n = 21)	4 (19.0)	15 (71.4)	10 (47.6)	6 (28.6)	4 (19.0)	13 (61.9)	8 (38.1)	11 (52.4)

3. Results

3.1. Population

A total of 182 lesions clinically suspicious for BCC in 154 patients were included in this study; 113 (62.1%) were confirmed histopathologically as BCCs and 69 (37.9%) as non-BCCs. The histopathological analysis entailed 35 (19.2%) completely excised lesions, 132 (72.5%) lesions acquired by punch biopsy, and 15 (8.2%) shave biopsies. Among the 113 BCCs, the nodular BCC subtype was seen most frequently in 52 (46%) lesions, followed by the superficial subtype in 35 (31%) and 4 (3.5%) infiltrative cases. Among the non-BCC cases, actinic keratosis (AK) was the most common diagnosis with a total of 24 lesions equaling a prevalence of 34.8%. Additional diagnoses included: squamous cell carcinoma (SCC), Bowen's disease, nevus, melanoma, sebaceous hyperplasia, scar tissue/fibrous papule, dermatofibroma, lentigo solaris/seborrheic keratosis, eczema, clear cell acanthoma, molluscum contagiosum, trichoblastoma, angioma, atypical fibroxanthoma, and granuloma (Figures 1–5) (Table 2).

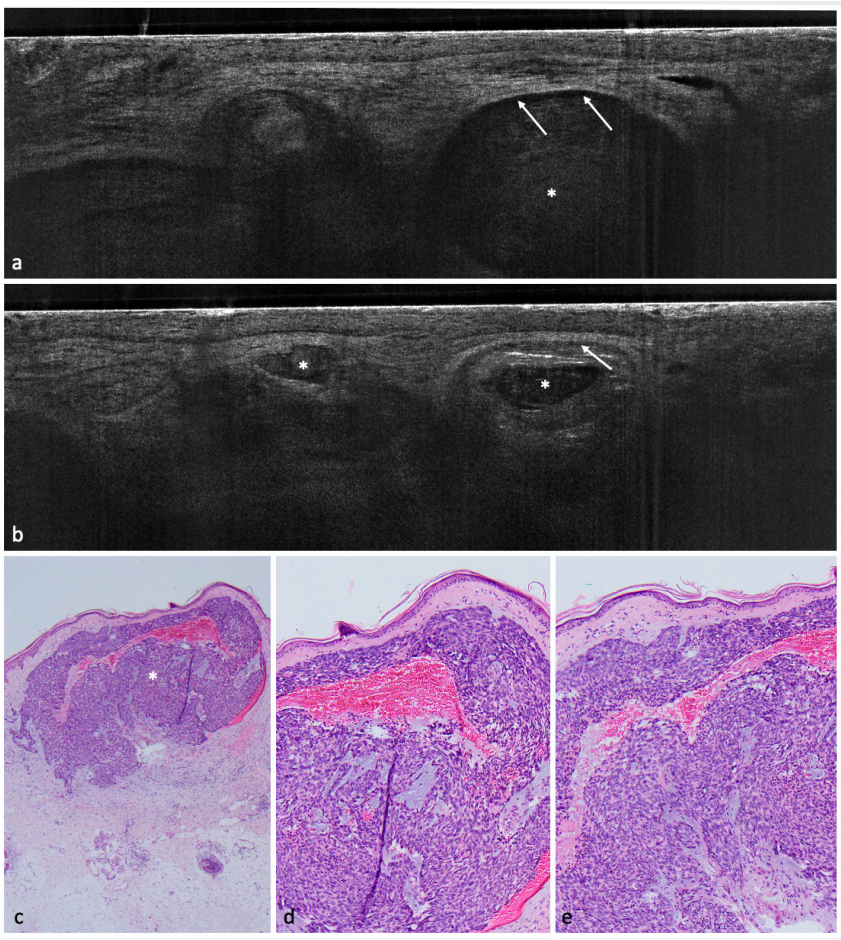

Figure 1. Nodular BCC on the lower leg of a 68-year-old female patient. (**a**,**b**) LC-OCT images. The nodular BCC presents itself with a fine granular texture corresponding to basaloid cells, peritumoral clefting (white arrows) and homogeneous areas with possibly liquefactive necrosis with remaining cell debris (white asterisks). (**c**) (40×), (**d**) (100×), and (**e**) (100×): corresponding histological HE-stained sections with peripheral palisading, clefting, and a central necrosis.

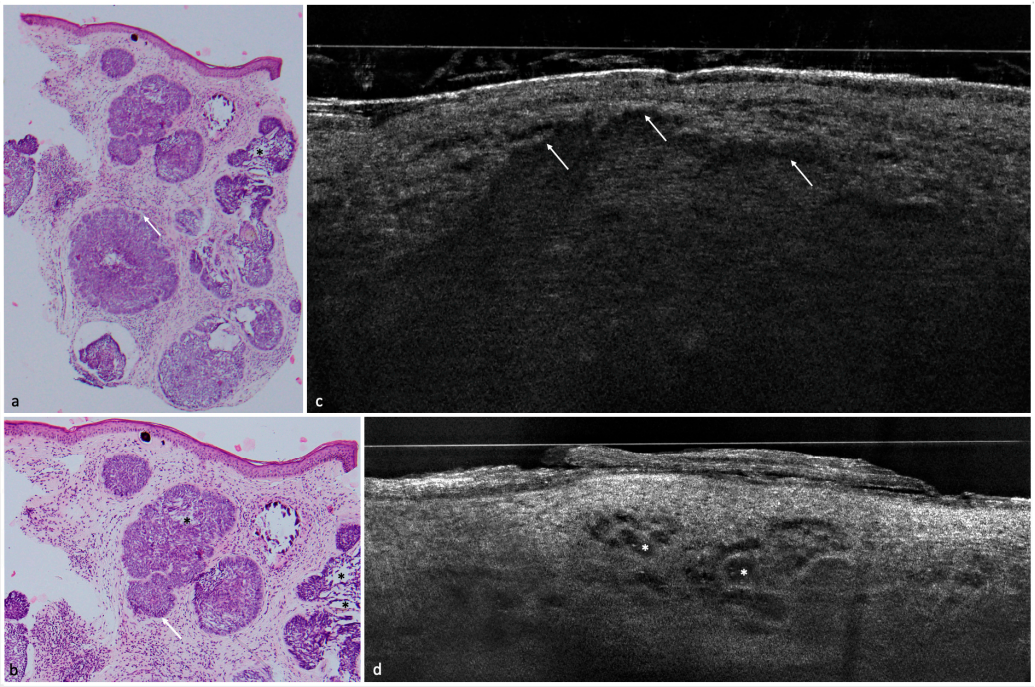

Figure 2. Nodular BCC with cystic parts in the nasolabial fold of a 76-year-old patient. (**a**) (200×) and (**b**) (100×): histological HE-stained sections. Peritumoral clefting (white arrows) and cystic structures (asterisk). (**c**) LC-OCT image of the same lesion. Arrows again indicate clefting, the BCC has a fine granular texture. (**d**) dark hyporeflective area (asterisk) in a cystic BCC corresponding to glomerular vessels.

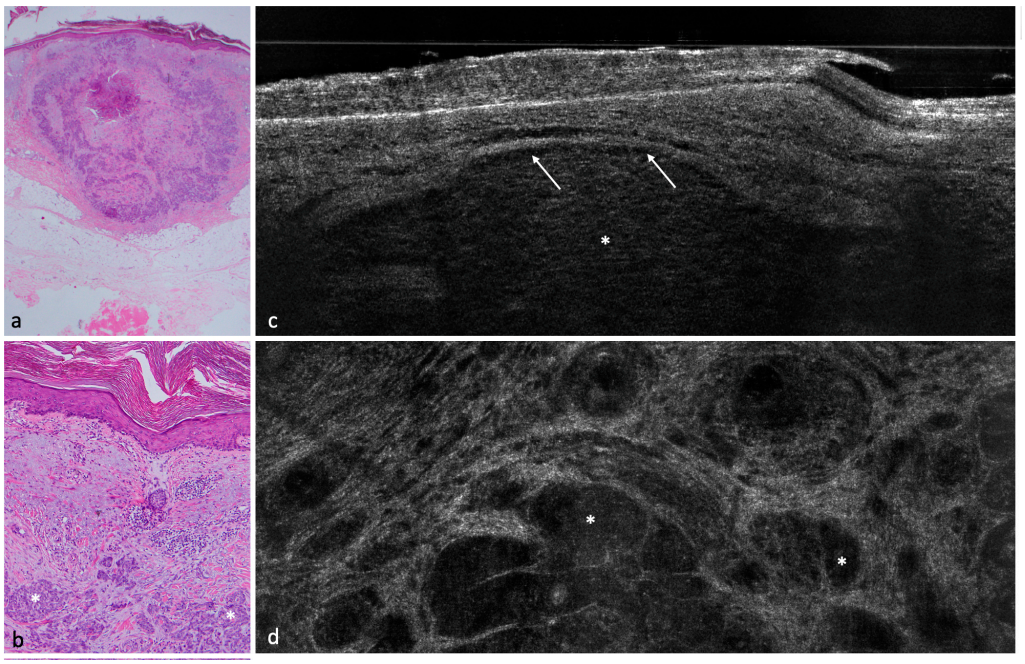

Figure 3. Nodular BCC on the right temple of a 64-year-old male patient. (**a**) (20×) and (**b**) (100×): histological HE-stained sections of the tumor. (**c**) (vertical) and (**d**) (horizontal): LC-OCT images of the corresponding lesion. Again, peripheral clefting can be seen (white arrow) as well as basaloid nests (asterisks).

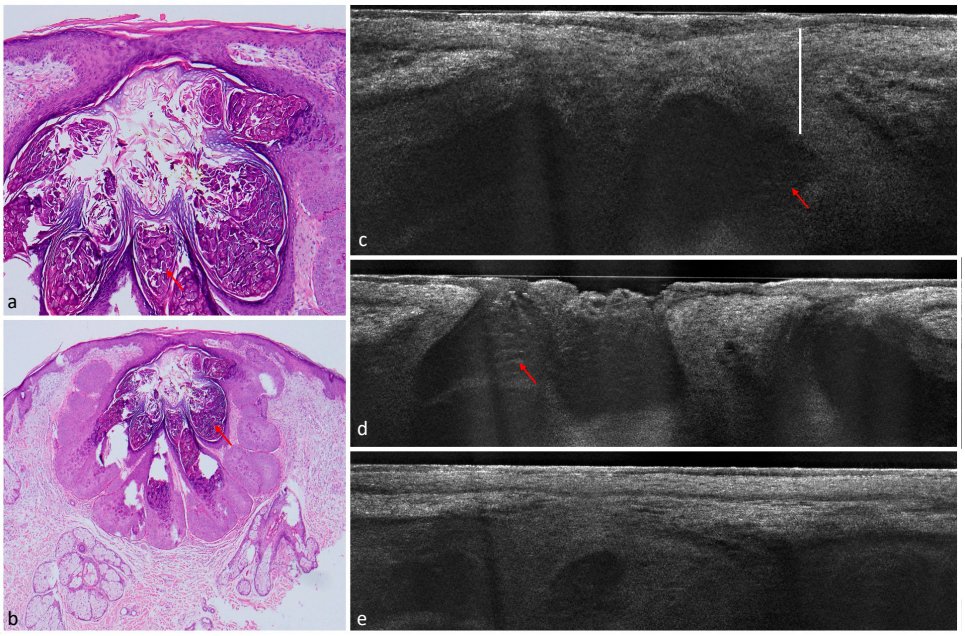

Figure 4. Molluscum contagiosum on the forehead of a 58-year-old male patient. (**a**) (100×) and (**b**) (40×): histological hematoxylin and eosin (HE)-stained sections. In histology, a cup-shaped multilobular lesion can be identified. Red arrows indicate intracytoplasmatic inclusion bodies (Henderson–Paterson bodies) which contain virus particles. (**c**–**e**) LC-OCT image of the molluscum contagiosum. It shows acanthosis (white bar) and hyporeflective areas with hazy structures, which probably correspond to the Henderson–Paterson bodies (red arrow).

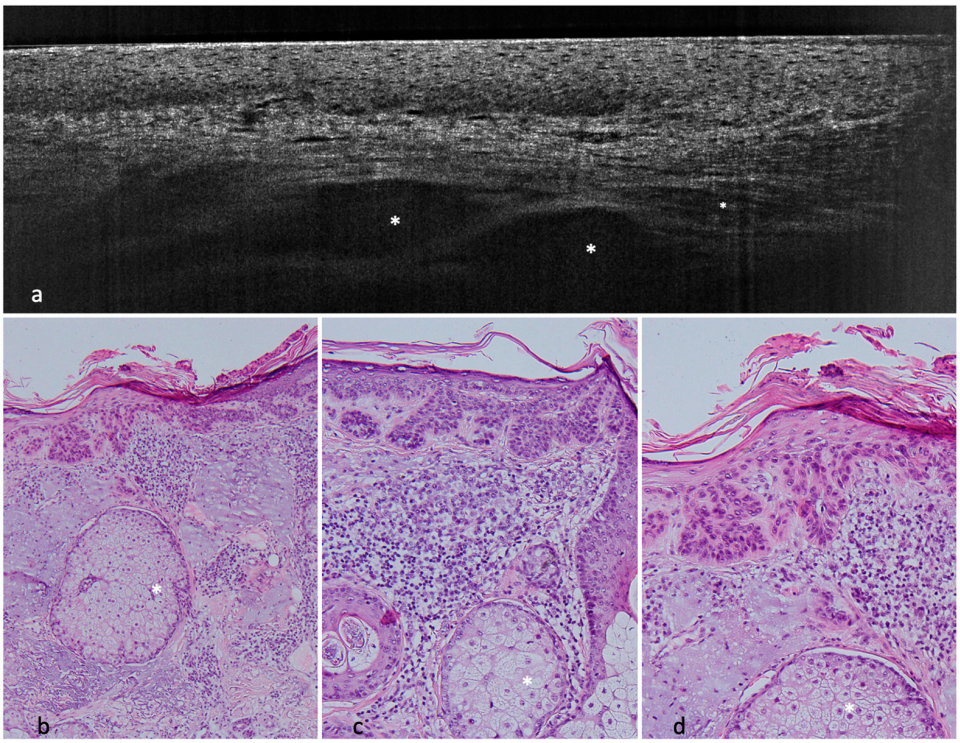

Figure 5. Sebaceous hyperplasia on the nose of a 70-year-old male patient. (**a**) LC-OCT image. The enlarged sebaceous glands are visible as hyporeflective ovoid structures (white asterisk). When looking carefully, roundish sebocytes might be spotted within the glands. (**b**) (100×) and (**c**) (200×) and (**d**) (200×): histological HE-stained sections. Enlarged, regularly structured sebaceous glands (white asterisk).

Table 2. Epidemiological data.

Characteristic	Patient-Based	Lesion-Based
Mean age (+/−SD)	70.8 (12.3)	71.7 (12.0)
Sex, n(%)		
Male	102 (66.2)	
Female	52 (33.8)	
Localisation, n (%)		
Ear	1 (0.6)	1 (0.5)
Face	76 (49.4)	85 (46.7)
Head	4 (2.6)	6 (3.3)
Neck	3 (1.9)	4 (2.2)
Scalp	3 (1.9)	4 (2.2)
Trunk	49 (31.8)	62 (34.1)
Lower limb	9 (5.8)	10 (5.5)
Upper limb	9 (5.8)	10 (5.5)
Number of lesions n (%)		
1	132 (85.7)	
2	17 (11.0)	
3	4 (2.6)	
4	1 (0.6)	
Histological diagnosis, n (%)		
BCC	91 (59.1)	113 (62.1)
non-BCC	63 (40.9)	69 (37.9)
AK	21 (33.3)	24 (34.8)
SCC	8 (12.7)	9 (13.0)
Sebaceous hyperplasia	7 (11.1)	7 (10.1)
Bowen	4 (6.3)	5 (7.2)
Other non-BCC *	23 (36.5)	24 (34.8)
BCC subtypes, n (%)		
Superficial BCC	25 (27.5)	35 (31.0)
Nodular BCC	44 (48.4)	52 (46.0)
Fibrosing BCC	4 (4.4)	4 (3.5)
Nodular superficial BCC	12 (13.2)	15 (13.3)
Nodular Fibrosing BCC	2 (2.2)	3 (2.7)
Mixed	3 (3.3)	3 (2.7)

* Other non-BCC subtypes include lentigo maligna/melanoma, nevus, scar, dermatofibroma, lentigo solaris/seborrheic keratosis, eczema, clear cell acanthoma, molluscum contagiosum, fibrous papule, trichoblastoma, angioma, atypical fibroxanthoma, aspecific crust, and granuloma.

3.2. Image Quality and Diagnostic Confidence

Average LC-OCT image quality was rated as high in 162 cases (89%) and as low in 20 cases (11%); no image was considered unreadable (image quality 3).

A high diagnostic confidence (1) by at least one observer was only scored in 48% of the dermoscopic images, compared to 70% of the LC-OCT cases. The interobserver agreement on the confidence level was very good. With LC-OCT, this was the case in 173 out of 182 (95%) of the observations (weighted kappa = 0.90 (95% CI, 8.84 to 0.97), $p \sim 0$). For der-

moscopy, the number of interobserver agreements was 177 out of 182 (97.3%) observations (weighted kappa = 0.96 (95% CI, 0.92 to 0.99), $p \sim 0$).

Our average diagnostic confidence with LC-OCT was 1.7; if we consider the subgroup of lesions with high image quality (1), we reported a confidence level of 1.1 (limbs) and 1.2 (head, trunk); in the subgroup of lesions with low image quality (2), diagnostic confidence sank to 2.3 (trunk), 2.5 (head), and 2.8 (limbs). Diagnostic confidence was therefore influenced by image quality but not by anatomical site.

3.3. Diagnostic Performance

Diagnostic accuracy of dermoscopy and LC-OCT for ruling out BCCs in suspicious lesions was 88% and 91%, respectively. Concerning sensitivity and specificity compared to the gold standard histology, dermoscopy scored a sensitivity of 90% and a specificity of 86%, while LC-OCT showed a high sensitivity (98%) and a good but lower specificity (80%). Sensitivity and specificity slightly increased when image quality was high, to 93% and 99%, respectively. If considering the subgroup of LC-OCT images with a high diagnostic confidence, however (70% of the lesions), the LC-OCT performance increased significantly, with a sensitivity of 100% and a specificity of 97% compared to the gold standard histology ($p = 1$, McNemar's test).

In daily clinical practice, the combination of dermoscopy and LC-OCT enables the clinician to confidently make an almost perfect diagnosis at the bedside. The combination of both reaches an accuracy of 92.9% in all cases and an accuracy of 98.2% in confident cases, providing a certain security for the clinician and guiding further steps in the treatment process.

3.4. BCC Subtype

The diagnostic accuracy of LC-OCT for all BCC subtypes was 90%; we reported an overall sensitivity of 77% and a specificity of 96%. When only looking at cases with either a high LC-OCT quality (n = 101, 11% of the lesions) or lesions with a high LC-OCT confidence level (n = 93, 84% of the lesions), the performance of LC-OCT showed no significant difference to histology for all subtypes ($p > 0.05$, McNemar's test). Diagnostic accuracy, sensitivity, and specificity for each subtype were: superficial BCC, 90%, 77%, 96%; nodular BCC, 88%, 96%, 82%; mixed BCC, 90%, 67%, 96%. This values slightly increased when selecting only high image quality (Table 3).

If we consider only pure BCC subtypes (86 lesions), the diagnostic accuracy increased to 92%. Sensitivity and specificity were for superficial BCCs 82% and 100%, for nodular BCCs 100% and 81%, and for fibrosing BCCs 75% and 100%, respectively.

Table 3. LC-OCT performance.

(**a**) All lesions				
All lesions		**LC-OCT**		
		BCC	Non-BCC	Total
Histology	BCC	111	2	113
	Non-BCC	14	55	69
	Total	125	57	182
		Dermoscopy		
		BCC	Non-BCC	Total
Histology	BCC	102	11	113
	Non-BCC	10	59	69
	Total	112	70	182

Table 3. *Cont.*

(**b**) High confidence lesions				
High confidence level for at least one of the 2 observers		**LC-OCT**		
		BCC	Non-BCC	Total
Histology	BCC	93	0	93
	Non-BCC	1	33	34
	Total	94	33	127
		Dermoscopy		
		BCC	Non-BCC	Total
Histology	BCC	61	2	63
	Non-BCC	0	24	24
	Total	61	26	87
(**c**) Performance for BCC				
All BCC lesions				
N (%)	111 (100)			
Global accuracy	84%			
	Superficial BCC (N = 35)	Nodular BCC (N = 51)	Fibrosing BCC (N = 4)	Mixed (N = 21)
Accuracy	90%	88%	99%	90%
Sensitivity	77%	96%	75%	67%
Specificity	96%	82%	100%	96%
p value (Mac Nemar's test)	0.23	0.03	1	0.55
Good image quality				
N (%)	101 (91)			
Global accuracy	86%			
	Superficial BCC (N = 31)	Nodular BCC (N = 49)	Fibrosing BCC (N = 2)	Mixed (N = 19)
Accuracy	91%	90%	100%	91%
Sensitivity	81%	96%	100%	68%
Specificity	96%	85%	100%	96%
P value (Mac Nemar's test)	0.51	0.11	-	0.50
High confidence level for at least one of the 2 observers				
N (%)	93 (84)			
Global accuracy	84			
	Superficial BCC (N = 31)	Nodular BCC (N = 43)	Fibrosing BCC (N = 1)	Mixed (N = 18)
Accuracy	89%	89%	100&	89%
Sensitivity	77%	95%	100%	67%
Specificity	95%	84%	100%	95%
p value (Mac Nemar's test)	0.34	0.11	-	0.75

3.5. Diagnostic Criteria

The following nine parameters were entered in the first model of the logistic regression: vertical parameters: hyperkeratosis, thinning of the epidermis, poorly defined DEJ, hyporeflective ovoid structures, dark rim/clefting; horizontal parameters: polarization of nuclei in the epidermis, palisading, clefting, and tumor nests. Through a backward elimination approach, non-significant parameters were removed one by one so that the three most impactful parameters to discriminate between BCC and non-BCC were: poorly defined DEJ, dark rim/clefting, and hyporeflective ovoid structures. These findings were in line with previous work [10,11].

Concerning BCC subtypes, following parameters were inserted in the logistic regression: thinning of the epidermis, shoal of fish pattern of the lobules, and string of pearls pattern of the lobules. After logistic regression, thinning of the epidermis and string of pearls were the most impactful key criteria to influence the distinction between superficial BCC and other BCC subtypes (Figures 1–3).

3.6. Other Diagnoses

With dermoscopy, 10 lesions were mistakenly classified as BCC: two AK, two sebaceous hyperplasias (Figure 5), one Bowen's disease, one SCC, one nevus, one dermatofibroma, one molluscum contagiosum (Figure 1), and one pyogenic granuloma. Eleven BCCs were instead classified as: five SCC, two AK, one lentigo maligna/melanoma, one nevus, one scar, and one dermatofibroma. Using LC-OCT, we reported 14 false positive cases: eight AK, two seborrheic keratosis, one Bowen's disease, one sebaceous hyperplasia, one molluscum contagiosum, and one pyogenic granuloma. Two cases of nodular BCCs were mistakenly diagnosed as a scar and an SCC.

Keratinocyte skin cancer (KC), consisting of actinic keratoses (AKs), squamous cell carcinoma (SCC), and Bowen carcinomas (BCs), made up 38 of the 182 suspicious lesions. The performance of LC-OCT differed on KC compared to BCCs, showing a change in sensitivity, specificity, and confidence. Compared to dermoscopy, LC-OCT was more specific but less sensitive (N = 182, McNemar's p value = 0.02).

4. Discussion

In this study, we aimed to analyze the diagnostic performance of LC-OCT for BCCs among clinically unclear lesions, which can be missed with dermoscopy since they display unspecific patterns. We determined our diagnostic confidence and our diagnostic accuracy, sensitivity, and specificity in comparison to dermoscopy and to the gold standard histology. Being in a real-life setting, we also focused on our capability of distinguishing superficial BCCs from other subtypes using LC-OCT, since this has a direct influence on the choice of the therapy. Moreover, we tried to identify morphological criteria specific for BCC compared to other non-BCC differential diagnoses, which could be helpful to avoid unnecessary biopsies in the case of a benign diagnosis and to direct the patient to the correct therapeutic path in the case of malignant lesions other than BCC.

4.1. BCC Morphologic Criteria and Comparison with Histology

While clinical examination and dermoscopy are able to diagnose most clear-cut BCCs, equivocal lesions are a special target of non-invasive diagnostic techniques [5]. To date, a few preliminary studies have described morphological criteria for diagnosing BCC using the novel device LC-OCT, with good histopathological correlations [10,11]. Suppa et al. examined 89 BCCs and described tumor lobules, with (in superficial BCCs) or without connection (in nodular BCCs) to the epidermis and branched lobules (in infiltrative BCCs). In our previous study [11], we reported overlapping findings and defined, analogously to OCT terminology, the presence of a string of pearls pattern in superficial BCCs and of a shoal of fish pattern in infiltrative BCCs. Moreover, we reported an overall BCC subtype agreement between LC-OCT and histology of 90.4%, with a sensitivity of 82% and a specificity of 100% for superficial BCCs.

4.2. Diagnostic Accuracy, Sensitivity, and Specificity

Our diagnostic accuracy for BCCs was very high with both dermoscopy (88%) and LC-OCT (91%); compared to the gold standard histology, LC-OCT reached a high sensitivity (98%) but a slightly lower specificity (80%) in contrast to dermoscopy (86%).

Nevertheless, LC-OCT's specificity was higher than shown in recent studies on the use of other diagnostic techniques: OCT (range: 73–75%) or RCM (range: 38–59%). Such tools have been used in similar studies to better characterize unclear lesions. Ulrich et al., for example, analyzed the sensitivity and specificity of OCT for the assisted diagnosis of

non-pigmented BCC in a similar way in a previous observational study [13]. The additional use of OCT resulted in a specificity of 75.3% (LC-OCT: 80%), a sensitivity of 95.7% (LC-OCT: 98%), and an accuracy of 87.4% (LC-OCT: 92.9%).

The combination of dermoscopy and LC-OCT reached, in our study, an accuracy of 92.9% in all cases and of 98.2% in confident cases, providing a certain security for the clinician and guiding further steps in the treatment process. Using both tools in clinical practice enables the clinician to confidently make a very accurate diagnosis at the bedside.

Dermoscopy alone scored a lower sensitivity (90%) than expected [14]. This was probably due to the setting of clinically equivocal lesions, further supported by the fact that for only 48% of the lesions examined, the clinicians had a high level of confidence in their diagnosis with dermoscopy. This finding supports the fact that the enrolled lesions were equivocal. Our confidence improved markedly (70%) using LC-OCT.

Interestingly, if we consider only lesions with a high level of diagnostic confidence with LC-OCT (the majority), sensitivity and specificity values for the diagnosis of BCC reach those of the gold standard histology (100% and 97%, McNemar's p value = 1).

4.3. Diagnostic Confidence

The abovementioned findings point out that the clinician can significantly increase diagnostic confidence after dermoscopy based on LC-OCT images and avoid a potentially unnecessary biopsy if reassured by high confidence (which was the case in most lesions in our study). The potential practical consequences are the reduction in pain and discomfort for the patient and surgery related costs and complications.

Our diagnostic confidence was not influenced by the anatomical site of the examined lesions, but was negatively influenced by the image quality. In fact, diagnostic confidence was significantly lower (1.2 vs. 2.5) in the subgroup of high vs. low image quality. This emphasizes the value of correct and standardized image acquisition protocols and required training for imaging performing personnel.

4.4. BCC Subtyping

After correctly diagnosing a BCC out of clinically equivocal lesions, the next step requires its classification into the superficial or non-superficial subtypes; in fact, a superficial BCC can be easily treated with topical drugs or further local treatments, while other more invasive subtypes should be referred to (micrographically controlled) surgery.

We identified the absence of the thinning of the epidermis and a string of pearls pattern with lobules connected to the DEJ as the most useful criteria for diagnosing superficial BCCs. The string of pearls pattern, present in 80% of our superficial BCCs, was described as hemispheric lobules (63%) or lobules connected to the epidermis (100%) in Suppa et al.'s findings. We demonstrated that we are able to use LC-OCT to distinguish between superficial and non-superficial BCC subtypes with high diagnostic accuracy. We reached a sensitivity and specificity for diagnosing superficial BCCs of 77% and 96%, respectively, increasing to 82% and 100% when considering only pure subtypes [11].

Mixed BCC subtypes are a diagnostic challenge, since their components vary in their amount and can be easily missed. However, when nodular or fibrosing components are present, the BCC becomes a surgery candidate and should not be (except for very superficial nodular components) treated with less invasive methods. Therefore, superficial BCCs could be treated non-invasively after LC-OCT without histopathological examination.

For nodular BCC detection, LC-OCT showed the highest sensitivity with 100%, whereas specificity was highest for superficial (100%) and infiltrating (100%) BCCs. However, it needs to be mentioned that for the infiltrating BCC subtype, only a few lesions (n = 4) were collected in the real-life setting and the category classified as mixed subtype includes nodular superficial, nodular fibrosing, and other mixed subtypes. This may be seen as a limitation of this study.

Again, the performance of LC-OCT for all subtypes including mixed subtypes showed no significant difference to histology for all subtypes ($p > 0.05$, McNemar's test) when only

looking at cases with either a high LC-OCT quality (n = 101, 11% of the lesions) or lesions with a high LC-OCT confidence level (n = 93, 84% of the lesions).

In a second step, we tried to identify with the help of logistic regressions a few key criteria able to distinguish between BCC and non-BCCs; these were: poorly defined DEJ, hyporeflective ovoid structures or nests/lobules (Figure 3), and dark rim/clefting (Figure 1). These criteria were consistent with previous findings [10,11].

4.5. Differential Diagnosis and Related Pitfalls

Although LC-OCT is a promising tool for the bedside differential diagnosis of BCC, there still remain pitfalls. Fourteen lesions (eight actinic keratosis, two lentigo solaris/seborrheic keratosis, one Bowen's disease, one sebaceous hyperplasia, one molluscum contagiosum, one pyogenic granuloma) were misdiagnosed as BCCs.

The actinic keratosis belonged to the bowenoid subtype, causing a roundish contour of the epidermis with atypical keratinocytes that can be confounded with a string of pearls pattern. In this case, the expert observer should pay attention to the bright hyperkeratosis and continuity of the DEJ, Analogously, tumor lobules can be easily caused by granulomas, sebaceous lobules [15], and even molluscum bodies [16]. In such cases, the roundish or polycyclic dermal lobules are very well defined and sharply contoured, and usually contain brighter granular structures (Figure 4: molluscum contagiosum, Figure 5: sebaceous hyperplasia) or fibrotic–calcific tissue (granuloma). Furthermore, the DEJ is usually preserved and is overlined by a normal epidermis, which can, however, be thinned by the dermal structures. Sebaceous hyperplasia is also usually connected to hair follicles.

One case of BCC was misdiagnosed as a scar, probably due to the hyperreflective connective tissue masking the presence of tumor lobules, while another one was classified as an SCC due to the surrounding field cancerization in an elderly patient with hyperkeratosis, keratinocyte atypia, elastosis, and collagen alterations. For this reason, particular attention is needed in such patients when performing a bedside mapping of multiple suspicious lesions.

5. Conclusions

To sum up, we were able to reach a very good diagnostic confidence and performance in distinguishing BCCs from other BCC-suspicious lesions compared to dermoscopy and the gold standard histology. The study had limitations such as the small number of non-BCC lesions and the presence of only histologically confirmed lesions. Nevertheless, we believe LC-OCT is able to support the clinician in the process of diagnosing and subtyping BCC, as a key role to optimize the diagnostic approach and the treatment. It is particularly useful to screen BCCs in the context of clinically equivocal lesions, which can be difficult to diagnose with dermoscopy only. Moreover, it is possible to screen for superficial BCCs to be treated with less invasive methods than surgery. Larger studies on specific lesion subgroups such as facial papules are needed to gain more experience in this interesting field of dermatology.

Author Contributions: Conceptualization, J.W., C.R. and E.C.S.; methodology, J.W., C.R., E.C.S. and S.S.; validation, J.W., C.R., E.C.S., S.S. and D.H.; formal analysis, J.W., C.R., E.C.S., S.S., D.H., C.G. and F.D.; investigation, J.W., C.R., E.C.S., S.S., D.H., C.G. and F.D.; resources, C.R., E.C.S., J.W. and L.E.F.; data curation, C.R., S.S. and C.G.; writing—original draft preparation, C.G. and C.R.; writing—review and editing, E.C.S., S.S., D.H., C.G., C.R., F.D. and L.E.F.; supervision, J.W. and E.C.S.; project administration, J.W., C.R., E.C.S. and S.S.; funding acquisition, C.R. All authors have read and agreed to the published version of the manuscript.

Funding: The study was partially funded by the FöFoLe, a Funding program for research and teaching and Research Grant of the medical faculty of the Ludwig Maximilian University of Munich, protocol number 10-22.

Institutional Review Board Statement: The study was conducted according to the guidelines of the Declaration of Helsinki, and approved by the Institutional Review Board of the LMU Munich (Protocol Number 17-699).

Informed Consent Statement: Informed consent was obtained from all subjects involved in the study.

Data Availability Statement: Fully anonymized data are available on motivated request.

Acknowledgments: The authors thank DAMAE Medical together with Maxime Cazalas and Melanie Pedrazzani for providing the device needed for this study and for their constant professional assistance.

Conflicts of Interest: The authors declare no relevant conflict of interest. The prototype of the LC-OCT device was made available for the study free of charge by DAMAE at both centers.

References

1. Lomas, A.; Leonardi-Bee, J.; Bath-Hextall, F. A systematic review of worldwide incidence of nonmelanoma skin cancer. *Br. J. Dermatol.* **2012**, *166*, 1069–1080. [CrossRef] [PubMed]
2. Peris, K.; Fargnoli, M.C.; Garbe, C.; Kaufmann, R.; Bastholt, L.; Seguin, N.B.; Bataille, V.; Marmol, V.D.; Dummer, R.; Harwood, C.A.; et al. Diagnosis and treatment of basal cell carcinoma: European consensus-based interdisciplinary guidelines. *Eur. J. Cancer* **2019**, *118*, 10–34. [CrossRef] [PubMed]
3. Lang, B.M.; Balermpas, P.; Bauer, A.; Blum, A.; Brölsch, G.F.; Dirschka, T.; Follmann, M.; Frank, J.; Frerich, B.; Fritz, K.; et al. S2k Guidelines for Cutaneous Basal Cell Carcinoma—Part 2: Treatment, Prevention and Follow-up. *J. Dtsch. Dermatol. Ges.* **2019**, *17*, 214–230. [CrossRef] [PubMed]
4. Heppt, M.V.; Leiter, U.; Steeb, T.; Amaral, T.; Bauer, A.; Becker, J.C.; Breitbart, E.; Breuninger, H.; Diepgen, T.; Dirschka, T.; et al. S3 guideline for actinic keratosis and cutaneous squamous cell carcinoma—Short version, part 1: Diagnosis, interventions for actinic keratoses, care structures and quality-of-care indicators. *J. Dtsch. Dermatol. Ges.* **2020**, *18*, 275–294. [CrossRef] [PubMed]
5. Ferrante di Ruffano, L.; Dinnes, J.; Deeks, J.J.; Chuchu, N.; Bayliss, S.E.; Davenport, C.; Takwoingi, Y.; Godfrey, K.; O'Sullivan, C.; Matin, R.N.; et al. Optical coherence tomography for diagnosing skin cancer in adults. *Cochrane Database Syst. Rev.* **2018**, *12*, Cd013189. [CrossRef] [PubMed]
6. Dinnes, J.; Deeks, J.J.; Chuchu, N.; Saleh, D.; Bayliss, S.E.; Takwoingi, Y.; Davenport, C.; Patel, L.; Matin, R.N.; O'Sullivan, C.; et al. Reflectance confocal microscopy for diagnosing keratinocyte skin cancers in adults. *Cochrane Database Syst. Rev.* **2018**, *12*, Cd013191. [CrossRef] [PubMed]
7. Longo, C.; Lallas, A.; Kyrgidis, A.; Rabinovitz, H.; Moscarella, E.; Ciardo, S.; Zalaudek, I.; Oliviero, M.; Losi, A.; Gonzalez, S.; et al. Classifying distinct basal cell carcinoma subtype by means of dermatoscopy and reflectance confocal microscopy. *J. Am. Acad. Dermatol.* **2014**, *71*, 716–724.e711. [CrossRef] [PubMed]
8. Ogien, J.; Levecq, O.; Azimani, H.; Dubois, A. Dual-mode line-field confocal optical coherence tomography for ultrahigh-resolution vertical and horizontal section imaging of human skin. *Biomed. Opt. Express* **2020**, *11*, 1327–1335. [CrossRef] [PubMed]
9. Dubois, A.; Xue, W.; Levecq, O.; Bulkin, P.; Coutrot, A.L.; Ogien, J. Mirau-based line-field confocal optical coherence tomography. *Opt. Express* **2020**, *28*, 7918–7927. [CrossRef]
10. Suppa, M.; Fontaine, M.; Dejonckheere, G.; Cinotti, E.; Yelamos, O.; Diet, G.; Tognetti, L.; Miyamoto, M.; Orte Cano, C.; Perez-Anker, J.; et al. Line-field confocal optical coherence tomography of basal cell carcinoma: A descriptive study. *J. Eur. Acad. Dermatol. Venereol.* **2021**, *35*, 1099–1110. [CrossRef] [PubMed]
11. Ruini, C.; Schuh, S.; Gust, C.; Kendziora, B.; Frommherz, L.; French, L.E.; Hartmann, D.; Welzel, J.; Sattler, E. Line-field optical coherence tomography: In vivo diagnosis of basal cell carcinoma subtypes compared to histopathology. *Clin. Exp. Dermatol.* **2021**, *46*, 1471–1481. [CrossRef]
12. Ruini, C.; Schuh, S.; Sattler, E.; Welzel, J. Line-field confocal optical coherence tomography-Practical applications in dermatology and comparison with established imaging methods. *Ski. Res. Technol.* **2021**, *27*, 340–352. [CrossRef]
13. Ulrich, M.; von Braunmuehl, T.; Kurzen, H.; Dirschka, T.; Kellner, C.; Sattler, E.; Berking, C.; Welzel, J.; Reinhold, U. The sensitivity and specificity of optical coherence tomography for the assisted diagnosis of nonpigmented basal cell carcinoma: An observational study. *Br. J. Dermatol.* **2015**, *173*, 428–435. [CrossRef] [PubMed]
14. Altamura, D.; Menzies, S.W.; Argenziano, G.; Zalaudek, I.; Soyer, H.P.; Sera, F.; Avramidis, M.; DeAmbrosis, K.; Fargnoli, M.C.; Peris, K. Dermatoscopy of basal cell carcinoma: Morphologic variability of global and local features and accuracy of diagnosis. *J. Am. Acad. Dermatol.* **2010**, *62*, 67–75. [CrossRef] [PubMed]

15. Lenoir, C.; Diet, G.; Cinotti, E.; Tognetti, L.; Orte Cano, C.; Rocq, L.; Trepant, A.L.; Monnier, J.; Perez-Anker, J.; Rubegni, P.; et al. Line-field confocal optical coherence tomography of sebaceous hyperplasia: A case series. *J. Eur. Acad. Dermatol. Venereol.* **2021**, *35*, e509–e511. [CrossRef] [PubMed]
16. Verzi, A.E.; Micali, G.; Lacarrubba, F. Line-field confocal optical coherence tomography in molluscum contagiosum: A case series. *J. Eur. Acad. Dermatol. Venereol.* **2021**, *35*, e934–e936. [CrossRef] [PubMed]

4.2 Paper 2

Published in:

Ruini C, Schuh S, Gust C, Kendziora B, Frommherz L, French LE, Hartmann D, Welzel J, Sattler E. Line-field optical coherence tomography: in vivo diagnosis of basal cell carcinoma subtypes compared with histopathology. Clin Exp Dermatol. 2021 Dec;46(8):1471-1481. doi: 10.1111/ced.14762. Epub 2021 Sep 24.

Original article

CED
Clinical and Experimental Dermatology

Line-field optical coherence tomography: *in vivo* diagnosis of basal cell carcinoma subtypes compared with histopathology

C. Ruini,[1,2] S. Schuh,[3] C. Gust,[1] B. Kendziora,[1] L. Frommherz,[1] L. E. French,[1,4] D. Hartmann,[1] J. Welzel[3] and E. Sattler[1]

[1]*Department of Dermatology and Allergy, University Hospital, LMU, Munich, Germany;* [2]*PhD School in Clinical and Experimental Medicine, University of Modena and Reggio Emilia, Italy;* [3]*Department of Dermatology and Allergy, University Hospital, Augsburg, Germany; and* [4]*Dr Phillip Frost Department of Dermatology and Cutaneous Surgery, University of Miami, Miller School of Medicine, Miami, FL, USA*

doi:10.1111/ced.14762

Summary

Background. Basal cell carcinoma (BCC) is the most common skin cancer in the general population. Treatments vary from Mohs surgery to topical therapy, depending on the subtype. Dermoscopy, reflectance confocal microscopy (RCM) and optical coherence tomography (OCT) have gained a foothold in daily clinical practice to optimize diagnosis and subtype-oriented treatment. The new technique of line-field confocal OCT (LC-OCT) allows imaging at high resolution and depth, but its use has not yet been investigated in larger studies.

Aim. To evaluate the main LC-OCT criteria for the diagnosis and subtyping of BCC compared with histopathology, OCT and RCM.

Methods. In total, 52 histopathologically confirmed BCCs were evaluated for imaging criteria. Their frequency, predictive values and ROC curves were calculated. A multinominal regression with stepwise variables selection to distinguish BCC subtypes was performed.

Results. Nodular BCCs were mainly characterized by atypical keratinocytes, altered dermoepidermal junction (DEJ), tumour nests in the dermis, dark clefting, prominent vascularization and white hyper-reflective stroma. Superficial BCCs showed a thickening of the epidermis due to a series of tumour lobules with clear connection to the DEJ (string of pearls pattern). Infiltrative BCCs were characterized by elongated hyporeflective tumour strands, surrounded by bright collagen (shoal of fish pattern). The overall BCC subtype agreement between LC-OCT and conventional histology was 90.4% (95% CI 79.0–96.8).

Conclusion. LC-OCT allows noninvasive, real-time identification of BCCs and their subtypes in vertical, horizontal and three-dimension mode compared with histology, RCM and OCT. Further larger studies are needed to better explore the clinical applications of this promising device.

Introduction

Basal cell carcinoma (BCC) is the most commonly occurring type of skin cancer in the general population. Because advanced tumours can be locally destructive and disfiguring, early detection and treatment are essential to limit destructive surgical procedures and their complications, economic burden and patient discomfort.[1] In a real-life setting, clinical and dermoscopic examination helps with identification of

Correspondence: Dr Cristel Ruini, Department of Dermatology and Allergy, University Hospital, LMU Munich, Frauenlobstr. 9-11, Munich, 80337, Germany
E-mail: cristel.ruini@med.uni-muenchen.de

Conflict of interest: the authors declare that they have no conflicts of interest.

JW and ES contributed equally to this work and should be considered joint senior authors.

Accepted for publication 25 May 2021

lesions suspicious for BCC. Patients with such lesions may then proceed to diagnostic or therapeutic procedures. Histology is accepted as the gold-standard assessment tool for BCC subtyping, which then directly guides the treatment offered to patients.[1] As biopsies are expensive and time-consuming and carry additional risks, noninvasive diagnostic methods have gained a foothold in daily clinical practice.[2] Among these, reflectance confocal microscopy (RCM), conventional and high-definition optical coherence tomography (OCT) and multiphoton microscopy have been used to increase diagnostic accuracy and to allow noninvasive BCC subtyping.[3–9] The main imaging criteria for diagnosing BCCs have been described in numerous studies as having diagnostic sensitivity and specificity values > 90%.[9–11]

Nevertheless, such technologies have minor disadvantages. Although RCM has a high resolution (horizontal < 1.25 μm, vertical < 5.0 μm), its penetration depth of 200–250 μm only reaches the superficial dermis. By contrast, OCT has a penetration depth of up to 1.5 mm, but its resolution is only about 7.5 μm (lateral) to 5 μm (axial).

The new technique of line-field confocal OCT (LC-OCT) allows the simultaneous display of horizontal and vertical images with both cellular resolution (axial 1.1 μm, lateral 1.3 μm) and a detection depth ($\sim$500 μm) that reaches to the mid-dermis. Healthy skin, various skin tumours and mite infestations have all been investigated by LC-OCT in pilot studies.[1–18] Moreover, a recently published study[18] described the main morphological criteria for BCC subtypes in LC-OCT. The aim of the current work was to evaluate the advantages and limitations of LC-OCT in the diagnosis of BCC and in the differentiation of BCC subtypes validated by histopathology in a clinical setting. A secondary aim was to compare a subgroup of LC-OCT BCC images with corresponding RCM and OCT images of the same lesion, focusing on diagnostic confidence.

Methods

The study protocol was reviewed and approved by the institutional review board of LMU Munich (approval no. 17-699) and written informed consent was obtained from all participants.

Study population

Patients were prospectively recruited and evaluated for the main imaging criteria in the context of a global study on pigmented and nonpigmented lesions examined with LC-OCT. We later included in the statistical analysis only previously untreated cases that had been completely excised after image review and confirmed as BCCs by subsequent histopathological examination and complete excision: 25 nodular (n)BCCs, 11 superficial (s)BCCs, 5 infiltrative (i)BCCs and 11 nodular–superficial (ns)BCCs. Four of the five iBCCs also included minor nodular components, but were clustered as infiltrative based on their predominant appearance. The nsBCCs had a homogeneous distribution of both components.

Images

Clinical, dermoscopic and LC-OCT images [horizontal, vertical, three-dimensional (3D) mode] were collected in all cases. Additionally and depending on patient consent. OCT images in horizontal (*en face*) view (6 × 6 mm in 31 cases: 13 nBCCs, 9 sBCCs, 2 iBCCs and 7 mBCCs) and RCM multiple Vivastacks (500 × 500 μm) and Vivablocks (5 × 5 mm) images (22 cases: 9 nBCCs, 4 sBCCs, 1 iBCC and 7 nsBCCs). In each case, the whole tumour area was scanned. Images were evaluated by four trained dermatologists (CR, SS, LF, ES) and agreement reached by consensus. Discordant cases were discussed with two dermatologists (DH, JW) who are experts in dermatopathology. Histopathological slides were analysed by the senior pathologist of each centre.

Imaging devices

The LC-OCT system (DAMAE Medical, Paris, France) is classified as a class 1 supercontinuum laser, and uses a central wavelength of 800 nm. Combining the principle of OCT interferometry with the spatial filtering of RCM, the device collects multiple A-scans parallel to the skin surface to a depth of $\sim$500 μm, while constantly adjusting its focus. It has three imaging modalities displayed as a grey scale: vertical or *en coupe*, horizontal or *en face* and 3D stack for a 3D reconstruction, with a vertical and horizontal field of view of 1.2 × 0.5 mm^2. Details have been described in previous studies.[14,17,19–21] Conventional OCT images were acquired with Vivosight (Michelson Diagnostics Ltd, Maidstone, Kent, UK), RCM images with Vivascope 1500 (Mavig GmbH, Munich, Germany) and clinical–dermoscopic images with Fotofinder (FotoFinder GmbH, Berlin, Germany) and Dermogenius 2 (Dermoscan GmbH, Regensberg, Germany).

Imaging features

The main diagnostic patterns were selected based on previous publications. The dermoscopic features are described in Table 1. For LC-OCT, a selection of criteria based on histological diagnostic features and previously described OCT and RCM terminology was developed (Table 1).[22–25] In addition, image quality and confidence with diagnosis and subtype were reported semiquantitatively (low < 50%, average 50–75%, high > 75%).

Statistical analysis

For descriptive statistics, mean ± SD were calculated for numerical variables, while absolute numbers with percentage values were used for nominal variables. To evaluate the diagnostic accuracy of LC-OCT in detecting different BCC subtypes, the sensitivity, specificity, positive predictive value (PPV), negative predictive value (NPV), and area under the curve of the receiver-operating characteristic curve were calculated. Dermatopathology was considered the gold standard. Multinomial regression with stepwise selection of variables was used to search for LC-OCT characteristics that would differentiate between BCC subtypes. Variables without explanatory value as measured by the Akaike information criterion were excluded by bidirectional elimination. All statistics were performed in *R* software (V3.6.0, 2; *R* Foundation for Statistical Computing, Vienna, Austria). $P < 0.05$ was considered statistically significant.

Results

Epidemiology

In total, 52 patients (35 men, 17 women, mean age 71 years) with Fitzpatrick skin phototypes I–III with

Table 1 Main line-field confocal optical coherence tomography in detecting different basal cell carcinoma subtypes evaluated in the study with their relative and absolute frequencies.

	BCC subtype									
	All		Nodular		Superficial		Infiltrative		Nodular–superficial	
Orientation	%	*n/N*	%	*n/N*	%	*n/N*	%	*n/N*	%	*n/N*
En coupe (vertical)										
Epidermis										
Hyperkeratosis	32.7	17/52	32.0	8/25	9.1	1/11	60.0	3/5	45.5	5/11
Thinning	46.2	24/52	44.0	11/25	36.4	4/11	40.0	2/5	63.6	7/11
Scales	26.9	14/52	24.0	6/25	27.3	3/11	40.0	2/5	27.3	3/11
Keratin plugs	5.8	3/52	8.0	2/25	0	0/11	0	0/5	9.1	1/11
Ulceration	21.2	11/52	16.0	4/25	18.2	2/11	20.0	1/5	36.4	4/11
Atypical keratinocytes	76.9	40/52	68.0	17/25	81.8	9/11	0	0/5	100.0	11/11
DEJ and dermis										
Alteration of the DEJ profile	98.1	51/52	96.0	24/25	100.0	11/11	100.0	5/5	100.0	11/11
Tumour nests/lobules	98.1	51/52	100.0	25/25	100.0	11/11	80.0	4/5	100.0	11/11
Clefting	96.2	50/52	100.0	25/25	90.9	10/11	80.0	4/5	100.0	11/11
Prominent vessels/neoangiogenesis	96.2	50/52	92.0	23/25	100.0	11/11	100.0	5/5	100.0	11/11
Bright structures	42.3	22/52	56.0	14/25	18.2	2/11	20.0	1/5	45.5	5/11
Shoal of fish pattern	13.5	7/52	4.0	1/25	0	0/11	100.0	5/5	9.1	1/11
String of pearls pattern	42.3	22/52	12.0	3/25	90.9	10/11	20.0	1/5	72.7	8/11
White hyper-reflective stroma	94.2	49/52	92.0	23/25	90.9	10/11	100.0	5/5	100.0	11/11
Black areas/cysts	19.2	10/52	12.0	3/25	18.2	2/11	40.0	2/5	27.3	3/11
Cell polarization	67.3	35/52	64.0	16/25	72.7	8/11	80.0	4/5	63.6	7/11
En face (horizontal)										
Atypical honeycomb	76.9	40/52	68.0	17/25	81.8	9/11	0	0/5	100.0	11/11
Clefting	53.8	28/52	60.0	15/25	45.5	5/11	40.0	2/5	54.5	6/11
Cord-like structures	11.5	6/52	8.0	2/25	36.4	4/11	0	0/5	0	0/11
Dark silhouettes	46.2	24/52	40.0	10/25	63.6	7/11	60.0	3/5	36.4	4/11
Tumour nests/lobules	65.5	33/52	72.0	18/25	36.4	4/11	60.0	3/5	72.7	8/11
Canalicular vessels	71.2	37/52	76.0	19/25	72.7	8/11	80.0	4/5	54.5	6/11
Collagen alterations	98.1	51/52	100.0	25/25	90.9	10/11	100.0	5/5	100.0	11/11

BCC, basal cell carcinoma; DEJ, dermoepidermal junction.

histologically confirmed BCCs were enrolled in the study. Most BCCs arose in the head and neck area (51.9%), followed by the trunk (34.6%) and limbs (13.5%).

Diagnostic confidence

Diagnostic confidence for BCC subtype (high, average and low, respectively) was 44.2%, 42,3% and 13.5% for dermoscopy, and 78.8%, 15.4% and 5.8% for LC-OCT. LC-OCT increased the examiners' diagnostic confidence by 36.5%. Diagnostic confidence (high and average, respectively) was 68% and 24% for OCT, and 44% and 31.5% for RCM was: high. LC-OCT image quality was high in 75% of cases and average in the remaining 25%.

Imaging features

The main dermoscopic features are shown in Table S1, and the main overall LC-OCT features of BCCs are shown in Table 1.

In vertical mode, nBCCs were mainly characterized by atypical keratinocytes in the epidermis above them (68%), an altered dermoepidermal junction (DEJ) profile as determined by connected or underlying tumour lobules (96%), tumour nests/lobules in the dermis (100%), dark clefting (100%), prominent vessels (92%) and white hyper-reflective stroma (92%). In horizontal mode, an atypical honeycomb pattern (68%), tumour nests/lobules (72%), dark silhouettes (40%) and collagen alterations (100%) were seen (Figs 1 and 2; Fig. S1, Video S1, Table 1).

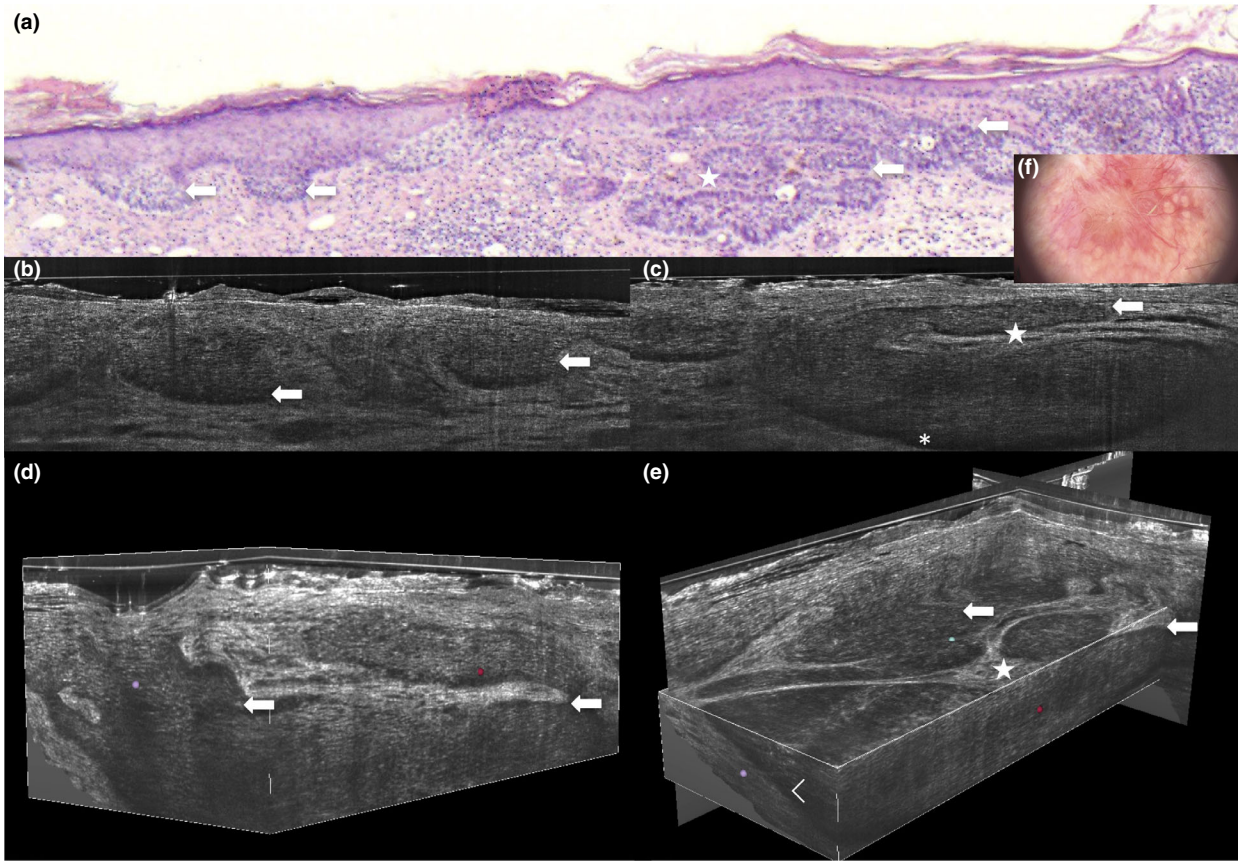

Figure 1 (a–f) Appearance of a nodular–superficial basal cell carcinoma of the face in a 60-year-old man as visualized by (a) conventional microscopy (haematoxylin and eosin, original magnification × 100), (b–e) line-field confocal optical coherence tomography in (b, c) vertical and (d, e) three-dimensional mode, and (f) dermoscopy (original magnification × 10). Note the hyporeflective ovoid structures arranged in a string of pearls pattern (arrow), together with the beginning of nodular components (arrow), which have lost their connection to the epidermis, separated by a discrete stromal reaction (star).

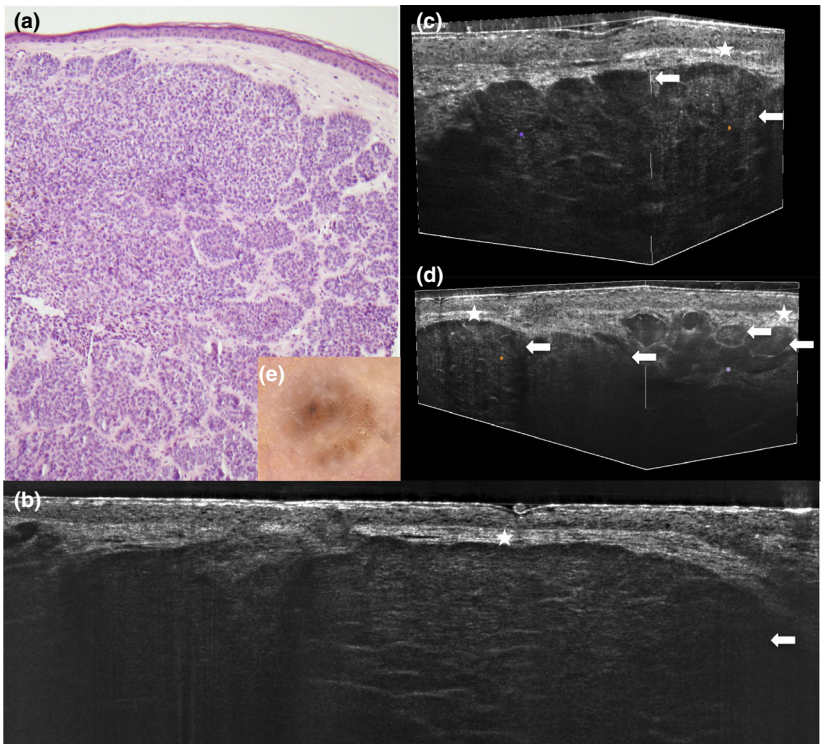

Figure 2 (a–e) Appearance of a nodular–micronodular basal cell carcinoma of the face in a 75-year-old woman, as visualized by (a) conventional microscopy (haematoxylin and eosin, original magnification × 140); (b–d) line-field confocal optical coherence tomography in (b) vertical and (c, d) three-dimensional mode, and (e) dermoscopy (original magnification × 10). Note the hyporeflective ovoid structures/lobules of different sizes in the dermis (arrow), pushing towards the thinned epidermis and surrounded by stromal reaction (star).

For sBCCs, atypical keratinocytes were noticed in 81.1% of cases, while an altered DEJ profile, tumour nests/lobules, white hyper-reflective stroma and prominent vessels were seen in 100% of cases. Cell polarization was seen in 72.7% of cases, and the 'string of pearls' pattern in 90.9% (Figs 1 and 3, Figs S1 and S3).

By contrast, the infiltrative subtypes were characterized by the so-called 'shoal of fish' pattern (100%) (Fig. 4). Mixed subtypes equally displayed the 'string of pearls' patterns as well as deeper ovoid tumour nests/lobules with no connection to the epidermis.

Agreement

The overall BCC subtype agreement between LC-OCT and conventional histology was 90.4% (95% CI 79.0–96.8), compared with 84% for OCT and 62.5% for RCM.

The sensitivity, specificity, PPV and NPV values of LC-OCT for different BCC subtypes are shown in Table 2, with ROC curves in Fig. 5. Multinomial regression with stepwise selection of variables identified the following features as most useful in distinguishing BCC subtypes: epidermal thinning, atypical honeycomb pattern, prominent vessels/neoangiogenesis, shoal of fish pattern, string of pearls pattern and white hyper-reflective stroma. Bidirectional elimination excluded (*en face*) tumour nests and (*en face*) clefting (Tables S2 and S3).

Discussion

In vivo BCC morphology has been widely characterized using, among others, the techniques of RCM and OCT. Longo *et al.* developed an RCM algorithm for differentiating BCC subtypes, with the key criteria being cord-like structures for sBCCs, large tumour nests and clefting for nBCCs, and dark silhouettes and abundant bright compact collagen for iBCCs.[10] Conventional OCT has been used for the noninvasive characterization of BCCs,[2,26–28] and the specific features identified were hyporeflective ovoid structures originating from the stratum basale/DEJ,

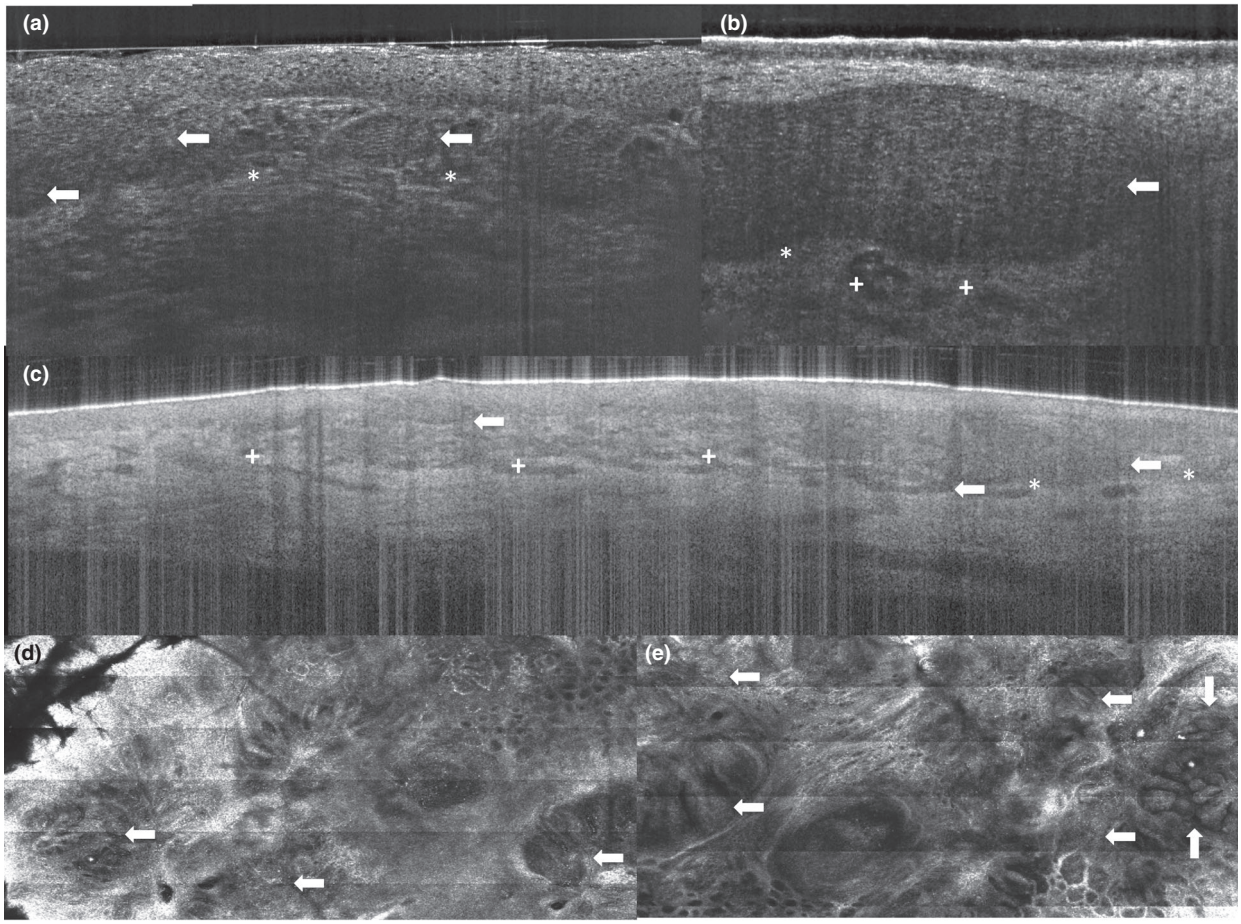

Figure 3 (a–e) Superficial basal cell carcinoma of the leg in a 54-year-old woman as visualized by (a, b) line-field confocal optical coherence tomography in vertical mode, (c) optical coherence tomography and (d,e) Vivastack reflectance confocal microscopy. Note the hyporeflective ovoid structures or tumour nests/lobules of different sizes in the dermis arranged in a string of pearls pattern (arrow), surrounded by stromal reaction (star) and dilated vessels (+).

corresponding to tumour nests, either with contact to the DEJ (string of pearls pattern) in sBCCs, or separated from the DEJ in nBCCs; and a dark rim, white hyper-reflective stroma, cysts and shoal of fish structures in iBCCs.[11] Dedicated Cochrane reviews have confirmed a role for both RCM and OCT in the diagnosis of clinically challenging BCCs.[9,12] In a pilot study, a combination of OCT and RCM showed good correlation to key histopathological features of infiltrative BCCs.[29]

LC-OCT can be seen as a method for combining the aforementioned diagnostic tools. LC-OCT images can be intuitively evaluated by physicians trained in non-invasive diagnostic technologies and with at least basic knowledge of skin histopathology. In fact, vertical (*en coupe*) scans are directly comparable to OCT images and histology, while horizontal (*en face*) scans can be related to RCM and dermoscopy. Preliminary studies conducted with available LC-OCT prototypes reported good correlations with histopathology in pilot settings.[14,30] However, there is a lack of systematic studies on large numbers of cases, with only one very recent study analysing 66 BCCs of pure histological subtypes.[18] Suppa *et al.* described lobules, blood vessels and small bright cells within epidermis as the most common criteria for BCCs. They also associated hemispheric lobules, connection with the epidermis and absence of stretching of the stroma with sBCCs; macrolobules, absence of connection to the epidermis with nBCCs; and branched lobules with iBCCs.[18] We observed similar features, but we have described our nomenclature based on the standard histological patterns, known RCM criteria for cytology and known OCT criteria for morphology.

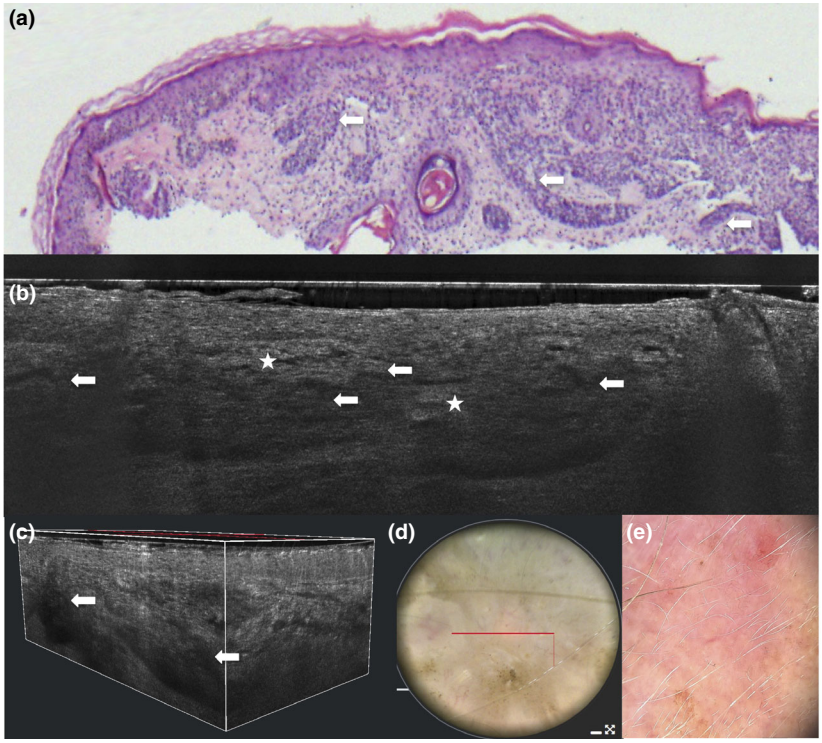

Figure 4 (a–e) Infiltrative basal cell carcinoma of the face in a 60-year-old man as visualized by (a) conventional microscopy (haematoxylin and eosin, original magnification × 40), (b, c) line-field confocal optical coherence tomography in (b) vertical and (c) three-dimensional mode, (d) clinical examination and (e) dermoscopy (original magnification × 10). Note the bizarrely configured, hyporeflective, branched strands arranged in a shoal of fish pattern (arrow), separated by a discrete stromal reaction (star).

The most intuitive BCC feature in our analysis is the tumour nest/lobule, which corresponds to its histological counterpart. Dark peritumoral clefting corresponding to mucin clearly delimitates the nests, which are surrounded by a bright collagenic stromal reaction in most cases.

Compared with conventional OCT, LC-OCT provides a higher resolution, which allows visualization of cellular components. In particular, larger cells, such as keratinocytes and activated melanocytes, can be clearly seen. In BCCs, slightly atypical keratinocytes in the epidermis and atypical cells in the tumour/lobules (described as cells of different sizes, shapes and contours) are visible. The cells in the tumour nests/lobules are hyporeflective with a hyper-reflective border and can either be polarized in overlapping strands or sometimes occur in a classic peripheral palisading. Analogously, pigmented BCCs sometimes show more hyperreflective components, possibly corresponding to melanocytes infiltrating the BCC, or to melanophages or pigmented keratinocytes, in line with previous experience with RCM and OCT.

The alteration of the DEJ seen in RCM and OCT becomes an alteration of the DEJ profile in LC-OCT compared with healthy skin, as tumour nests/lobules appear to be either connected to the epidermis (in sBCCs) or pushing it upwards (in nBCCs).

In our experience, nBCCs are extremely well characterized with ovoid nests/lobules in the dermis, pushing against the DEJ and causing a thinning of the epidermal layers. Micronodular tumours were also distinguishable by their smaller lobular components. Sometimes, dark holes were seen inside the nests, probably due to cysts and/or necrosis.

In the case of sBCCs, the tumour nests/lobules, which were slightly elongated, were clearly identifiable as a series of small ovoid nests/lobules connected with the DEJ and with each other through streamlined cords (string of pearls pattern). In contrast to conventional OCT, however, the epidermis does not appear irregularly thickened, but can be mostly distinguished from the tumour lobules connected to it.

Infiltrative tumours are usually more difficult to diagnose, as they do not have well-defined roundish

Table 2 Diagnostic accuracy of line-field confocal optical coherence tomography in detecting different basal cell carcinoma subtypes.

BCC type	Point estimates (95% CI)
Nodular	
Apparent prevalence	0.48 (0.34–0.62)
True prevalence	0.48 (0.34–0.62)
Sensitivity	0.96 (0.80–1.00)
Specificity	0.96 (0.81–1.00)
Positive predictive value	0.96 (0.80–1.00)
Negative predictive value	0.96 (0.81–1.00)
Positive likelihood ratio	25.92 (3.78–177.68)
Negative likelihood ratio	0.04 (0.01–0.28)
Kappa	0.92 (0.82–1.00)
AUC	0.96 (0.91–1.00)
Superficial	
Apparent prevalence	0.17 (0.08–0.30)
True prevalence	0.21 (0.11–0.35)
Sensitivity	0.82 (0.48–0.98)
Specificity	1.00 (0.91–1.00)
Positive predictive value	1.00 (0.66–1.00)
Negative predictive value	0.95 (0.84–0.99)
Positive likelihood ratio	Inf (NaN–Inf)
Negative likelihood ratio	0.18 (0.05–0.64)
Kappa	0.88 (0.71–1.00)
AUC	0.98 (0.95–1.00)
Infiltrative BCCs	
Apparent prevalence	0.12 (0.04–0.23)
True prevalence	0.10 (0.03–0.21)
Sensitivity	1.00 (0.48–1.00)
Specificity	0.98 (0.89–1.00)
Positive predictive value	0.83 (0.36–1.00)
Negative predictive value	1.00 (0.92–1.00)
Positive likelihood ratio	47.00 (6.76–326.73)
Negative likelihood ratio	0.00 (0.00–NaN)
Kappa	0.90 (0.70–1.00)
AUC	0.92 (0.75–1.00)
Nodular–superficial BCCs	
Apparent prevalence	0.23 (0.13–0.37)
True prevalence	0.21 (0.11–0.35)
Sensitivity	0.91 (0.59–1.00)
Specificity	0.95 (0.83–0.99)
Positive predictive value	0.83 (0.52–0.98)
Negative predictive value	0.97 (0.87–1.00)
Positive likelihood ratio	18.64 (4.76–72.94)
Negative likelihood ratio	0.10 (0.01–0.62)
Kappa	0.83 (0.65–1.00)
AUC	0.90 (0.79–1.00)

AUC, area under the curve; Inf, infimum; NaN, not a number (undefined).

nests but rather elongated, slightly hyporeflective strands/branched lobules, surrounded by a bright collagen reaction. This feature defines the 'shoal of fish' pattern, also visible in OCT.

BCC subtyping is crucial for choosing an appropriate therapy, while superficial and thin nodular BCCs can

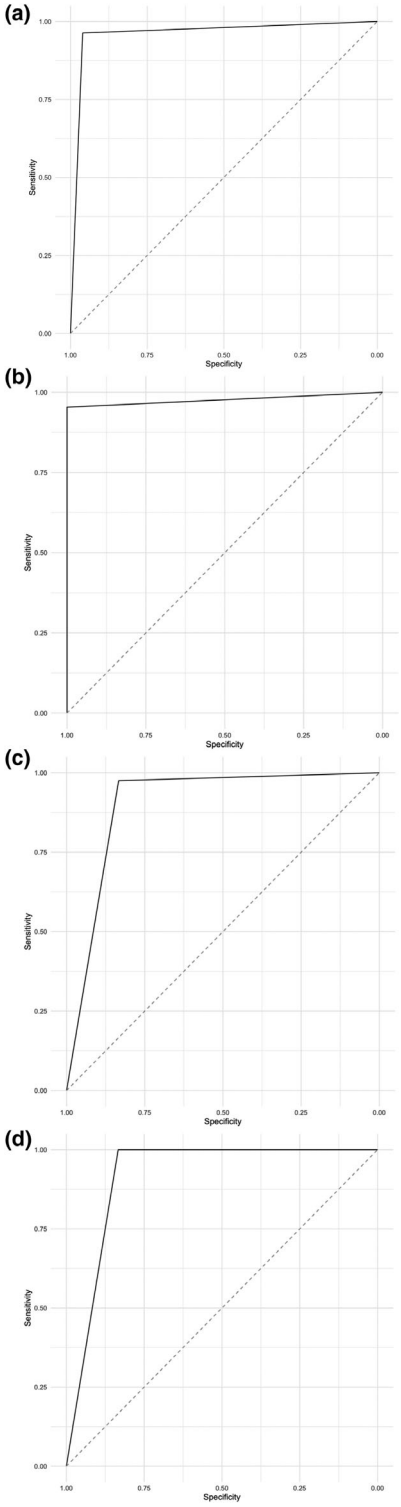

Figure 5 Receiver-operating characteristic curves: (a) nodular basal cell carcinoma (BCC), (b) superficial BCC, (c) infiltrative BCC and (d) nodular–superficial BCC.

be treated with local therapy options, thick nodular and infiltrative BCCs should be excised with (Mohs) surgery. Up to 40% of BCCs in daily clinical practice are of mixed subtype, and a normal punch biopsy is often too small to ensure complete lesion sampling.[31]

In vivo mapping with LC-OCT is able to scan the whole lesion and is able to identify the individual components of mixed tumours, providing an advantage compared with standard punch biopsies.

In our analysis, one case of superficial BCC was wrongly evaluated as nodular–superficial, probably due to numerous sebaceous glands acting as confounders; such entities appear as roundish hyporeflective structures with hyper-reflective borders, usually containing lobules of large (sebaceous) cells. To avoid confounding, we suggest combined evaluation of vertical and horizontal images, as sebaceous glands and sebaceous hyperplasia appear in horizontal mode as sharply demarcated, concentric, roundish structures in continuity with hair follicles, in contrast to BCC tumour nests.

In LC-OCT horizontal sections, the following BCC patterns were found: an atypical honeycomb pattern defined by polygonal bright keratinocytes of different sizes, shapes and contours; canalicular blood vessels; bright collagen stromal reaction/elastosis; and ovoid hyporeflective tumour nests with dark clefting and palisading. In our experience, these characteristics appeared less well defined than with RCM.

In our opinion, the main advantages of LC-OCT are the nearly cellular resolution and the good penetration depth reaching the dermis, combined with the instant switch from vertical to horizontal mode, the user-friendly software and the fast camera-guided image acquisition in three dimensions, which allows navigation of the whole tumour.

Nevertheless, some limitations exist. For example, distinguishing between nBCCs and sBCCs can sometimes be difficult, the tight connection of the tumour islands to the DEJ might be overlooked. In addition, some deep nodular components might not be visualized because of limits to the penetration depth of LC-OCT (which is less than conventional OCT), so that the possibility of missing deeper nodular components exists. For the same reason, determination of BCC thickness of the BCC is limited with LC-OCT compared with conventional OCT, as it is with RCM. Infiltrative BCCs require caution, as elongated tumour strands can sometimes be misinterpreted as blood vessels by nonexpert observers. Some significant differential diagnoses, for example with melanocytic tumours, are more difficult using LC-OCT compared with RCM because of the slightly lower resolution of the LC-OCT device. All the cited technologies can encounter limits in scanning difficult-to-reach anatomical areas, such as the inner eyelids. In doubtful cases, short-term follow-up or a biopsy should be performed.

This work was limited by the smaller number of iBCCs and RCM/OCT acquisitions. Moreover, the multiple but small Vivastacks images for mapping the whole tumour area might be responsible for the lower diagnostic confidence attributed to RCM. A larger, systematic comparison study should be conducted to further analyse the advantages and pitfalls of the different technologies.

Conclusion

Our study describes the most common LC-OCT features of BCCs compared with histological findings, and shows that the device provides significant additional morphological details compared with naked eye examination and dermoscopy for diagnosing BCCs and their histological subtypes. This could have important practical consequences as it allows the clinician to immediately assign the correct treatment for the patient. Similar to other, already established, noninvasive diagnostic methods, LC-OCT is quick, painless and intuitively comparable to histology following dedicated training.

Acknowledgement

We thank DAMAE Medical for providing the LC-OCT device used for this study.

What's already known about this topic?

- The novel imaging technique of LC-OCT has been shown in small case series to be able to noninvasively characterize healthy skin and potentially nonmelanoma skin cancer, as a result of its good resolution and penetration depth.
- There is to date just one systematic study defining the LC-OCT diagnostic criteria for BCC.

What does this study add?

- LC-OCT is useful for the *in vivo* diagnosis and characterization of BCC subtypes with high sensitivity and specificity compared with histology.
- The comparison with other imaging technologies shows the advantages and limitations of this new imaging method.

References

1 Peris K, Fargnoli MC, Garbe C *et al*. Diagnosis and treatment of basal cell carcinoma: European consensus-based interdisciplinary guidelines. *Eur J Cancer* 2019; **118**: 10–34.

2 Nori S, Rius-Díaz F, Cuevas J *et al*. Sensitivity and specificity of reflectance-mode confocal microscopy for in vivo diagnosis of basal cell carcinoma: a multicenter study. *J Am Acad Dermatol* 2004; **51**: 923–30.

3 Garbarino F, Migliorati S, Farnetani F *et al*. Nodular skin lesions: correlation of reflectance confocal microscopy and optical coherence tomography features. *J Eur Acad Dermatol Venereol* 2020; **34**: 101–11.

4 Manfredini M, Arginelli F, Dunsby C *et al*. High-resolution imaging of basal cell carcinoma: a comparison between multiphoton microscopy with fluorescence lifetime imaging and reflectance confocal microscopy. *Skin Res Technol* 2013; **19**: e433–43.

5 Paganelli A, Garbarino F, Ciardo S *et al*. Disguised basal cell carcinomas: how to track them down with reflectance confocal microscopy. *J Eur Acad Dermatol Venereol* 2020; **34**: e68–70.

6 Peccerillo F, Mandel V, Di Tullio F *et al*. Lesions mimicking melanoma at dermoscopy confirmed basal cell carcinoma: evaluation with reflectance confocal microscopy. *Dermatology* 2019; **235**: 35–44.

7 Ulrich M, Themstrup L, de Carvalho N *et al*. Dynamic optical coherence tomography in dermatology. *Dermatology* 2016; **232**: 298–311.

8 Boone M, Suppa M, Pellacani G *et al*. High-definition optical coherence tomography algorithm for discrimination of basal cell carcinoma from clinical BCC imitators and differentiation between common subtypes. *J Eur Acad Dermatol Venereol* 2015; **29**: 1771–80.

9 Dinnes J, Deeks JJ, Chuchu N *et al*. Reflectance confocal microscopy for diagnosing keratinocyte skin cancers in adults. *Cochrane Database Syst Rev* 2018; (12): CD013191.

10 Longo C, Lallas A, Kyrgidis A *et al*. Classifying distinct basal cell carcinoma subtype by means of dermatoscopy and reflectance confocal microscopy. *J Am Acad Dermatol* 2014; **71**: 716–24.e1.

11 Sinx KAE, van Loo E, Tonk EHJ *et al*. Optical coherence tomography for noninvasive diagnosis and subtyping of basal cell carcinoma: a prospective cohort study. *J Invest Dermatol* 2020; **140**: 1962–7.

12 Ferrante di Ruffano L, Dinnes J, Deeks JJ *et al*. Optical coherence tomography for diagnosing skin cancer in adults. *Cochrane Database Syst Rev* 2018; (12): CD013189.

13 Pedrazzani M, Breugnot J, Rouaud-Tinguely P *et al*. Comparison of line-field confocal optical coherence tomography images with histological sections: validation of a new method for in vivo and non-invasive quantification of superficial dermis thickness. *Skin Res Technol* 2020; **26**: 398–404.

14 Ruini C, Sattler E. Konfokale Line-Field-OCT: die eierlegende Wollmilchsau? [Line-field confocal optical coherence tomography: the golden goose?] (in German). *Aktuelle Dermatol*. 2020; **46**: 148–51.

15 Monnier J, Tognetti L, Miyamoto M *et al*. In vivo characterization of healthy human skin with a novel, non-invasive imaging technique: line-field confocal optical coherence tomography. *J Eur Acad Dermatol Venereol* 2020; **34**: 2914–21.

16 Ruini C, Schuh S, Pellacani G *et al*. In vivo imaging of *Sarcoptes scabiei* infestation using line-field confocal optical coherence tomography. *J Eur Acad Dermatol Venereol* 2020; **34**: e808–9.

17 Ruini C, Schuh S, Sattler E, Welzel J. Line-field confocal optical coherence tomography – practical applications in dermatology and comparison with established imaging methods. *Skin Res Technol* 2021; **27**: 340–52.

18 Suppa M, Fontaine M, Dejonckheere G *et al*. Line-field confocal optical coherence tomography of basal cell carcinoma: a descriptive study. *J Eur Acad Dermatol Venereol* 2020; **27**: 340–52.

19 Ogien J, Levecq O, Azimani H, Dubois A. Dual-mode line-field confocal optical coherence tomography for ultrahigh-resolution vertical and horizontal section imaging of human skin in vivo. *Biomed Opt Express* 2020; **11**: 1327.

20 Dubois A, Levecq O, Azimani H *et al*. Line-field confocal time-domain optical coherence tomography with dynamic focusing. *Opt Express* 2018; **26**: 33534–42.

21 Ogien J, Daures A, Cazalas M *et al*. Line-field confocal optical coherence tomography for three-dimensional skin imaging. *Front Optoelectron* 2020; **13**: 381–92.

22 Holmes J, von Braunmühl T, Berking C *et al*. Optical coherence tomography of basal cell carcinoma: influence of location, subtype, observer variability and image quality on diagnostic performance. *Br J Dermatol* 2018; **178**: 1102–10.

23 Themstrup L, De Carvalho N, Nielsen SM *et al*. In vivo differentiation of common basal cell carcinoma subtypes by microvascular and structural imaging using dynamic optical coherence tomography. *Exp Dermatol* 2018; **27**: 156–65.

24 De Carvalho N, Schuh S, Kindermann N *et al*. Optical coherence tomography for margin definition of basal cell carcinoma before micrographic surgery-recommendations regarding the marking and scanning technique. *Skin Res Technol* 2018; **24**: 145–51.

25 Welzel J, Schuh S. [Non-invasive diagnostics in dermatology] (in German). *J Dtsch Dermatol Ges* 2017; **15**: 999–1017.

26 Olsen J, Themstrup L, De Carvalho N *et al*. Diagnostic accuracy of optical coherence tomography in actinic keratosis and basal cell carcinoma. *Photodiagnosis Photodyn Ther* 2016; **16**: 44–9.

27 Ulrich M, Braunmuehl T, Kurzen H *et al*. The sensitivity and specificity of optical coherence tomography for the

assisted diagnosis of nonpigmented basal cell carcinoma: an observational study. *Br J Dermatol* 2015; **173**: 428–35.
28 Schuh S, Kaestle R, Sattler EC, Welzel J. Optical coherence tomography of actinic keratoses and basal cell carcinomas – differentiation by quantification of signal intensity and layer thickness. *J Eur Acad Dermatol Venereol* 2016; **30**: 1321–6.
29 Gill M, Sahu A, Alessi-Fox C *et al*. Angulated small nests and cords: key diagnostic histologic features of infiltrative basal cell carcinoma can be identified using integrated reflectance confocal microscopy-optical coherence tomography. *J Cutan Pathol* 2020; **48**: 53–65.
30 Dubois A, Levecq O, Azimani H *et al*. Line-field confocal optical coherence tomography for high-resolution noninvasive imaging of skin tumors. *J Biomed Opt* 2018; **23**: 1–9.
31 Cohen PR, Schulze KE, Nelson BR. Basal cell carcinoma with mixed histology: a possible pathogenesis for recurrent skin cancer. *Dermatol Surg* 2006; **32**: 542–51.

Supporting Information

Additional Supporting Information may be found in the online version of this article:

Figure S1. (a–d) Nodular basal cell carcinoma on the face of a 75-year-old woman as visualized under (a,b) line-field confocal optical coherence tomography in (a) vertical and (b) horizontal mode, (c) optical coherence tomography and (d) Vivastack reflectance confocal microscopy. Note the hyporeflective ovoid structures/lobules of different size in the dermis (arrow), surrounded by stromal reaction (*).

Figure S2. (a–d) Superficial basal cell carcinoma on the back of a 47-year-old man as visualized under (a) conventional microscopy (haematoxylin and eosin, original magnification × 100), (b) line-field confocal optical coherence tomography in vertical mode and (c) dermoscopy (original magnification × 10). Note the hyporeflective ovoid structures arranged in a string of pearls pattern (arrow), surrounded by a dark rim corresponding to peripheral clefting (*).

Figure S3. (a–c) Superficial basal cell carcinoma of the leg in a 54-year-old woman as visualized under (a) conventional microscopy (haematoxylin and eosin, original magnification × 100), (b) line-field confocal optical coherence tomography in vertical mode and (c) dermoscopy (original magnification × 10). Note the hyporeflective ovoid structures arranged in a string of pearls pattern (arrow), surrounded by dark rims corresponding to peripheral clefting (*). A hyperkeratotic crust (triangle) overlies the epidermal layer. Additionally, a sebaceous gland (rhombus) is visible.

Table S1. Main dermoscopy features of BCCs evaluated in the study with their relative and absolute frequencies.

Table S2. Multinomial logistic regression with stepwise selection of variables to search for LCOCT characteristics helping in the distinction of BCC subtypes.

Table S3. Final model.

Video S1. Line-field confocal optical coherence tomography three-dimensional acquisition of a pigmented nodular basal cell carcinoma.

5 Appendix

5.1 Paper 3

Published in:

Ruini C, Schuh S, Gust C, Kendziora B, Frommherz L, French LE, Hartmann D, Welzel J, Sattler EC. Line-field confocal optical coherence tomography for the in vivo real-time diagnosis of different stages of keratinocyte skin cancer: a preliminary study. J Eur Acad Dermatol Venereol. 2021 Dec;35(12):2388-2397. doi: 10.1111/jdv.17603. Epub 2021 Sep 24.

DOI: 10.1111/jdv.17603 JEADV

ORIGINAL ARTICLE

Line-field confocal optical coherence tomography for the in vivo real-time diagnosis of different stages of keratinocyte skin cancer: a preliminary study

C. Ruini,[1,2] S. Schuh,[3] C. Gust,[1] B. Kendziora,[1] L. Frommherz,[1] L.E. French,[1,4] D. Hartmann,[1] J. Welzel,[3,*,†] E.C. Sattler[1,†]

[1]Department of Dermatology and Allergy, University Hospital, LMU Munich, Germany
[2]PhD School in Clinical and Experimental Medicine, University of Modena and Reggio Emilia, Modena, Italy
[3]Department of Dermatology and Allergy, University Hospital, Augsburg, Germany
[4]Dr. Phillip Frost Department of Dermatology & Cutaneous Surgery, Miller School of Medicine, University of Miami, Coral Gables, FL, USA
*Correspondence: J. Welzel. E-mail: julia.welzel@uk-augsburg.de

Abstract

Background The treatment of keratinocyte cancers (KC) strictly depends on their differentiation and invasiveness. Non-invasive diagnostic techniques can support the diagnosis in real time, avoiding unnecessary biopsies. This study aimed to preliminarily define main imaging criteria and histological correlations of actinic keratosis (AK), Bowen's disease (BD) and squamous cell carcinoma (SCC) using the novel device line-field confocal optical coherence tomography (LC-OCT).

Methods Dermoscopy and LC-OCT images of 73 histopathologically confirmed lesions (46 AKs, 11 BD and 16 SCCs) were included in the study. Exemplary lesions (10 AKs, 5 BD and 5 SCCs) were additionally investigated with optical coherence tomography and reflectance confocal microscopy.

Results Most common LC-OCT findings of KC in the descriptive statistics were hyperkeratosis/parakeratosis, disruption of stratum corneum, broadened epidermis, basal and suprabasal keratinocyte atypia, dilated vessels/neoangiogenesis and elastosis/collagen alterations. In the univariate multinomial logistic regression, a preserved DEJ was less common in SCC compared with AK and BD, BD displayed marked keratinocyte atypia involving all epidermal layers (bowenoid pattern), while SCC showed ulceration, increased epidermal thickness, keratin plugs, acantholysis, not visible/interrupted DEJ and epidermal bright particles. LC-OCT increased the diagnostic confidence by 24.7% compared with dermoscopy alone.

Conclusions Our study describes for the first time specific LC-OCT features of different stages of KC and their histopathological correlates, focusing on keratinocyte morphology and architecture of the epidermis and DEJ. LC-OCT may open new scenarios in the bedside diagnosis, treatment planning and follow-up of KC.

Received: 19 February 2021; Accepted: 3 August 2021

Conflicts of interest

None declared.

Funding source

The study was partially funded by the FöFoLe Grant 10-22 of the LMU Munich.

Introduction

Keratinocyte skin cancer (KC), from its early stages of actinic keratosis (AK) and Bowen's disease (BD) to invasive squamous cell carcinoma (SCC), belongs to the most common tumours in elderly patients, related to chronic solar damage or immunosuppression.[1]

In order to prevent the transformation from subclinical keratinocyte dysplasia to invasive SCC and to lower the social and economic burden of the disease, early detection and treatment are essential.[2]

The diagnosis of KC is based on clinical and dermoscopical examination, eventually followed by a biopsy.[1] Dermoscopy has a good reported sensitivity and specificity in diagnosing and

†The authors share their senior authorship.
IRB approval status: Reviewed and approved by LMU Munich IRB; approval #17-699.

grading KC, although significantly higher for AKs (51.2%–98%; 95%) rather than SCCs (55%–79%; 84%–87%) and mainly calculated in the context of retrospective studies, so that further prospective studies are needed.[3–11] Non-invasive diagnostic methods such as reflectance confocal microscopy (RCM) and optical coherence tomography (OCT) have been widely used in the diagnosis of AKs[12–16], while few articles analysed the sensitivity and specificity of such tools for invasive SCCs.[14,17] RCM, which displays horizontal sections, allows a detection of characteristic AK patterns with high resolution[10,18]; however, its low penetration depth (up to 200–250 μm) can be a limit in evaluating the DEJ and the infiltration of the dermis in thick lesions. On the contrary, OCT does not permit a clear evaluation of cellular morphology in its vertical sections but is able to detect invasive lesions thanks to its higher penetration depth (up to 1.5 mm), and can display even their vascularity in dynamic mode.[19]

The new device line-field confocal OCT (LC-OCT) creates scans at higher resolution than conventional OCT, while reaching a higher detection depth compared to RCM, and can potentially be used for a non-invasive diagnosis of KC and several other skin diseases.[15,20–27] To date, no systematic studies on this topic have been published, so that we aimed to define main LC-OCT criteria for the diagnosis of KC, based on the histological criteria and the ones already described for similar diagnostic techniques. In addition, we preliminarily compared LC-OCT images with OCT and RCM to exemplarily point out the differences, strengths and limitations of the methods.

Materials and methods

Clinical, dermoscopic (FotoFinder GmbH, Germany and DermoGenius-DermoScan GmbH, Germany) and LC-OCT images of suspected KC were prospectively collected and analysed at the University of Munich and Augsburg. Cases were analysed by three imaging experts blinded to the histological diagnosis in a consensus, with an almost perfect agreement. In discordant cases, three more experts were involved for consensus. Only histopathologically confirmed lesions with a complete image set were included in the analysis. LC-OCT features were defined based on main histological parameters and the nomenclature chosen based on the current histology, OCT and RCM terminology. We chose not to define a novel terminology because LC-OCT allows a very intuitive comparison with the corresponding histological features because of its cellular resolution and visualization of vertical slices. Following criteria were investigated: epidermal thickness in μm (obtained with ten repeated measurements taken every 120 μm on the vertical image of the 1.2 mm long LC-OCT field of view in the centre of the lesion using the incorporated software tool), ulceration, disruption of stratum corneum (SC), hyperkeratosis, compact parakeratosis, scales, keratin plugs, thinning of the epidermis, broadened/acanthotic epidermis, suprabasal and basal atypical keratinocytes, bowenoid pattern, acantholysis, pyknotic cells, atypical honeycombed pattern, bright particles in the epidermis, dendritic cells, flattened rete ridges, well-defined dermo-epidermal junction (DEJ), not visible/interrupted DEJ, dilated vessels/neoangiogenesis, glomerular vessels, bright particles in the dermis and elastosis/collagen alterations. Keratinocytes were defined as atypical when visually markedly differing from each other in size, shape and contours compared with healthy skin. We defined the thickened, acanthotic epidermis with roundish ('bowenoid') contours built by enlarged atypical keratinocytes in all epidermal layers as 'bowenoid pattern'.

The level of diagnostic confidence was defined on a three-point scale from 0% to 100% as follows: high (>70%), average (51%–69%) and poor (<50%). LC-OCT images were acquired with a prototype device (DAMAE Medical, Paris), a class 1 supercontinuum laser with a central wavelength of 800 nm, with three imaging modalities: vertical and horizontal (1.2×0.5 mm^2) and 3D ($1.2 \times 0.5 \times 0.5$ mm^3). Instrument and acquisition procedures were described elsewhere.[21,28] Exemplary lesions (10 AKs, 5 BD and 5 SCCs) were imaged with a conventional OCT (VivoSight, Michelson-Diagnostics, UK) and RCM (VivaScope 1500–3000, Mavig, Germany) device.

Statistical analysis

For descriptive statistics, mean values with 95% confidence interval were calculated for numeric data, while absolute numbers with percentage portion were given for nominal data. To evaluate the discriminant value of LC-OCT features for the distinction between AK, BD and SCC, univariate multinomial logistic regressions were performed for each individual feature. Odds ratios (OR) with corresponding *P*-values representing the effect of one feature on the likelihood of a diagnosis being made were calculated for: (1) AK vs. BD and (2) BD vs. SCC (3) AK vs. SCC.

We additionally included all predictors that showed a significant OR in a multivariable multinomial logistic regression analysis, as done by Peppelman *et al.*[29] to estimate the correct classification rate that is reached by using all information contained in the predictors showing significance in the univariate multinomial logistic regression analyses. We excluded the results of this analysis from our results because of overfitting.

P-values of less than 0.05 were considered statistically significant. All statistical analyses were conducted using R (version 3.6.0, 2019, R Foundation for Statistical Computing).

All patients provided their written informed consent. The study was approved by the local ethics committee (No. 17-699).

Results

Population

123 lesions suspicious for KC were recruited prospectively of which 73 cases were enrolled after histopathologic confirmation (belonging to 25 females, 48 males, mean age 74.8 years, CI 72.7–76.9). Remaining cases were excluded due to missing histopathological confirmation of the diagnosis as gold standard. Forty-six

AKs (10 hypertrophic, 5 atrophic, 3 bowenoid), 11 BD and 16 invasive SCCs were analysed. Most common lesion site was the head and neck area (52.1% face, 28.8% scalp), followed by upper limbs (9.6%), lower limbs (5.5%), trunk (2.7%) and genital area (1.4%).

Diagnostic confidence

Our diagnostic confidence with LC-OCT was high in 74% and average in 26% of the cases; with dermoscopy, it was high in 49.3% and average in 49.3%. We therefore estimated an improvement of 24.7% compared with clinical examination and dermoscopy alone.

Morphological features

The descriptive statistics and the univariate multinomial logistic regressions of the dermoscopic features are available in Tables S1 and S2.

Main LC-OCT features of AKs in vertical mode as reported in the descriptive statistics were (Tables 1 and 2) (Figures 1 and 2, S1): hyperkeratosis with compact parakeratosis (95.7% and 67.1%, respectively), scales (67.4%), broadened acanthotic epidermis (68.2%) and keratinocyte atypia (95.5%). It was not always possible to exactly distinguish between basal and suprabasal layers. The DEJ was preserved in 82.6%. The dermis showed dilated vessels/neoangiogenesis (59.5%) and elastosis/collagen alterations (56.1%). BD was characterized by a marked keratinocyte atypia involving all epidermal layers (100%) but with a well-defined DEJ (80%) (Figures 1 and 3, S2). In 7 AKs and 2 BD, some parts of the DEJ were not visible.

In invasive SCC, hyperkeratosis (100%), ulceration (68.8%) and disruption of SC (100%), a marked keratinocyte atypia (100%) in a broadened epidermis (93.8%) was found, with an

Table 1 Descriptive statistics of LC-OCT features of actinic keratosis, Bowen's disease and squamous cell carcinoma evaluated in the study with their relative and absolute frequencies

Features	All subtypes		Actinic keratosis		Bowen's disease		Invasive squamous cell carcinoma	
	Mean	95% CI	Mean	95% CI	Mean	95% CI	Mean	95% CI
Epidermal thickness	155.8	134.0, 177.5	126.2	102.9, 149.5	168.5	107.1, 229.8	232.0	182.3, 281.7
	%	*n*	%	*n*	%	*n*	%	*n*
Epidermis								
Ulceration	23.9	17/71	6.8	3/44	27.3	3/11	68.8	11/16
Disruption of stratum corneum	82.2	60/73	71.7	33/46	100.0	11/11	100.0	16/16
Hyperkeratosis	97.3	71/73	95.7	44/46	100.0	11/11	100	16/16
Compact parakeratosis	83.6	61/73	67.1	35/46	100.0	11/11	93.8	15/16
Scales	78.1	57/73	67.4	31/46	90.9	10/11	100.0	16/16
Keratin plugs	50.7	37/73	39.1	18/46	54.5	6/11	81.2	13/16
Thinning of the epidermis	28.2	20/71	40.9	18/44	18.2	2/11	0.0	0/16
Broadened/acanthotic epidermis	78.9	56/71	68.2	30/44	100.0	11/11	93.8	15/16
Suprabasal atypical keratinocytes	71.2	52/73	54.3	25/46	100.0	11/11	100.0	16/16
Basal atypical keratinocytes	94.5	69/71	95.5	42/44	100.0	11/11	100.0	16/16
Bowenoid pattern	27.8	20/72	15.2	7/46	90.0	9/10	25.0	4/16
Acantholysis	23.2	16/69	15.9	7/44	20.0	2/10	46.7	7/15
Pyknotic cells	43.1	31/72	32.6	15/46	20.0	5/10	68.8	11/16
Atypical honeycombed pattern	97.2	70/72	95.7	44/46	100.0	10/10	100.0	16/16
Bright particles in the epidermis	31-4	22/70	25.0	11/44	10.0	1/10	62.5	10/16
Dendritic cells	5.7	4/70	4.5	2/44	20.0	2/10	0	0/16
Flattened rete ridges	56.5	39/69	65.1	28/43	5.5	6/11	33.3	5/15
Dermo-epidermal junction								
Well defined	68.1	49/72	82.6	38/46	80.0	8/10	18.8	3/16
Not visible/interrupted	28.8	21/73	15.2	7/46	36.4	4/11	81.2	13/16
Dermis								
Dilated vessels/neoangiogenesis	65.2	43/66	59.5	25/42	70.0	7/10	78.6	11/14
Glomerular vessels	13.6	9/66	9.5	4/42	20.0	2/10	21.4	3/14
Bright particles in the dermis	18.8	13/69	11.4	5/44	20.0	2/10	40.0	6/15
Elastosis/collagen alterations	61.9	39/63	56.1	23/41	70.0	7/10	75.0	9/12

CI, confidence interval; %, per cent (relative frequency); *n*, number (absolute frequency).

Table 2 Univariate multinomial logistic regression reporting odds ratios (OR) and *P*-values of main analysed LC-OCT parameters

Feature LC-OCT	Subtype	OR	*P*
Epidermal thickness	2|1	1.01	0.13
	3|1	1.01	$P < 0.001$***
	3|2	1.01	0.10
Ulceration	2|1	5.12	0.07050
	3|1	30.06	$P < 0.001$***
	3|2	5.87	$P < 0.05$*
Disruption of stratum corneum	2|1	5548.60	0.81
	3|1	9400.90	0.81
	3|2	15.70	0.98
Hyperkeratosis	2|1	978.45	0.88
	3|1	896.47	0.85
	3|2	12.36	0.98
Compact parakeratosis	2|1	2212.53	0.76
	3|1	4.72	0.15
	3|2	0.00	0.84
Scales	2|1	4.80	0.15
	3|1	8192.20	0.78
	3|2	1509.60	0.81
Keratin plugs	2|1	1.87	0.36
	3|1	6.74	$P < 0.01$**
	3|2	3.61	0.15
Thinning of the epidermis	2|1	0.32	0.18
	3|1	0.00	0.80
	3|2	0.00	0.85
Broadened/acanthotic epidermis	2|1	5689.80	0.80
	3|1	7.00	0.07
	3|2	0.00	0.99
Suprabasal atypical keratinocytes	2|1	12044.20	0.79
	3|1	20060.40	0.80
	3|2	12.60	0.99
Basal atypical keratinocytes	2|1	923.79	0.87
	3|1	867.28	0.84
	3|2	12.87	0.99
Bowenoid pattern	2|1	50.14	$P < 0.001$***
	3|1	1.86	0.38
	3|2	0.04	$P < 0.05$**
Acantholysis	2|1	1.32	0.75
	3|1	4.63	$P < 0.05$*
	3|2	3.50	0.18
Pyknotic cells	2|1	2.08	0.30
	3|1	4.55	$P < 0.05$*
	3|2	2.20	0.34
Atypical honeycombed pattern	2|1	1687.40	0.90
	3|1	3545.80	0.91
	3|2	12.4	0.98
Bright particles in the epidermis	2|1	0.33	0.32
	3|1	5.00	$P < 0.01$**
	3|2	15.00	$P < 0.05$*
Dendritic cells	2|1	5.250	0.12
	3|1	0.00	0.88
	3|2	0.00	0.84
Flattened rete ridges	2|1	0.64	0.52
	3|1	0.27	$P < 0.05$*
	3|2	0.42	0.28
Well-defined DEJ	2|1	0.84	0.85
	3|1	0.049	$P < 0.001$***
	3|2	0.058	$P < 0.01$**
Not visible/interrupted DEJ	2|1	3.18	0.12
	3|1	9.28	$P < 0.001$***
	3|2	2.92	0.19
Dilated vessels/neoangiogenesis	2|1	1.59	0.54
	3|1	2.49	0.21
	3|2	1.57	0.63
Glomerular vessels	2|1	2.38	0.36
	3|1	2.59	0.26
	3|2	1.09	0.93
Bright particles in the dermis	2|1	1.95	0.47
	3|1	5.20	$P < 0.05$*
	3|2	2.67	0.30
Elastosis/collagen alterations	2|1	1.83	0.43
	3|1	2.35	0.25
	3|2	1.29	0.79

Nomenclature: 1 = actinic keratosis, 2 = Bowen disease, 3 = squamous cell carcinoma. Abbreviations: DEJ, dermo-epidermal junction; OR, odds ratio; Significance levels: *$P < 0.05$, **$P < 0.01$, ***$P < 0.001$.

either interrupted or non-visible DEJ (81.2%). (Figures 1 and 4). Dilated vessels/neoangiogenesis (78.6%) and collagen alterations (75%) were noticed.

In horizontal sections, SC was disrupted in 71.7% of AKs and 100% of SCCs; an atypical honeycombed pattern as described in RCM [13] was found in 95.7% of AKs and 100% of SCCs, pyknotic (broken) cells in 32.6% AKs, 68.8% SCCs. Collagen alterations and dilated vessels/neoangiogenesis were seen in all types of lesions; in 90% of BD, glomerular vessels (the typical tortuous, dilated vessels inside the dermal papillae) were displayed (Figure 3).

Mean epidermal thickness was 126.2 μm in AKs, 168.5 μm in BDs and 232 μm in SCCs (Table 1).

Univariate multinomial logistic regression models were performed to identify the main LC-OCT patterns allowing the distinction between different entities (AK, BD and SCC).[2] Following features were helpful in distinguishing SCCs compared to AKs: increased epidermal thickness ($P < 0.001$), ulceration ($P < 0.001$), keratin plugs ($P < 0.001$), acantholysis ($P < 0.05$), bright particles in the epidermis ($P < 0.01$), flattened rete ridges ($P < 0.05$), not visible/interrupted DEJ ($P < 0.001$) and bright particles in the dermis ($P < 0.05$). Ulceration ($P < 0.05$) and bright particles in the epidermis ($P < 0.05$) could analogously help differentiate a SCC from a BD, while the OR for BD well-defined DEJ ($P < 0.01$) and bowenoid pattern

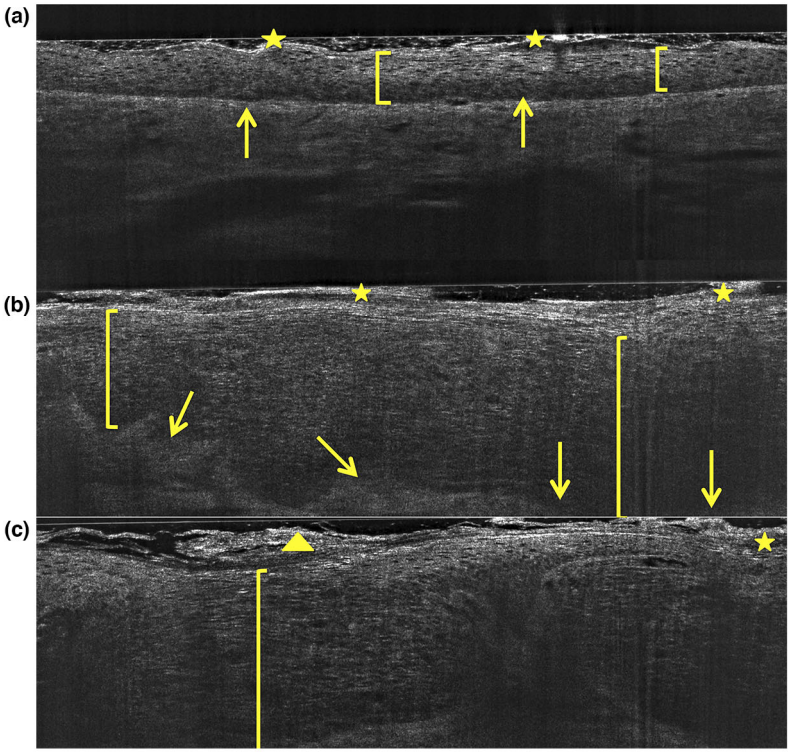

Figure 1 Different stages of keratinocyte skin cancer in LC-OCT, vertical mode: (a) AK of the face, (b) BD of the back, (c) SCC of the scalp. Hyperkeratosis and parakeratosis (star), atypical keratinocytes (bracket) are seen in all lesions; the DEJ (arrow) is preserved in (a) and (b), but not in (c), where strands of atypical keratinocytes infiltrating the dermis are seen (bracket) together with a thick, hyperkeratotic crust (triangle). AK, actinic keratosis; BD, Bowen disease; DEJ, dermo-epidermal junction; LC-OCT, line-field confocal optical coherence tomography; SCC, squamous cell carcinoma.

($P < 0.01$) was significantly higher for BD compared to SCC. The bowenoid pattern was the distinguishing feature of BD compared to AKs ($P < 0.001$).

Discussion

Differentiating stages of field cancerization noninvasively in real time is of outmost importance in the clinical practice since it allows an efficient therapy planning.

A dermoscopical 'progression model' was developed by Zalaudek *et al.*, who described a red pseudonetwork ('strawberry pattern') as typical for early AKs, and a red starburst pattern and yellow-white scales as a sign of transition to intraepidermal carcinoma. In BD, increasing neovascularization is seen as clustered glomerular vessels, while scales tend to become thicker and centrally coalesce. Advanced SCCs are characterized by irregular vessels, increased keratinization and ulceration.[3] Our findings were in line with the common literature on the topic: glomerular vessels were the most significant finding in dermoscopy of BD, while starburst pattern, scales and ulceration were seen in SCCs.

Conventional OCT, which provides vertical images intuitively comparable to histological sections and LC-OCT vertical mode, is able to detect common features of KC such as hyperkeratosis, epidermal disruption and loss of the DEJ. However, hyperkeratosis affects the imaging of underlying structures and an exact discrimination of the invasiveness is not always possible.[14,19,30–32] In their systematic review, Friis[19] described most common OCT features of AKs: disruption of layers, white streaks and dots and thickened epidermis. Schuh and Welzel demonstrated on a very large sample that AKs can be easily differentiated from normal skin and BCCs thanks to the decreased local signal intensity, as well as thicker SC and epidermis, finding moreover very good correlations between OCT and histopathological thickness of the skin layers.[33] In a paper focused on differentiation of non-melanoma skin cancers (NMSC), Batz *et al.* associated multifocal acanthosis to Bowen's disease and SCC, with SCC additionally showing hyperreflective nests and non-compressible dark borders.[34] No systematic study on OCT-guided diagnosis of SCC was published. Yet high-definition OCT (not commercially available anymore) was also used by Boone *et al.* for the in vivo discrimination of

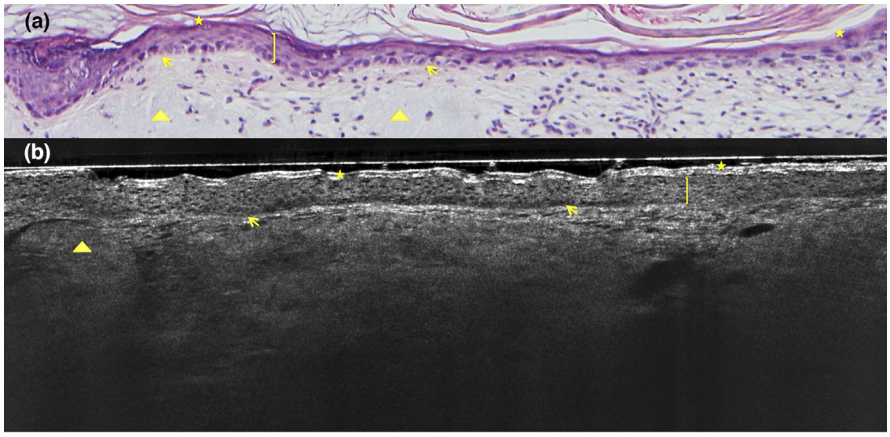

Figure 2 Atrophic AK of the face: H&E stained histology (100×) (a), LC-OCT in vertical mode (b) Note hyperkeratosis/parakeratosis (star), atypical keratinocytes (bracket) with preserved DEJ and flattened rete ridges (arrow), solar elastosis (triangle). AK, actinic keratosis; DEJ, dermo-epidermal junction; H&E, haematoxylin–eosin; LC-OCT, line-field confocal optical coherence tomography.

sun-damaged skin, AKs and SCCs based on the analysis of cellular, 3D microarchitectural structures and tissue scattering.[35]

In this article, we focused on LC-OCT features of AK, BD and SCC, in order to correlate the presence of specific descriptors with the stage of KC.

Hyperkeratosis was visible as a hyperreflective multilayer of polygonal cells with sometimes remaining nuclei (parakeratosis). Atypical keratinocytes were polygonal structures with a dark cytoplasm and bright contours, enlarged in comparison with those in healthy epidermis and with inhomogeneous size and shape. The cellular layering was intuitively comparable with the corresponding histological sections. However, it was not always easy to systematically differentiate basal and suprabasal keratinocyte atypia; to this regard, we noticed that the differences were easier detectable with higher grades of dysplasia (BD, SCC). Acantholysis was seen as darker spaces between the epidermal keratinocytes. Also, fragmented (pycnotic) keratinocytes could be detected.

The epidermal thickness systematically and significantly increased with the progression to invasive SCC.

In the dermis, increased vascularization and collagen fibre disarrangement, corresponding to elastosis (collagen reaction), were seen in all types of lesions in both vertical and horizontal sections. Small bright particles, probably corresponding to inflammatory infiltrates, could be visualized in both the epidermal and dermal layers.

We could visualize AKs and their main histopathological correlates with LC-OCT; the device also seemed to be potentially useful in AK subtyping. Although we only analysed a very small sample of AK subtypes (10 hypertrophic, 5 atrophic and 3 bowenoid), we were able to preliminarily observe the characteristic flattening of the rete in hypertrophic AKs, a thinned epidermis in atrophic AKs and the typical full thickness keratinocyte dysplasia with roundish contours in bowenoid AKs. In early AKs, the dermoscopic structureless red areas interrupted by follicular openings were associated with dilated and tortuous hyporeflective vessels in the superficial dermis and hyperreflective, follicular hyperkeratosis. A larger, systematic study on AKs subtyping should be performed to further investigate this interesting topic.

In BD, the enlarged atypical keratinocytes built a thickened, acanthotic epidermis with roundish ('bowenoid') contours of the enlarged atypical keratinocytes in all epidermal layers, which we defined as bowenoid pattern. This was the main feature to distinguish BD from AKs and SCCs.

In BDs and AKs, the DEJ was well preserved, seen as a darker band separating the basal keratinocytes from the bright dermal collagen; however, in 7 AKs and 2 BD, some parts of the DEJ were not visible, due to the increased thickness of the stratum corneum, pointing towards the limited penetration depth of LC-OCT, which does not always allow a complete examination of the epidermis and DEJ in thick hyperkeratotic lesions. Possible strategies to partially overcome this limit may be, as in conventional OCT and RCM, focusing on the lesion borders and/or removing thick hyperkeratotic crusts, thus with the risk of bleeding and inflammation impeaching the examination.

Squamous cell carcinomas are invasive, keratinizing tumours, composed of large keratinocytes displaying different grades of atypia, arising from the epidermis and extending into the dermis. In LC-OCT, disarranged masses of large polygonal cells with irregular contours could be seen; roundish bright homogeneous structures corresponding to horn pearls were visible. When visible, the dermis was infiltrated by tumour strands and masses, with increased and irregular vascularization (dilated vessels/neoangiogenesis) and bright collagen bundles

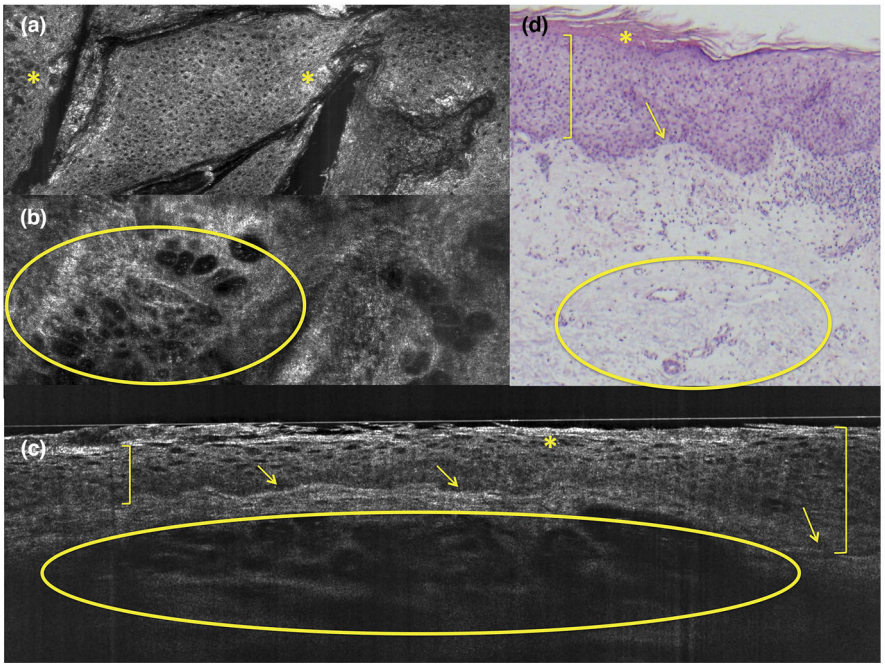

Figure 3 BD of the back: LC-OCT in horizontal mode at the epidermis (a) and junctional (b) level, vertical mode (c) and H&E stained histology (40×) (d). Atypical keratinocytes (bracket), hyperkeratosis with parakeratosis (asterisk), preserved DEJ (arrow), dilated vessels (circle) are seen. BD, Bowen disease; DEJ, dermo-epidermal junction; H&E, haematoxylin–eosin; LC-OCT, line-field confocal optical coherence tomography.

(elastosis/collagen alterations). In the descriptive statistics, these findings were more common in SCCs compared with AKs and BDs, although the model did not reach a statistical significance probably due to the small sample size.

If we take into account RCM, Peppelman and colleagues found architectural disarray in the stratum granulosum–spinosum and nest-like structures in the dermis as predictors of SCC compared to AK, based on 30 lesions.[29,36] Manfredini *et al.* listed erosion, architectural disarrangement and speckled nucleated cells in the dermis as the most common SCC features; buttonhole vessels were mostly found in in situ SCCs, while irregularly dilated vessels could be detected in invasive SCCs.[17] In horizontal LC-OCT images, which are intuitively comparable to RCM ones, we could describe an atypical honeycombed pattern constituted of dark polygonal cells in different sizes and shapes in all lesions; the grade of atypia increased from AK to SCC. Pyknotic cells were also visible. Collagen alterations/elastosis were seen, but we did not find any predominant vascular morphology.

A supplementary point was to evaluate whether specific LC-OCT descriptors were significantly associated with different stages of keratinocyte cancer. In fact, recognizing the invasiveness of the tumour is necessary for the therapeutic planning, since most AKs and BDs do not require a surgical approach. We therefore included all predictors that showed a significant odds ratio, in a multivariate multinomial logistic regression with bidirectional elimination based on previous studies about other diagnostic techniques,[29] and extrapolated dermoscopic and LC-OCT characteristics that can be useful in the correct classification of different subtypes of KC. In fact, a few patterns immediately help recognize different KC types. For example, a continuous DEJ is a typical feature of AK and BD, but cannot be seen in SCC, where an interrupted DEJ, marked collagen alterations and bright (inflammatory) particles in the dermis are prevalent. Even different types of AKs can be better recognized compared with dermoscopy: flattened rete ridges are typical for hypertrophic AKs, while a thinned epidermis was found in atrophic AKs. The model was conceived to calculate the correct classification rate of LC-OCT for AK, BD and SCC, which was 100%. However, due to overfitting, we based the interpretation of our results and discussion on the univariate multinomial logistic regressions. These results should be considered as preliminary and serve as a hint for future studies on larger samples, including more BD and SCCs compared with AKs.

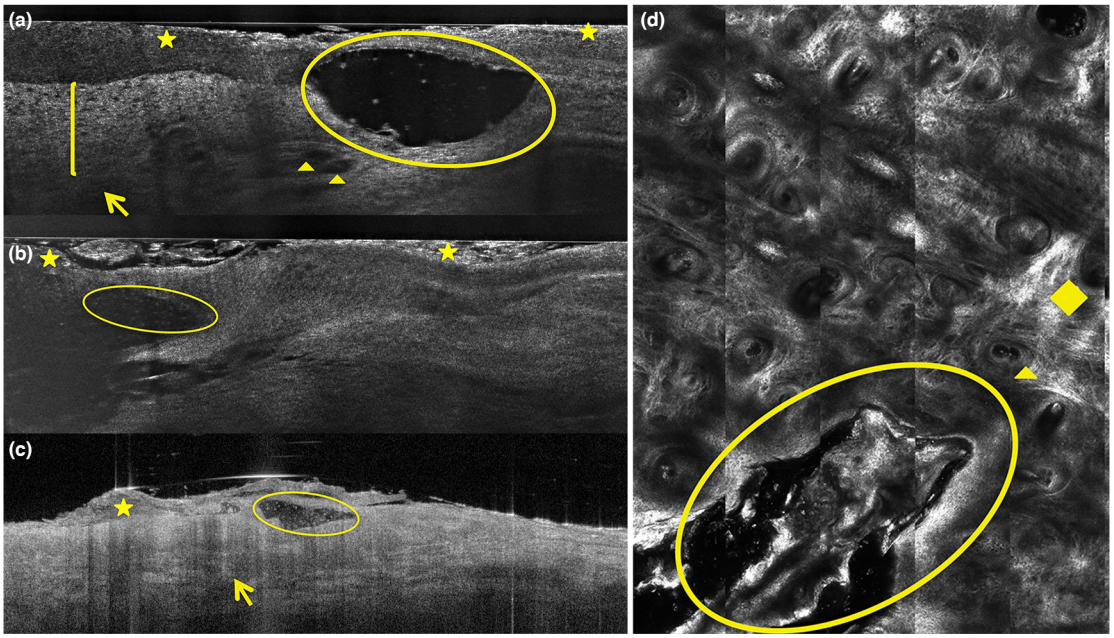

Figure 4 SCC of the scalp in vertical LC-OCT (a, b), OCT (c) and RCM (d). We see the following: a thick hyperkeratotic crust (asterisk), ulceration/blood crust (circle), atypical keratinocytes (bracket) with loss of the DEJ (arrow), dilated vessels (triangle), marked architectural disarrangement and elastosis (rhombus) also at the periphery of the lesion. DEJ, dermo-epidermal junction; H&E, haematoxylin–eosin; LC-OCT, line-field confocal optical coherence tomography; OCT, optical coherence tomography; RCM, reflectance confocal microscopy; SCC, squamous cell carcinoma.

Advantages and limitations of LC-OCT compared with other diagnostic techniques should be briefly discussed. The scanning camera allows the direct navigation of the examined area, as in conventional OCT and RCM 1500®. The unique combination of vertical and horizontal images at nearly cellular resolution makes histopathological correlations easier and reduces diagnostic pitfalls. The limited resolution compared with RCM does not impeach the evaluation of the keratinocyte atypia, but might complicate the differential diagnosis with melanocytic lesions. Offering less penetration depth than conventional OCT, LC-OCT can miss the deeper epidermal layers in the presence of massive hyperkeratosis, so that some thick early lesions might be misevaluated. Only conventional OCT offers a dynamic mode for blood flow.

Conclusions

We believe that the integration of clinical, dermoscopic and imaging data improves the therapeutic planning and follow-up of KC. In our experience, LC-OCT recognizes main features (keratinocyte morphology, architecture and DEJ structure) and allows the diagnosis of different stages of KC with intuitive and reliable histopathological correlations. Our findings open new scenarios in the non-invasive characterization of field cancerization. Further studies are needed to correlate the LC-OCT images to other histologic AK classifications such as PRO (a model focused on different stages of downward extension of basal keratinocytes 'protruding' into the papillary dermis)[37,38] and to standardize imaging algorithms for AKs, BD and SCCs.

Acknowledgments

The authors thank DAMAE medical for providing the LC-OCT device used for this study.

References

1 Leiter U, Heppt MV, Steeb T *et al*. S3 guideline for actinic keratosis and cutaneous squamous cell carcinoma (cSCC) - short version, part 2: epidemiology, surgical and systemic treatment of cSCC, follow-up, prevention and occupational disease. *J Dtsch Dermatol Ges* 2020; **18**: 400–413.
2 Malvehy J. A new vision of actinic keratosis beyond visible clinical lesions. *J Eur Acad Dermatol Venereol* 2015; **29**(Suppl 1): 3–8.
3 Zalaudek I, Giacomel J, Schmid K *et al*. Dermatoscopy of facial actinic keratosis, intraepidermal carcinoma, and invasive squamous cell carcinoma: a progression model. *J Am Acad Dermatol* 2012; **66**: 589–597.
4 Rosendahl C, Cameron A, Argenziano G, Zalaudek I, Tschandl P, Kittler H. Dermoscopy of squamous cell carcinoma and keratoacanthoma. *Arch Dermatol* 2012; **148**: 1386–1392.
5 Dinnes J, Deeks JJ, Chuchu N *et al*. Visual inspection and dermoscopy, alone or in combination, for diagnosing keratinocyte skin cancers in adults. *Cochrane Database Syst Rev* 2018; **12**: Cd011901.

6 Witkowski A, Łudzik J, DeCarvalho N *et al*. Non-invasive diagnosis of pink basal cell carcinoma: how much can we rely on dermoscopy and reflectance confocal microscopy? *Skin Res Technol* 2016; **22**: 230–237.
7 Valdés-Morales KL, Peralta-Pedrero ML, Cruz FJ, Morales-Sánchez MA. Diagnostic accuracy of dermoscopy of actinic keratosis: a systematic review. *Dermatol Pract Concept* 2020; **10**: e2020121.
8 Zalaudek I, Kreusch J, Giacomel J, Ferrara G, Catricala C, Argenziano G. How to diagnose nonpigmented skin tumors: a review of vascular structures seen with dermoscopy: part I. Melanocytic skin tumors. *J Am Acad Dermatol* 2010; **63**: 361–374.
9 Reinehr CP, Garbin GC, Bakos RM. Dermatoscopic patterns of nonfacial actinic keratosis: characterization of pigmented and nonpigmented lesions. *Dermatol Surg* 2017; **43**: 1385–1391.
10 Huerta-Brogeras M, Olmos O, Borbujo J *et al*. Validation of dermoscopy as a real-time noninvasive diagnostic imaging technique for actinic keratosis. *Arch Dermatol* 2012; **148**: 1159–1164.
11 Navarrete-Dechent C, Bajaj S, Marchetti MA, Rabinovitz H, Dusza SW, Marghoob AA. Association of shiny white blotches and strands with nonpigmented basal cell carcinoma: evaluation of an additional dermoscopic diagnostic criterion. *JAMA Dermatol* 2016; **152**: 546–552.
12 Ruini C, Hartmann D, Bastian M *et al*. Non-invasive monitoring of subclinical and clinical actinic keratosis of face and scalp under topical treatment with ingenol mebutate gel 150 mcg/g by means of reflectance confocal microscopy and optical coherence tomography: New perspectives and comparison of diagnostic techniques. *J Biophotonics* 2019; **12**: e201800391.
13 Ulrich M, Krueger-Corcoran D, Roewert-Huber J, Sterry W, Stockfleth E, Astner S. Reflectance confocal microscopy for noninvasive monitoring of therapy and detection of subclinical actinic keratoses. *Dermatology* 2010; **220**: 15–24.
14 Themstrup L, Pellacani G, Welzel J, Holmes J, Jemec GBE, Ulrich M. In vivo microvascular imaging of cutaneous actinic keratosis, Bowen's disease and squamous cell carcinoma using dynamic optical coherence tomography. *J Eur Acad Dermatol Venereol* 2017; **31**: 1655–1662.
15 Dejonckheere G, Suppa M, Del Marmol V, Meyer T, Stockfleth E. The actinic dysplasia syndrome - diagnostic approaches defining a new concept in field carcinogenesis with multiple cSCC. *J Eur Acad Dermatol Venereol* 2019; **33**(Suppl 8): 16–20.
16 Guida S, Longo C, Casari A *et al*. Update on the use of confocal microscopy in melanoma and non-melanoma skin cancer. *G Ital Dermatol Venereol* 2015; **150**: 547–563.
17 Manfredini M, Longo C, Ferrari B *et al*. Dermoscopic and reflectance confocal microscopy features of cutaneous squamous cell carcinoma. *J Eur Acad Dermatol Venereol* 2017; **31**: 1828–1833.
18 Navarrete-Dechent C, DeRosa AP, Longo C *et al*. Reflectance confocal microscopy terminology glossary for nonmelanocytic skin lesions: A systematic review. *J Am Acad Dermatol* 2019; **80**: 1414–1427.e3.
19 Friis KBE, Themstrup L, Jemec GBE. Optical coherence tomography in the diagnosis of actinic keratosis-A systematic review. *Photodiagnosis Photodyn Ther* 2017; **18**: 98–104.
20 Ruini C, Schuh S, Sattler E, Welzel J. Line-field confocal optical coherence tomography—Practical applications in dermatology and comparison with established imaging methods. *Skin Res Technol* 2021; **27**: 340–352. http://dx.doi.org/10.1111/srt.12949.
21 Ruini C, Sattler E. Konfokale Line-Field-OCT: die eierlegende Wollmilchsau?. *Aktuelle Dermatol* 2020; **46**: 148–151. http://dx.doi.org/10.1055/a-1072-7002.
22 Tognetti L, Fiorani D, Suppa M *et al*. Examination of circumscribed palmar hypokeratosis with line-field confocal optical coherence tomography: Dermoscopic, ultrasonographic and histopathologic correlates. *Indian J Dermatol Venereol Leprol* 2020; **86**: 206–208.
23 Monnier J, Tognetti L, Miyamoto M *et al*. In vivo characterization of healthy human skin with a novel, non-invasive imaging technique: line-field confocal optical coherence tomography. *J Eur Acad Dermatol Venereol* 2020; **34**: 2914–2921. http://dx.doi.org/10.1111/jdv.16857.
24 Dubois A, Levecq O, Azimani H *et al*. Line-field confocal optical coherence tomography for high-resolution noninvasive imaging of skin tumors. *J Biomed Opt* 2018; **23**: 1–9.
25 Ruini C, Schuh S, Hartmann D, French L, Welzel J, Sattler E. Noninvasive real-time imaging of mite skin infestations with line-field confocal optical coherence tomography. *Br J Dermatol* 2020; **184**.
26 Ogien J, Daures A, Cazalas M, Perrot J-L, Dubois A. Line-field confocal optical coherence tomography for three-dimensional skin imaging. *Front Optoelectron* 2020; **13**: 381–392. http://dx.doi.org/10.1007/s12200-020-1096-x.
27 Dubois A, Levecq O, Azimani H *et al*. Line-field confocal time-domain optical coherence tomography with dynamic focusing. *Opt Express* 2018; **26**: 33534–33542.
28 Ogien J, Levecq O, Azimani H, Dubois A. Dual-mode line-field confocal optical coherence tomography for ultrahigh-resolution vertical and horizontal section imaging of human skin. *Biomed Opt Express* 2020; **11**: 1327–1335.
29 Peppelman M, Nguyen KP, Hoogedoorn L, van Erp PE, Gerritsen MJ. Reflectance confocal microscopy: non-invasive distinction between actinic keratosis and squamous cell carcinoma. *J Eur Acad Dermatol Venereol* 2015; **29**: 1302–1309.
30 Olsen J, Themstrup L, De Carvalho N, Mogensen M, Pellacani G, Jemec GB. Diagnostic accuracy of optical coherence tomography in actinic keratosis and basal cell carcinoma. *Photodiagnosis Photodyn Ther* 2016; **16**: 44–49.
31 Ulrich M, Themstrup L, de Carvalho N *et al*. Dynamic optical coherence tomography of skin blood vessels - proposed terminology and practical guidelines. *J Eur Acad Dermatol Venereol* 2018; **32**: 152–155.
32 Ferrante di Ruffano L, Dinnes J, Deeks JJ *et al*. Optical coherence tomography for diagnosing skin cancer in adults. *Cochrane Database Syst Rev* 2018; **12**: Cd013189.
33 Schuh S, Kaestle R, Sattler EC, Welzel J. Optical coherence tomography of actinic keratoses and basal cell carcinomas - differentiation by quantification of signal intensity and layer thickness. *J Eur Acad Dermatol Venereol* 2016; **30**: 1321–1326.
34 Batz S, Wahrlich C, Alawi A, Ulrich M, Lademann J. Differentiation of different nonmelanoma skin cancer types using OCT. *Skin Pharmacol Physiol* 2018; **31**: 238–245.
35 Boone MA, Suppa M, Marneffe A, Miyamoto M, Jemec GB, Del Marmol V. A new algorithm for the discrimination of actinic keratosis from normal skin and squamous cell carcinoma based on in vivo analysis of optical properties by high-definition optical coherence tomography. *J Eur Acad Dermatol Venereol* 2016; **30**: 1714–1725.
36 Nguyen KP, Peppelman M, Hoogedoorn L, Van Erp PE, Gerritsen MP. The current role of in vivo reflectance confocal microscopy within the continuum of actinic keratosis and squamous cell carcinoma: a systematic review. *Eur J Dermatol* 2016; **26**: 549–565.
37 Schmitz L, Gupta G, Stücker M *et al*. Evaluation of two histological classifications for actinic keratoses - PRO classification scored highest interrater reliability. *J Eur Acad Dermatol Venereol* 2019; **33**: 1092–1097.
38 Schmitz L, Gambichler T, Gupta G *et al*. Actinic keratoses show variable histological basal growth patterns - a proposed classification adjustment. *J Eur Acad Dermatol Venereol* 2018; **32**: 745–751.

Supporting information

Additional Supporting Information may be found in the online version of this article:

Figure S1. Hypertrophic AK of the scalp: in vertical LC-OCT (a) and H&E stained histology (40×): hyperkeratosis/parakeratosis (star) together with atypical keratinocytes (bracket) are seen, while the DEJ is preserved (arrow); solar elastosis is present (triangle).

Figure S2. Detail of the cellular morphology of a clear cell BD in LC-OCT in horizontal mode (a) and H&E stained histology (100×) (b). Hyperkeratosis with parakeratosis (star) and large atypical keratinocytes (bracket) are seen.

Table S1. Descriptive statistics of dermoscopic features of actinic keratosis, Bowen's disease, and squamous cell carcinoma evaluated in the study with their relative and absolute frequencies.

Table S2. Univariate multinomial logistic regression reporting odds ratios (OR) and *P*-values of main analysed dermoscopic patterns.

5.2 Paper 4

Published in:

Ruini C, Schuh S, Gust C, Hartmann D, French LE, Sattler EC, Welzel J. In-Vivo LC-OCT Evaluation of the Downward Proliferation Pattern of Keratinocytes in Actinic Keratosis in Comparison with Histology: First Impressions from a Pilot Study. Cancers (Basel). 2021 Jun 8;13(12):2856. doi: 10.3390/cancers13122856. PMID: 34201052; PMCID: PMC8228287.

cancers

MDPI

Article

In-Vivo LC-OCT Evaluation of the Downward Proliferation Pattern of Keratinocytes in Actinic Keratosis in Comparison with Histology: First Impressions from a Pilot Study

Cristel Ruini [1,2,*], Sandra Schuh [3], Charlotte Gust [1], Daniela Hartmann [1], Lars Einar French [1,4], Elke Christina Sattler [1,†] and Julia Welzel [1,*,†]

1 Department of Dermatology and Allergy, University Hospital, LMU Munich, 80337 Munich, Germany; charlotte.gust@t-online.de (C.G.); daniela.hartmann@med.uni-muenchen.de (D.H.); lars.french@med.uni-muenchen.de (L.E.F.); elke.sattler@med.uni-muenchen.de (E.C.S.)
2 PhD School in Clinical and Experimental Medicine, University of Modena and Reggio Emilia, 41125 Modena, Italy
3 Department of Dermatology and Allergy, University Hospital, 86156 Augsburg, Germany; Sandra.Schuh@uk-augsburg.de
4 Dr. Phillip Frost Department of Dermatology & Cutaneous Surgery, Miller School of Medicine, University of Miami, Miami, FL 33125, USA
* Correspondence: Cristel.Ruini@med.uni-muenchen.de (C.R.); Julia.Welzel@uk-augsburg.de (J.W.)
† The two authors share the senior authorship.

Simple Summary: Actinic keratoses (AKs) are extremely common in the elderly population; they are universally recognized as precursors of invasive squamous cell carcinoma, and their risk of progression relates to the basal growth pattern of keratinocytes in the histological slides, based on a model called "PRO" classification. Since AKs can be investigated at bedside with non-invasive devices such the new line-field confocal optical coherence tomography (LC-OCT), we hypothesized that it was also possible to use such devices for reproducing the PRO classification and assessing the progression risk of AK without an invasive biopsy. In this pilot study, we demonstrated the feasibility of the LC-OCT severity grading of AKs based on the histological PRO classification, obtaining a good correlation between the two models and strong interobserver agreement.

Abstract: It is known that actinic keratoses (AKs) can progress to invasive squamous cell carcinoma (SCC). The histological PRO grading of AKs is based on the growth pattern of basal keratinocytes and relates to their progression risk. AKs can be non-invasively characterized by line-field confocal optical coherence tomography (LC-OCT). The aim of the study was to define criteria for an LC-OCT grading of AKs based on the PRO classification and to correlate it with its histological counterpart. To evaluate the interobserver agreement for the LC-OCT PRO classification, fifty AKs were imaged by LC-OCT and biopsied for histopathology. PRO histological grading was assessed by an expert consensus, while two evaluator groups separately performed LC-OCT grading on vertical sections. The agreement between LC-OCT and histological PRO grading was 75% for all lesions (weighted kappa 0.66, 95% CI 0.48–0.83, $p \leq 0.001$) and 85.4% when comparing the subgroups PRO I vs. PRO II/III (weighted kappa 0.64, 95% CI 0.40–0.88, $p \leq 0.001$). The interobserver agreement for LC-OCT was 90% (Cohen's kappa 0.84, 95% CI 0.71–0.91, $p \leq 0.001$). In this pilot study, we demonstrated that LC-OCT is potentially able to classify AKs based on the basal growth pattern of keratinocytes, in-vivo reproducing the PRO classification, with strong interobserver agreement and a good correlation with histopathology.

Keywords: actinic keratosis; PRO; dysplasia; keratinocyte cancer; field cancerization; line-field confocal optical coherence tomography; bedside histology; skin imaging; non-invasive diagnostics in dermatology

Citation: Ruini, C.; Schuh, S.; Gust, C.; Hartmann, D.; French, L.E.; Sattler, E.C.; Welzel, J. In-Vivo LC-OCT Evaluation of the Downward Proliferation Pattern of Keratinocytes in Actinic Keratosis in Comparison with Histology: First Impressions from a Pilot Study. *Cancers* **2021**, *13*, 2856. https://doi.org/10.3390/cancers13122856

Academic Editors: Aimilios Lallas, Salvador González, Melissa Gill and Ángeles Juarranz

Received: 24 March 2021
Accepted: 4 June 2021
Published: 8 June 2021

1. Introduction

Actinic keratoses (AKs) or solar keratoses are scaly, pink to reddish brown macules appearing as single to multiple elements on sun-exposed areas of elderly patients' skin. Clinically, AKs are divided into three main categories, from slightly palpable, to moderately thick, to hyperkeratotic [1].

Originally described as keratoma senilis, they were renamed by Hermann Pinkus, who combined their keratotic texture and their relationship with sunlight exposure [2]. Scalp, face, ears, neck, forearms and dorsal hands are the most involved body sites; males are more often affected than females [3]. In addition to UV radiation, other risk factors include fair skin, advanced age and chronic immunosuppression [4,5].

AKs are at risk of progressing to invasive squamous cell carcinoma (SCC) [6–11]. In fact, AKs and SCC share overlapping cytological features (atypical keratinocytes, loss of polarity, nuclear pleomorphism, altered maturation, higher mitotic index), which probably express the continuum of DNA damage due to chronic sun exposure, leading to the concept of field cancerization [12–15]. By definition, dysplastic alterations in AKs have to be confined to foci within the epidermis, while tumor strands invading the dermo-epidermal junction (DEJ) characterize invasive SCCs [16,17]. The most common histological classification divides AKs into three subgroups based on the distribution of the atypical keratinocytes within the epidermis, from the lower third (AK I), to two-thirds (AK II), to full thickness atypia (AK III) [9]. Surprisingly, this model does not correlate with progression to SCC, since the highest risk for invasion is instead associated with AKs with atypical keratinocytes restricted to the lower epidermis third (AK I). Recent studies observed that advanced basal proliferation of keratinocytes was related to progression to invasive SCC [18,19]. For this reason, a new AK histopathological classification focused on the basal growth pattern of keratinocytes was developed; the model was named "PRO I-III", since it was focused on different stages of downward extension of basal keratinocytes, "protruding" into the papillary dermis. The earlier stage PRO I was characterized by the "crowding" of atypical keratinocytes in the basal layer, PRO II by their "budding" in round nests into the upper papillary dermis and PRO III by the "papillary sprouting", with spikes of atypical keratinocytes protruding into the dermis and thicker than the overlying epidermis [19–21].

Multiple AKs often arise on sun-damaged and elderly skin, in the context of a field cancerization. Since it is not possible to predict which AKs will undergo progression into SCC through clinical examination, the whole field cancerization should be treated [22] Non-invasive diagnostic technologies such as reflectance confocal microscopy (RCM), optical coherence tomography (OCT) and line-field confocal optical coherence tomography (LC-OCT) have been successfully used to enhance the diagnostic accuracy of AKs and to characterize the field cancerization in vivo [12,23–25].

As LC-OCT provides a cellular resolution, we hypothesized that it should be possible to in-vivo grade the basal growth pattern of AKs based on LC-OCT images. The aim of this study was to evaluate the agreement between the LC-OCT and histological PRO classification of AKs. A secondary aim was to assess the interobserver agreement in performing the LC-OCT PRO grading.

2. Materials and Methods

Fifty histologically confirmed AKs of the face, imaged with LC-OCT between January 2020 and 2021 at the Departments of Dermatology of the universities of Munich and Augsburg, were analyzed in the study. The lesions belonged to 26 males and 17 females, mean age 73.8 years (CI 57;86); we included the first sequentially recruited fifty lesions with a histologically confirmed diagnosis of AK and a complete set of evaluable LC-OCT images and histopathological slides. Previously treated and/or not histologically confirmed lesions were excluded a priori from the analysis. During the selection process, 5 additional histologically confirmed AKs were excluded before performing the evaluation and were therefore not included in the panel of the fifty lesions since the quality of LC-OCT acquisition was not sufficient to analyze the required parameters (availability of only

horizontal sections and not of vertical sections, artefacts such as oil bubbles). The whole lesion was imaged and analyzed with multiple LC-OCT scans, examining the epidermis, the DEJ and the dermis from the skin surface to a depth of approximately 500 µm. LC-OCT images sized 1.2 × 0.5 mm^2 were acquired with a prototype device (DAMAE Medical, Paris), a class 1 supercontinuum laser with a central wavelength of 800 nm. Instrument and acquisition procedures have been described elsewhere [26,27]. Image acquisition was within a time frame of 0–7 days before the biopsy. The histologic specimens were 34 deep shave biopsies (with scalpel), 10 punch biopsies, 2 curettages (deep shave with ring curette) and 4 excisions. They were included in paraffin and stained with hematoxylin & eosin (H&E), according to the standard procedures, and evaluated as in daily routine examinations. Only completely evaluable tissue specimens with a vertical orientation were examined in the study.

We considered an H&E stained histological slide the gold standard. We did not perform any supplementary analysis with additional devices. PRO classification was made on both histological slides and LC-OCT vertical images based on the criteria of the original study by Schmitz et al. [21]: PRO I was defined by atypical keratinocytes crowded at basal epidermal layers (crowding), PRO II showed a slight protrusion into the upper papillary dermis with round nests of atypical keratinocytes (budding), thinner than the overlying epidermis, and PRO III displayed spikes of atypical cells thicker than the overlying epidermis (papillary sprouting). In the event that two or more patterns were present in the same image set, the higher score was chosen according to the literature [20,21]. LC-OCT images in vertical mode were evaluated, blinded to H&E slides, by a pair of dermatologists expert in non-invasive diagnostic techniques (observer round) and, separately, by a board-certified dermatopathologist/dermatologist and a dermatologist educated in dermopathology, both experts in non-invasive diagnostic techniques (consensus round). In case of discrepancy regarding the grading, the dermatopathologist set the final decision, being the most experienced in the PRO classification. Hematoxylin & Eosin (H&E) stained slides were evaluated in a consensus by a board-certified dermatopathologist expert in both classification systems and a dermatologist educated in dermatopathology, blinded to LC-OCT images. Since the PRO classification was performed on histological slides in standard vertical sections, only vertical LC-OCT images were examined, while horizontal sections were not analyzed in order to avoid confounders and bias.

Cohen's weighted kappa coefficient with linear weights was used to calculate the correlation between LC-OCT and histopathological PRO score including confidence intervals (CI); the two cases labeled as indefinable with LC-OCT were excluded from the analysis. The correlation was also estimated into the different subgroups (PRO I and II/III). The interobserver agreement was calculated with Cohen´s kappa coefficient, also taking into account the non-definable cases. A p-value lower than 0.05 was considered significant [28].

The study was approved by the ethical committee of the LMU Munich (Protocol Number 17–699).

3. Results

3.1. PRO Grading

Seventeen AKs were histologically classified as PRO I, 22 as PRO II and 11 as PRO III. LC-OCT PRO grading was defined as in Figure 1. The LC-OCT PRO grading was in agreement with the histological grading in 75% of the observations. The weighted kappa for LC-OCT and histological classification was 0.66 (95% CI 0.48 to 0.83; $p \leq 0.001$). Two cases were not classifiable with LC-OCT due to excessive lesion thickness. Discordant cases were either underestimated (12%) or overestimated (12%) (Table S1, Figure 2).

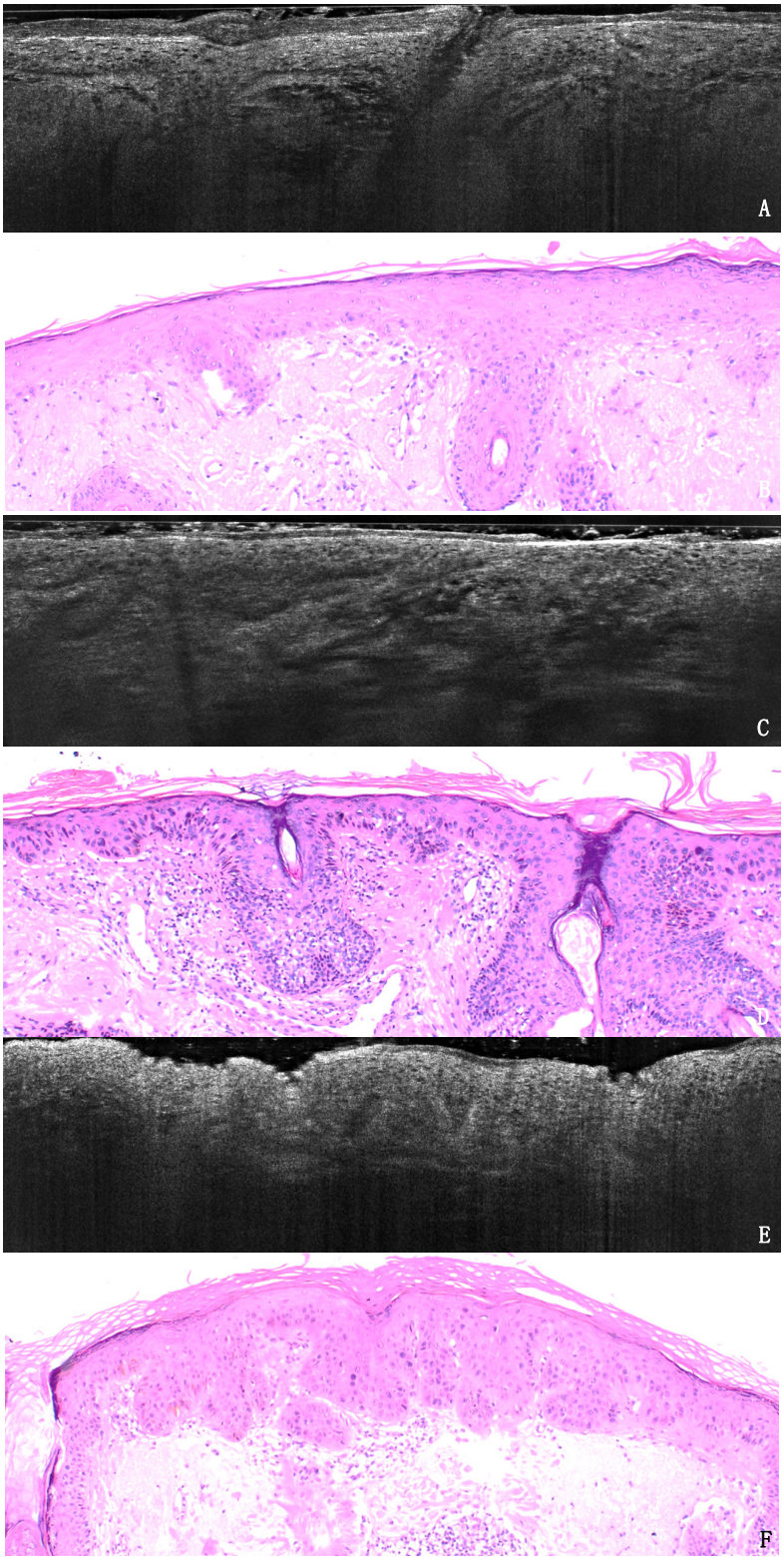

Figure 1. Example of three AK lesions in LC-OCT (**A**,**C**,**E**) and histology (**B**,**D**,**F**) in H&E sections, original magnification 40×. (**A**,**B**). AK PRO I shows basal crowding of keratinocytes in an otherwise regularly layered epidermis, with no protrusions into the dermis. (**C**,**D**). AK PRO II displays spikes of atypical keratinocytes slightly protruding into the papillary dermis. (**E**,**F**). AK PRO III shows the extended downward growth of atypical keratinocytes with spikes thicker than the overlying epidermis.

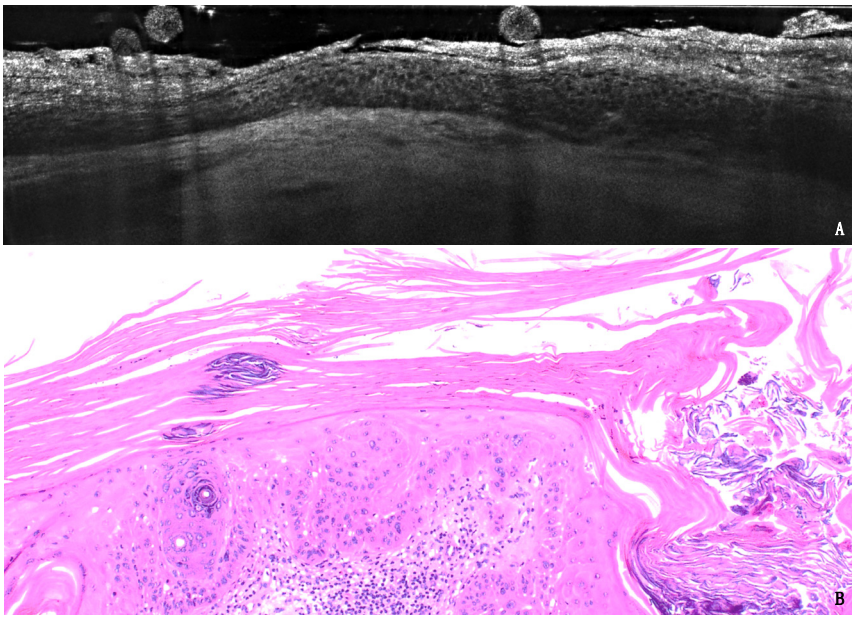

Figure 2. Example of AK lesion with discordant PRO grading between LC-OCT (**A**) and histology (40×, **B**): the hypertrophic AK on the scalp of an 85-year-old male patient was graded PROII in LC-OCT and PROIII in H&E, probably because of the diffuse hyperkeratoses impeding the evaluation of the deepest layers of the lesions.

If we take into account the subgroups, the agreement between LC-OCT and histology was 66.7% for PRO I, 86.5% for PRO II and 64% for PRO III. In the comparison between PRO I and PRO II-III grouped together as the higher progression risk category, the overall concordance was 85.4% (weighted kappa = 0.64, 95% CI, 0.40 to 0.88; $p \leq 0.001$) (Figure 3).

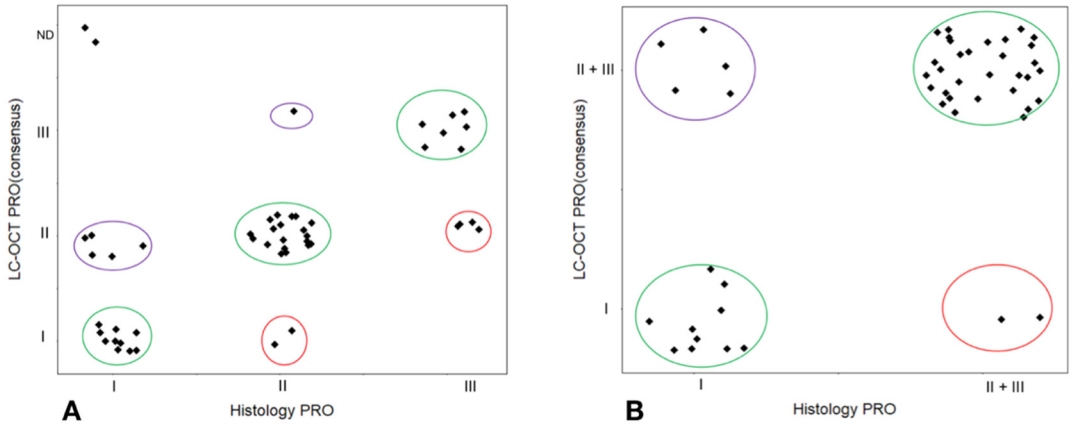

Figure 3. Overall (**A**) and subgroup (**B**) correlation between LC-OCT and histopathological PRO grading of AKs. ND: not definable.

3.2. Agreement

The interobserver agreement for LC-OCT PRO grading between the observer round and consensus round was 90%, with a Cohen´s kappa = 0.84 (95% CI 0.71 to 0.97; $p \leq 0.001$). (Figure 4).

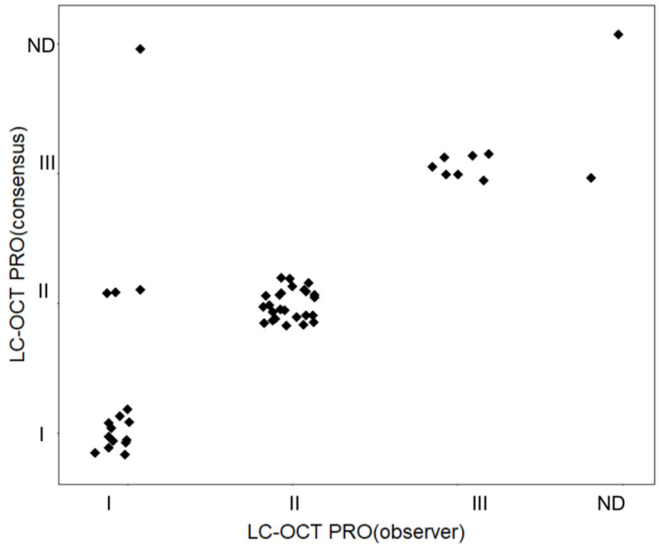

Figure 4. Interobserver agreement in the LC-OCT PRO classification of AKs. ND: not definable.

4. Discussion

AKs are one of the most common skin conditions in the elderly population, mainly arising on sun-exposed areas of the skin in the context of a field cancerization. Following the current guidelines, all AKs should be treated, since it is not possible to predict which ones will grow into an invasive SCC [29]. The type of treatment should be determined based on the clinical features, the patients' comorbidities and the previous therapies. Various local and field treatments, including surgery, laser ablation, photodynamic therapy and diverse topical treatments such as 5-fluorouracile, diclofenac, imiquimod and potassium hydroxide, can be used. It is known that diagnosis and follow-up of AKs can be improved by non-invasive diagnostic technologies such as RCM, OCT and LC-OCT, which provide a painless bedside examination of keratinocyte cancer (KC) [12,15,24,25,30–33]. RCM has been used for grading increasing keratinocyte dysplasia into different levels, with good correlation with histopathology, but it does not refer to specific classification systems [23].

We therefore focused on the in-vivo evaluation of the growth pattern of basal keratinocytes through LC-OCT, based on the recent PRO classification. The latter proved, in fact, to ensure the best interobserver agreement and the best risk stratification (in terms of progression risk to SCC) compared to other AK classifications [19–21]. We chose to use LC-OCT since it delivers dermoscopy-guided and real-time cross-sectional imaging of skin lesions with cellular resolution, so that the cytological and architectural features of the epidermis can be displayed in real time. It can visualize the epidermal layers, the DEJ and the superficial dermis, and its vertical acquisitions can be intuitively compared to histological slides [30,34,35]. Moreover, additional features such as perifollicular proliferation and adnexal extension can be visible, up to a depth of 500 µm. A direct and practical consequence is the potential in-vivo assessment of AK progression risk, since PRO III AKs are associated with a higher risk of developing an invasive SCC compared to PRO I [19–21].

In our study, we were able to visualize and grade the downward extension of AKs non-invasively through LC-OCT, defining key imaging patterns that can be used as reference images. We reported strong interobserver agreement in grading the basal growth pattern of keratinocytes in the examined AKs. Moreover, we reported good agreement in the PRO classification of AKs between LC-OCT and traditional histopathology. Additionally, we reached an overall agreement of 85.4% when comparing the subgroup of PRO I and the subgroup of PRO II/III AKs, which are the lesions at higher risk of progression to SCC compared to PRO I.

LC-OCT displays the protrusions of atypical basal keratinocytes into the upper dermis (spikes) and allows the measurement of their thickness compared to the overlying epidermis. This visual evaluation permits a reproducible LC-OCT grading of AKs based on the

PRO histological classification. We were able to classify PRO I as lesions with no visible spikes, PRO II as lesions with spikes slightly protruding into the papillary dermis and PRO III as lesions with more prominent spikes, thicker than the overlying epidermis (Figure 1, Figure 5). Our criteria can be used as a reference model for LC-OCT grading of AKs. The high reproducibility (90%) between observers demonstrates that skilled imaging experts are able to perform an in-vivo evaluation of cyto-architectural atypia with LC-OCT.

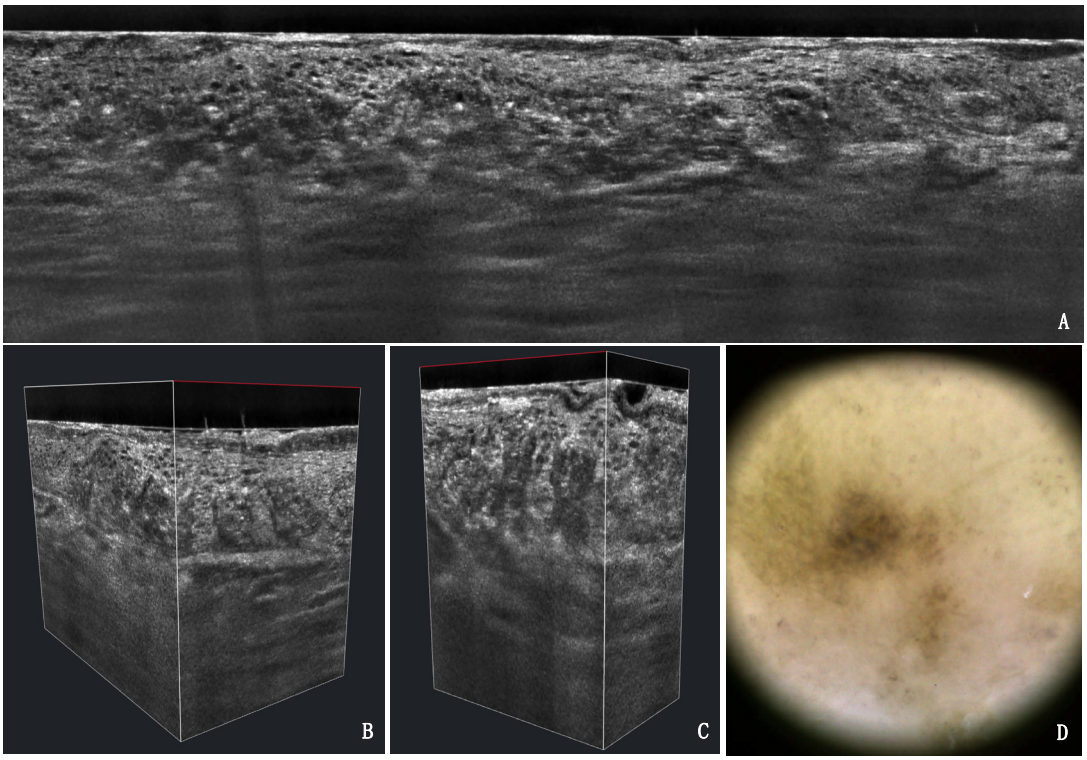

Figure 5. LC-OCT vertical (**A**), 3D (**B**,**C**) and dermoscopy (**D**) of a pigmented PRO III AK lesion on the dorsum of the hand of an 82-year-old male patient. The typical papillary sprouting as well as the pigmented basal keratinocytes are visible.

LC-OCT can be therefore considered a useful tool for the diagnosis and therapeutic monitoring of AKs and might be successfully used in both clinical trials and daily routine. As OCT and RCM, it can be used for a live, in-vivo mapping of several lesions in different progression stages and perilesional skin in the context of field cancerization, avoiding multiple surgical biopsies and related consequences (pain, discomfort, scars, inflammatory reactions, failed localization). Compared to conventional OCT, LC-OCT has a higher resolution and allows the assessment of cytological features and not only structural details. Compared to RCM, LC-OCT displays vertical sections simultaneously to horizontal slides as in RCM. Thus, it is much easier in LC-OCT images to determine the degree of basal proliferation and compare it with histology.

Some limitations have to be taken into account. In our study, two large and thick hyperkeratotic lesions were not fully evaluable. This sheds light on the good but still not perfect penetration depth of the LC-OCT, which does not fully display the basal layer in the presence of severe hyperkeratosis. In such cases, it is useful to examine the margins of the lesion, since the basal growth pattern of keratinocytes does not depend on the lesion thickness. Moreover, in this regard, it was easier for the observers to evaluate the downward growth pattern of basal keratinocytes in the context of a PRO classification, compared to the distribution of the atypical keratinocytes through the epidermis, as in other classifications. Another limitation of the study was the small sample size (50 lesions, belonging to 43 patients). Since some lesions arose on the same patient, a bias derived from this aspect cannot be excluded; however, we only included independent lesions, arising on

different anatomical sites and separately imaged and biopsied, so that we considered the number of cases acceptable for a lesion-centered, pilot study [36]. An additional, crucial point that has to be taken into account is represented by the observer´s experience, not only in non-invasive diagnostic techniques but also in dermatopathology. All observers in this study had knowledge of dermatopathology and non-invasive imaging; it was not possible to perform a correlation of the LC-OCT grading and the level of experience of the observer.

The agreement between LC-OCT and histology was lower in PRO I compared to PRO II/III, due to overestimation. Five cases graded as PRO I in histology were evaluated as PRO II/III with LC-OCT. This might be due to confounders such as hair follicles and shafts, which might appear as longitudinal structures in the sections, but also to the larger field of view, providing a global analysis of the examined area. LC-OCT can, in fact, scan the whole AK lesion in a three-dimensional way, guided by a camera, displaying multiple scans; on the contrary, the pathologist only has a few histological sections at their disposal, since only a few slides are obtained from each tissue block in the daily diagnostic routine. From this perspective, LC-OCT might provide additional details regarding non-invasive AK grading, correctly directing lesions to either conservative or surgical therapy based on their basal growth pattern.

5. Conclusions

LC-OCT is able to perform a reliable in-vivo evaluation of basal keratinocyte growth pattern based on the histopathological PRO classification of AKs, with strong agreement with histopathology and between different observers. Larger studies, also potentially aided by artificial intelligence algorithms, are needed to validate the method.

Supplementary Materials: The following are available online at https://www.mdpi.com/article/10.3390/cancers13122856/s1, Table S1: PRO grading evaluated with LC-OCT in the observer round, consensus round and histopathology.

Author Contributions: Conceptualization, J.W. and E.C.S.; methodology, J.W., C.R., E.C.S. and S.S.; validation, J.W., C.R., E.C.S., S.S. and D.H.; formal analysis, J.W., C.R., E.C.S., S.S., D.H. and C.G.; investigation, J.W., C.R., E.C.S., S.S, D.H. and C.G.; resources, C.R., E.C.S., J.W. and L.E.F.; data curation, C.R., S.S. and C.G.; writing—original draft preparation, C.R.; writing—review and editing, E.C.S., S.S, D.H., C.G. and L.E.F.; supervision, J.W and E.C.S.; project administration, J.W., C.R., E.C.S. and S.S.; funding acquisition, C.R. All authors have read and agreed to the published version of the manuscript.

Funding: The study was partially funded by the FöFoLe (Förderprogramm für Forschung und Lehre) Grant 10-22 of the Ludwig Maximilian University of Munich (LMU Munich).

Institutional Review Board Statement: The study was conducted according to the guidelines of the Declaration of Helsinki and approved by the Institutional Review Board of the LMU Munich (Protocol Number 17-699).

Informed Consent Statement: Informed consent was obtained from all subjects involved in the study.

Data Availability Statement: Fully anonymized data are available on request.

Acknowledgments: The authors thank DAMAE medical together with Maxime Cazalas and Melanie Pedrazzani for providing the device needed for this study and for their constant professional assistance.

Conflicts of Interest: The authors declare no relevant conflict of interest.

References

1. Olsen, E.A.; Abernethy, M.L.; Kulp-Shorten, C.; Callen, J.P.; Glazer, S.D.; Huntley, A.; McCray, M.; Monroe, A.B.; Tschen, E.; Wolf, J.E., Jr. A double-blind, vehicle-controlled study evaluating masoprocol cream in the treatment of actinic keratoses on the head and neck. *J. Am. Acad. Dermatol.* **1991**, *24*, 738–743. [CrossRef]

2. Pinkus, H. Keratosis senilis; a biologic concept of its pathogenesis and diagnosis based on the study of normal epidermis and 1730 seborrheic and senile keratoses. *Am. J. Clin. Pathol.* **1958**, *29*, 193–207. [CrossRef]
3. Frost, C.; Williams, G.; Green, A. High incidence and regression rates of solar keratoses in a queensland community. *J. Investig. Dermatol.* **2000**, *115*, 273–277. [CrossRef]
4. Traianou, A.; Ulrich, M.; Apalla, Z.; De Vries, E.; Bakirtzi, K.; Kalabalikis, D.; Ferrandiz, L.; Ruiz-de-Casas, A.; Moreno-Ramirez, D.; Sotiriadis, D.; et al. Risk factors for actinic keratosis in eight European centres: A case-control study. *Br. J. Dermatol.* **2012**, *167* (Suppl. 2), 36–42. [CrossRef]
5. Stockfleth, E.; Ulrich, C.; Meyer, T.; Christophers, E. Epithelial malignancies in organ transplant patients: Clinical presentation and new methods of treatment. *Recent Results Cancer Res.* **2002**, *160*, 251–258.
6. Cockerell, C.J.; Wharton, J.R. New histopathological classification of actinic keratosis (incipient intraepidermal squamous cell carcinoma). *J. Drugs Dermatol. JDD* **2005**, *4*, 462–467.
7. Heaphy, M.R., Jr.; Ackerman, A.B. The nature of solar keratosis: A critical review in historical perspective. *J. Am. Acad. Dermatol.* **2000**, *43*, 138–150. [CrossRef] [PubMed]
8. Ackerman, A.B.; Mones, J.M. Solar (actinic) keratosis is squamous cell carcinoma. *Br. J. Dermatol.* **2006**, *155*, 9–22. [CrossRef] [PubMed]
9. Rowert-Huber, J.; Patel, M.J.; Forschner, T.; Ulrich, C.; Eberle, J.; Kerl, H.; Sterry, W.; Stockfleth, E. Actinic keratosis is an early in situ squamous cell carcinoma: A proposal for reclassification. *Br. J. Dermatol.* **2007**, *156*, 8–12. [CrossRef]
10. de Berker, D.; McGregor, J.M.; Mohd Mustapa, M.F.; Exton, L.S.; Hughes, B.R. British Association of Dermatologists' guidelines for the care of patients with actinic keratosis 2017. *Br. J. Dermatol.* **2017**, *176*, 20–43. [CrossRef] [PubMed]
11. Tokez, S.; Alblas, M.; Nijsten, T.; Pardo, L.; Wakkee, M. Predicting keratinocyte carcinoma in patients with actinic keratosis: Development and internal validation of a multivariable risk-prediction model. *Br. J. Dermatol.* **2020**, *183*, 495–502. [CrossRef]
12. Dejonckheere, G.; Suppa, M.; Del Marmol, V.; Meyer, T.; Stockfleth, E. The actinic dysplasia syndrome—Diagnostic approaches defining a new concept in field carcinogenesis with multiple cSCC. *J. Eur. Acad. Dermatol. Venereol.* **2019**, *33* (Suppl. 8), 16–20. [CrossRef]
13. Schmitz, L.; Stücker, M.; Gambichler, T.; Stockfleth, E.; Dirschka, T. Histological intralesional heterogeneity of actinic keratoses relates to field cancerization. *J. Dtsch. Dermatol. Ges.* **2018**, *16*, 1211–1217. [CrossRef] [PubMed]
14. Fernandez Figueras, M.T. From actinic keratosis to squamous cell carcinoma: Pathophysiology revisited. *J. Eur. Acad. Dermatol. Venereol.* **2017**, *31* (Suppl. 2), 5–7. [CrossRef] [PubMed]
15. Ruini, C.; Witkowski, A.M.; Cesinaro, A.; Teixeira De Carvalho, N.; Pellacani, G. From actinic keratosis to squamous cell carcinoma: Evidence of morphologic and biologic progression. *J. Am. Acad. Dermatol.* **2015**, *72*, S8–S10. [CrossRef]
16. Cockerell, C.J. Histopathology of incipient intraepidermal squamous cell carcinoma ("actinic keratosis"). *J. Am. Acad. Dermatol.* **2000**, *42*, 11–17. [CrossRef]
17. Cockerell, C.J. Pathology and pathobiology of the actinic (solar) keratosis. *Br. J. Dermatol.* **2003**, *149* (Suppl. 66), 34–36. [CrossRef] [PubMed]
18. Fernandez-Figueras, M.T.; Carrato, C.; Saenz, X.; Puig, L.; Musulen, E.; Ferrandiz, C.; Ariza, A. Actinic keratosis with atypical basal cells (AK I) is the most common lesion associated with invasive squamous cell carcinoma of the skin. *J. Eur. Acad. Dermatol. Venereol.* **2015**, *29*, 991–997. [CrossRef]
19. Schmitz, L.; Gambichler, T.; Kost, C.; Gupta, G.; Stucker, M.; Stockfleth, E.; Dirschka, T. Cutaneous squamous cell carcinomas are associated with basal proliferating actinic keratoses. *Br. J. Dermatol.* **2019**, *180*, 916–921. [CrossRef] [PubMed]
20. Schmitz, L.; Gupta, G.; Stücker, M.; Doerler, M.; Gambichler, T.; Welzel, J.; Szeimies, R.M.; Bierhoff, E.; Stockfleth, E.; Dirschka, T. Evaluation of two histological classifications for actinic keratoses—PRO classification scored highest inter-rater reliability. *J. Eur. Acad. Dermatol. Venereol.* **2019**, *33*, 1092–1097. [CrossRef]
21. Schmitz, L.; Gambichler, T.; Gupta, G.; Stücker, M.; Stockfleth, E.; Szeimies, R.M.; Dirschka, T. Actinic keratoses show variable histological basal growth patterns—A proposed classification adjustment. *J. Eur. Acad. Dermatol. Venereol.* **2018**, *32*, 745–751. [CrossRef] [PubMed]
22. Schmitz, L.; Kahl, P.; Majores, M.; Bierhoff, E.; Stockfleth, E.; Dirschka, T. Actinic keratosis: Correlation between clinical and histological classification systems. *J. Eur. Acad. Dermatol. Venereol.* **2016**, *30*, 1303–1307. [CrossRef]
23. Pellacani, G.; Ulrich, M.; Casari, A.; Prow, T.W.; Cannillo, F.; Benati, E.; Losi, A.; Cesinaro, A.M.; Longo, C.; Argenziano, G.; et al. Grading keratinocyte atypia in actinic keratosis: A correlation of reflectance confocal microscopy and histopathology. *J. Eur. Acad. Dermatol. Venereol.* **2015**, *29*, 2216–2221. [CrossRef]
24. Schuh, S.; Kaestle, R.; Sattler, E.C.; Welzel, J. Optical coherence tomography of actinic keratoses and basal cell carcinomas—differentiation by quantification of signal intensity and layer thickness. *J. Eur. Acad. Dermatol. Venereol.* **2016**, *30*, 1321–1326. [CrossRef]
25. Ruini, C.; Hartmann, D.; Bastian, M.; Ruzicka, T.; French, L.E.; Berking, C.; von Braunmühl, T. Non-invasive monitoring of subclinical and clinical actinic keratosis of face and scalp under topical treatment with ingenol mebutate gel 150 mcg/g by means of reflectance confocal microscopy and optical coherence tomography: New perspectives and comparison of diagnostic techniques. *J. Biophotonics* **2019**, *12*, e201800391. [CrossRef]
26. Ogien, J.; Daures, A.; Cazalas, M.; Perrot, J.-L.; Dubois, A. Line-field confocal optical coherence tomography for three-dimensional skin imaging. *Front. Optoelectron.* **2020**, *13*, 381–392. [CrossRef]

27. Dubois, A.; Levecq, O.; Azimani, H.; Davis, A.; Ogien, J.; Siret, D.; Barut, A. Line-field confocal time-domain optical coherence tomography with dynamic focusing. *Opt. Express* **2018**, *26*, 33534–33542. [CrossRef] [PubMed]
28. Watson, P.; Petrie, A. Method agreement analysis: A review of correct methodology. *Theriogenology* **2010**, *73*, 1167–1179. [CrossRef]
29. Heppt, M.V.; Leiter, U.; Steeb, T.; Amaral, T.; Bauer, A.; Becker, J.C.; Breitbart, E.; Breuninger, H.; Diepgen, T.; Dirschka, T.; et al. S3 guideline for actinic keratosis and cutaneous squamous cell carcinoma—Short version, part 1: Diagnosis, interventions for actinic keratoses, care structures and quality-of-care indicators. *J. Dtsch. Dermatol. Ges.* **2020**, *18*, 275–294. [CrossRef]
30. Ruini, C.; Schuh, S.; Sattler, E.; Welzel, J. Line-field confocal optical coherence tomography-Practical applications in dermatology and comparison with established imaging methods. *Skin Res. Technol.* **2020**. [CrossRef]
31. Nguyen, K.P.; Peppelman, M.; Hoogedoorn, L.; Van Erp, P.E.; Gerritsen, M.P. The current role of in vivo reflectance confocal microscopy within the continuum of actinic keratosis and squamous cell carcinoma: A systematic review. *Eur. J. Dermatol.* **2016**, *26*, 549–565. [CrossRef] [PubMed]
32. Olsen, J.; Themstrup, L.; De Carvalho, N.; Mogensen, M.; Pellacani, G.; Jemec, G.B. Diagnostic accuracy of optical coherence tomography in actinic keratosis and basal cell carcinoma. *Photodiagnosis Photodyn. Ther.* **2016**, *16*, 44–49. [CrossRef] [PubMed]
33. Boone, M.A.; Suppa, M.; Pellacani, G.; Marneffe, A.; Miyamoto, M.; Alarcon, I.; Ruini, C.; Hofmann-Wellenhof, R.; Malvehy, J.; Jemec, G.B.; et al. High-definition optical coherence tomography algorithm for discrimination of basal cell carcinoma from clinical BCC imitators and differentiation between common subtypes. *J. Eur. Acad. Dermatol. Venereol.* **2015**, *29*, 1771–1780. [CrossRef]
34. Pedrazzani, M.; Breugnot, J.; Rouaud-Tinguely, P.; Cazalas, M.; Davis, A.; Bordes, S.; Dubois, A.; Closs, B. Comparison of line-field confocal optical coherence tomography images with histological sections: Validation of a new method for in vivo and non-invasive quantification of superficial dermis thickness. *Skin Res. Technol.* **2020**, *26*, 398–404. [CrossRef] [PubMed]
35. Monnier, J.; Tognetti, L.; Miyamoto, M.; Suppa, M.; Cinotti, E.; Fontaine, M.; Perez, J.; Orte Cano, C.; Yélamos, O.; Puig, S.; et al. In vivo characterization of healthy human skin with a novel, non-invasive imaging technique: Line-field confocal optical coherence tomography. *J. Eur. Acad. Dermatol. Venereol.* **2020**. [CrossRef] [PubMed]
36. Zwinderman, A.H.; Glas, A.S.; Bossuyt, P.M.; Florie, J.; Bipat, S.; Stoker, J. Statistical models for quantifying diagnostic accuracy with multiple lesions per patient. *Biostatistics* **2008**, *9*, 513–522. [CrossRef]

5.3 Paper 5

Published in:

Schuh S, Ruini C, Perwein MKE, Daxenberger F, Gust C, Sattler EC, Welzel J. Line-Field Confocal Optical Coherence Tomography: A New Tool for the Differentiation between Nevi and Melanomas? Cancers (Basel). 2022 Feb 23;14(5):1140. doi: 10.3390/cancers14051140. PMID: 35267448; PMCID: PMC8909859.

cancers

MDPI

Article

Line-Field Confocal Optical Coherence Tomography: A New Tool for the Differentiation between Nevi and Melanomas?

Sandra Schuh [1,*], Cristel Ruini [2], Maria Katharina Elisabeth Perwein [1], Fabia Daxenberger [2], Charlotte Gust [2], Elke Christina Sattler [2,†] and Julia Welzel [1,*,†]

[1] Department of Dermatology and Allergology, University Hospital, 86179 Augsburg, Germany; maria.perwein@web.de
[2] Department of Dermatology and Allergy, University Hospital, LMU Munich, 80337 Munich, Germany; cristel.ruini@med.uni-muenchen.de (C.R.); fabia.daxenberger@gmail.com (F.D.); charlotte.gust@t-online.de (C.G.); elke.sattler@med.uni-muenchen.de (E.C.S.)
* Correspondence: sandra.schuh@uk-augsburg.de (S.S.); julia.welzel@uk-augsburg.de (J.W.)
† These authors contributed equally to this work.

Simple Summary: Typical benign nevi and advanced melanomas can be easily discriminated, but there are still some melanocytic lesions where even experts are not sure about the correct diagnosis and degree of malignity. The high penetration depth of optical coherence tomography (OCT) allows an assessment of tumor thickness of the lesion precisely, but without cellular resolution the differentiation of melanocytic lesions remains difficult. On the other hand, reflectance confocal microscopy (RCM) allows for very good morphological identification of either a nevus or a melanoma, but cannot show the infiltration depth of the lesion because of its low penetration depth. Since the new device of line-field confocal optical coherence tomography (LC-OCT) technically closes the gap between these other two devices, in this study, we wanted to examine if it is possible to differentiate between nevi and melanomas with LC-OCT, and which criteria are the most important for it.

Abstract: Until now, the clinical differentiation between a nevus and a melanoma is still challenging in some cases. Line-field confocal optical coherence tomography (LC-OCT) is a new tool with the aim to change that. The aim of the study was to evaluate LC-OCT for the discrimination between nevi and melanomas. A total of 84 melanocytic lesions were examined with LC-OCT and 36 were also imaged with RCM. The observers recorded the diagnoses, and the presence or absence of the 18 most common imaging parameters for melanocytic lesions, nevi, and melanomas in the LC-OCT images. Their confidence in diagnosis and the image quality of LC-OCT and RCM were evaluated. The most useful criteria, the sensitivity and specificity of LC-OCT vs. RCM vs. histology, to differentiate a (dysplastic) nevus from a melanoma were analyzed. Good image quality correlated with better diagnostic performance (Spearman correlation: 0.4). LC-OCT had a 93% sensitivity and 100% specificity compared to RCM (93% sensitivity, 95% specificity) for diagnosing a melanoma (vs. all types of nevi). No difference in performance between RCM and LC-OCT was observed (McNemar's p value = 1). Both devices falsely diagnosed dysplastic nevi as non-dysplastic (43% sensitivity for dysplastic nevus diagnosis). The most significant criteria for diagnosing a melanoma with LC-OCT were irregular honeycombed patterns (92% occurrence rate; 31.7 odds ratio (OR)), the presence of pagetoid spread (89% occurrence rate; 23.6 OR) and the absence of dermal nests (23% occurrence rate, 0.02 OR). In conclusion LC-OCT is useful for the discrimination between melanomas and nevi.

Keywords: melanoma; nevus; skin cancer; line-field confocal optical coherence tomography; optical coherence tomography; reflectance confocal microscopy; skin imaging; non-invasive diagnostics in dermatology

check for updates

Citation: Schuh, S.; Ruini, C.; Perwein, M.K.E.; Daxenberger, F.; Gust, C.; Sattler, E.C.; Welzel, J. Line-Field Confocal Optical Coherence Tomography: A New Tool for the Differentiation between Nevi and Melanomas? *Cancers* **2022**, *14*, 1140. https://doi.org/10.3390/cancers14051140

Academic Editors: Reinhard Dummer and Florentia Dimitriou

Received: 29 January 2022
Accepted: 22 February 2022
Published: 23 February 2022

Publisher's Note: MDPI stays neutral with regard to jurisdictional claims in published maps and institutional affiliations.

1. Introduction

Optical coherence tomography (OCT) and reflectance confocal microscopy (RCM) already play important roles in routine non-invasive skin cancer diagnosis [1]. OCT is well established for non-melanoma skin cancer (NMSC), whereas RCM is most commonly used for pigmented lesions [2–4]. With OCT it is possible to create vertical images until mid to deep dermal level, to reconstruct 3D images, measure tumor thickness, monitor topically treated lesions over the course of time, and even to distinguish BCC subtypes, but lacks cellular resolution [2,3]. This is why melanocytic lesions cannot be visualized very well with OCT. With the high resolution of RCM, pigmented tumors can be examined horizontally in cellular detail. Since the penetration depth of RCM is limited, it is only possible to measure from the stratum corneum to the stratum papillare of the dermis [4,5].

The new line-field confocal optical coherence tomography (LC-OCT) method offers the combination of the advantages of both devices—a high penetration depth like OCT and a similar high resolution like RCM, together with the visualization of images in horizontal and vertical views [6–11].

Therefore, LC-OCT was used in this study to investigate melanocytic lesions and to find out the most common and most useful parameters for diagnosis, especially for the differentiation between (dysplastic) nevi and melanomas. The improved distinction between nevus and melanoma with LC-OCT allows a fast, in vivo, and non-invasive diagnosis. If the lesion can be categorized as a nevus immediately with LC-OCT, no excision is necessary. In addition to the benefit to the patient that no invasive procedure is needed, this new technique will help to avoid unnecessary surgeries, leading to lower healthy insurance costs, as well as to offering more free capacities for other necessary melanoma surgeries. This study assesses the influence of image quality on diagnostic performance with LC-OCT and RCM and determines the potential of LC-OCT (vs. RCM vs. histology) to identify a melanoma vs. a nevus reliably and accurately. To our knowledge, this is the first work about melanocytic lesions, especially concerning the differentiation of nevi and melanomas with the new LC-OCT device.

2. Materials and Methods

2.1. LC-OCT

The LC-OCT device used in our study is based on a time-domain-OCT (TD-OCT), which takes several A-scans from the skin's surface down to a maximal depth of 500 µm for the acquisition of B-scans, while constantly refocusing. It has an axial resolution of 1.1 µm and a lateral resolution of 1.3 µm. The LC-OCT technique consists of a two-beam interference microscope, with a laser source of 800 nm wavelength with a continuous spectrum and a line camera as a photodetector. The laser classification is 1 M according to EN 60825-1. Like in conventional OCT, the images are depicted in grey scale. The CE-marked LC-OCT deepLive™ (DAMAE Medical, Paris, France) is a mobile central unit with a monitor and a handheld probe. To generate high quality images and reduce the optical index between the glass plate of the probe and skin layers, paraffin oil was used. The device is non-invasive, painless, and is applied without pressure. LC-OCT has three available modes to create images in real time: vertical (en-coupe) sections, as in OCT and histology, horizontal (en-face) images as in RCM, and 3D images. The field of view for both the vertical and horizontal sections is 1.2 mm × 0.5 mm. The 3D images can be taken as horizontal stacks from the top of the skin with steps of 1 µm. Short videos can also be acquired with up to 26, 16, or 8 frames/s (basic, high definition, ultra-high definition). Moreover, a dermoscopic image (resolution 5 µm, field of view 2.5 mm) is taken simultaneously, which makes it possible to navigate in the lesion and choose the correct position. Captured images can be exported and saved globally or as a single patient/lesion file in TIFF, DICOM, or JPEG formats. The additional program 3DSlicer (The Slicer Community, Open-Source Software) allows the reconstruction of 3D cubes of the horizontal LC-OCT stacks [9,10].

2.2. RCM and OCT

In our study we used commercially distributed RCM devices (VivaScope® 1500 and VivaScope® 1500/3000 Combo, Mavig GmbH, Munich, Germany), which have a penetration depth of 300 µm. Both have a lateral resolution of 1 µm and an axial resolution between 3–5 µm. The light source is an 830 nm diode laser. The 1500 device has an integrated dermoscopic camera for navigation, creates image sizes of 500 µm × 500 µm, and builds mosaics of single greyscale pictures up to 8 mm × 8 mm (VivaBlock®). The other mode, which we used in the study for the comparison with LC-OCT, is the VivaStack®, where single images can be taken from the skin's surface to the stratum papillare in several steps. The conventional OCT used in this study is the commercially available, handheld-based OCT device VivoSight® (Michelson Diagnostics Ltd., Maidstone, Kent, UK). We additionally measured 30 of all the melanocytic lesions with conventional OCT for comparative reasons. The OCT acquires images of 6 mm × 6 mm with 1.5 mm detection depth. It has a lateral resolution of 7.5 µm and an axial resolution of 10 µm, and contains a laser source of 1305 nm. With the addition of dynamic OCT, blood flow and blood vessels can be visualized. Further details on the devices are described elsewhere [2,12].

2.3. Patients

Patients with suspicious melanocytic lesions or nevi that were planned for excision were enrolled in the study at the Department of Dermatology and Allergology at the University Hospital of Augsburg and at the University Hospital of the Ludwig Maximilian University, Munich in Germany between November 2019 and January 2021. The study was approved by the local ethics committee (No. 17-699) and conducted according to the principles of the Declaration of Helsinki and international guidelines concerning human studies. Written informed consent was obtained from all patients prior to inclusion into the study.

2.4. Measurements

A clinical examination was done to identify the lesion as suspicious for a melanoma or a (dysplastic) nevus prior to excision. Clinical and dermoscopic images of each lesion were acquired using Fotofinder® (FotoFinder Systems GmbH, Bad Birnbach, Germany), DermoGenius 2® (DermoScan GmbH, Regensburg, Germany), ILLUCO IDS-1100 (DermoScan GmbH, Regensburg, Germany), or an iPhone 12 Pro Camera (Apple Inc., Cupertino, CA, USA). After dermoscopy, the lesions were scanned with LC-OCT (deepLive™, DAMAE Medical, Paris, France) in horizontal, vertical, and 3D. After that, OCT images (vertical and dynamic en-face) as well as RCM pictures were taken (VivaStacks® and VivaBlocks®). Horizontal LC-OCT and RCM images were taken at the level of the stratum corneum, the epidermis, the dermo-epidermal junction (DEJ), and the papillary dermis. For measurements with RCM and LC-OCT, a few drops of paraffin oil were used before the scan. OCT examinations did not require preparation of the skin. After the examination, a biopsy, shave, or excision of the lesion was taken and sent for histological analysis. All lesions were compared with standard histology in haematoxylin/eosin.

After all images had been reviewed, the observers graded LC-OCT and RCM image quality during a consensus meeting with semi-quantitative scores as poor (3), acceptable (2), good (1), or excellent (0), and the confidence level from low (3), medium (2), high (1), to very high (0). After histology, the final diagnosis was noted. Both centers are regular users of OCT, RCM, and LC-OCT. Both centers had at least 3 months of practical experience and training with LC-OCT before the study.

In addition to the well-known clinical and dermoscopic diagnostic criteria for melanocytic lesions, we used the following patterns for the different methods: LC-OCT criteria in horizontal and vertical view (see Tables S1 and S2) and RCM parameters (see Tables S3 and S4). In 30 cases, conventional OCT images were also recorded for demonstration purposes. Since RCM is superior to OCT in diagnosing melanocytic lesions and OCT cannot show the

cellular details of melanomas and nevi, OCT criteria were not evaluated and OCT was not included in the systematic study [13,14].

2.5. Statistical Analysis

For the collection of data, Microsoft® Office Excel® for Mac 2021 was used. Statistical analysis was performed with R version 4.0.0 (R Foundation for Statistical Computing; Vienna, Austria). The accuracy, specificity, sensitivity of each technique, PPV (percentage of positive diagnoses that were correct), and NPV (percentage of negative diagnoses that were correct) were calculated. The specificity and sensitivity of LC-OCT for the diagnosis of a melanoma were compared with the specificity and sensitivity of RCM, and then both devices with histology using McNemar's test, which considers the paired nature of the data. Furthermore, the investigators' responses concerning the recognized parameters for melanocytic lesions, the diagnoses, the image quality, and confidence level were noted. For the intra-method correlation between image quality and confidence level, Spearman's correlation coefficients (r) were calculated. A p-value < 0.05 was considered as statistically significant. When the data failed the normality test, a Wilcoxon test for paired tests was used to compare image quality and confidence level between LC-OCT and RCM. We also performed univariate and multivariate logistic regression analyses for the criteria that were more useful in discriminating a melanoma from a nevus (dysplastic or not), and used a backward elimination approach.

3. Results

3.1. Study Population

A total of 75 patients with 84 melanocytic lesions were evaluated with LC-OCT before excision. A total of 36 of the 84 lesions were also measured with RCM. Five patients had two lesions, one patient had five lesions, and the others had one pigmented lesion. The mean age of the patients was 51 years. Lesions were mainly located on the trunk (57.1%), limb (25%), and the head (17.9%). Histology was available for all 84 lesions. Histology identified 42 (50%) of 84 lesions as banal nevi, 13 (15.5%) as dysplastic nevi and 28 (33.3%) as melanomas. A total of 65.5% of the lesions were histologically diagnosed as nevi (dysplastic or not). Furthermore, 82.1% of the lesions were completely excised, 16.7% were biopsied, and 1.2% were shaved. One lesion was histologically diagnosed as a pigmented actinic keratosis and was therefore excluded for further evaluation. In terms of invasion levels, nine melanomas were in situ melanomas (32%), and nine invasive melanomas were up to 1 mm thick (32%). A total of seven melanomas had a tumor thickness between 1 and 2 mm (25%), two melanomas were between 2 and 4 mm thick (7%), and one melanoma was thicker than 4 mm (4%). Regarding the subtype, 17 melanomas were classified as superficial spreading melanomas (61%), 2 were nodular (7%), 2 were acrolentiginous (7%), and 7 lentigo maligna (3) or invasive lentigo maligna melanomas (4) (25%). TNM classifications for the melanomas were T0 (9), IA (9), IB (7), IIA (1), IIB (1), and IIIC (1). All melanomas with a tumor thickness up to 2 mm were excised with a safety margin of 1 cm, while melanomas with a tumor thickness $\geq$ 2mm received excision with a safety margin of 2 cm. In patients with a melanoma with a tumor thickness > 1 mm, a sentinel lymph node biopsy (or in high-risk cases with a tumor thickness > 0.75 mm) was conducted.

3.2. LC-OCT and RCM Image Quality and Confidence Level

A total of 1 out of 36 lesions imaged with RCM and 4 from 84 lesions imaged with LC-OCT were classified as having poor image quality. The diagnostic confidence level depended on image quality for LC-OCT and RCM (Table 1, Figure 1).

Lower image quality led to a poorer confidence level (Table 2). We found no difference between RCM and LC-OCT in terms of average image quality or average diagnostic confidence level (Table 2). A total of 77.8% of the lesions had good LC-OCT image quality (scored 0 or 1), while 72.2% had good RCM image quality. The average quality was evaluated as 1.2 for LC-OCT vs. 1.3. for RCM. However, the image quality (p = 0.49) and

the confidence level ($p = 0.40$) were not significantly different between LC-OCT and RCM ($p = 0.49$). In total, 86.1% of the lesions had a high LC-OCT confidence level (scored 0 or 1), while 77.8% had a high RCM confidence level. The average confidence level was calculated as 1.2 for LC-OCT vs. 1.2 for RCM.

Table 1. Influence of image quality on the LC-OCT and RCM confidence level. LC-OCT and RCM image quality was scored from 0 (higher quality) to 3 (lower quality). LC-OCT and RCM confidence level was scored from 0 (higher confidence level) to 3 (lower confidence level).

		LC-OCT		
For all lesions (*n* = 84)	**Quality = 0 (*n* = 4)**	**Quality = 1 (*n* = 58)**	**Quality = 2 (*n* = 18)**	**Quality = 3 (*n* = 4)**
Average confidence level	0.8	1.2	1.4	2.3
For lesions also imaged with RCM (*n* = 36)	Quality = 0 (*n* = 1)	Quality = 1 (*n* = 27)	Quality = 2 (*n* = 7)	Quality = 3 (*n* = 1)
Average confidence level	1	1.1	1.3	3
		RCM		
***n* = 36**	**Quality = 0 (*n* = 0)**	**Quality = 1 (*n* = 26)**	**Quality = 2 (*n* = 9)**	**Quality = 3 (*n* = 1)**
Average confidence level	-	1.1	1.4	2

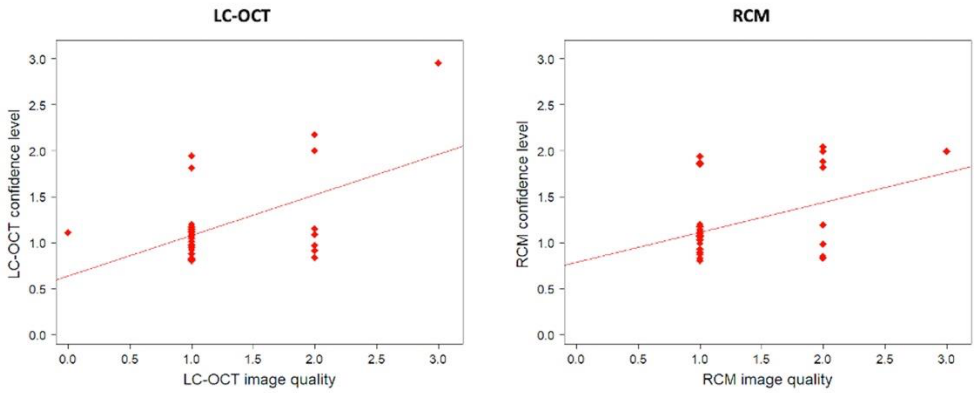

Figure 1. Correlation between confidence level and image quality for LC-OCT and RCM. There was a statistically significant positive correlation between LC-OCT confidence levels and image quality for LC-OCT ($r_s(36) = 0.40$; $p = 0.02$), as well as for RCM ($r_s(36) = 0.43$; $p = 0.008$).

Table 2. Comparison of image quality and confidence level between LC-OCT and RCM.

	LC-OCT	**RCM**
Image quality	*n* (%)	*n* (%)
Score 0	1 (2.8)	0 (0)
Score 1	27 (75.0)	26 (72.2)
Score 2	7 (19.4)	9 (25.0)
Score 3	1 (2.8)	1 (2.8)
Confidence level	*n* (%)	*n* (%)
Score 0	0 (0)	0 (0)
Score 1	31 (86.1)	28 (77.8)
Score 2	4 (11.1)	8 (22.2)
Score 3	1 (2.8)	0 (0)

3.3. LC-OCT and RCM Performance for Diagnosing a Melanoma vs. a Nevus

Table 3 shows LC-OCT performances for diagnosing a melanoma vs. a nevus (dysplastic or not), and Table 4 for diagnosing a melanoma vs. a nevus vs. a dysplastic nevus for all 84 lesions.

Table 3. LC-OCT performances for diagnosing melanomas vs. nevi (dysplastic or not) compared to histology.

All Lesions		Histology			
		Melanoma	**Nevus**	**Other**	**Total**
LC-OCT	Melanoma	26	0	0	26
	Nevus	2	55	0	57
	Other	0	0	1	1
	Total	28	55	1	84

Table 4. LC-OCT performances for diagnosing melanomas vs. nevi vs. dysplastic nevi compared to histology.

All Lesions		Histology				
		Nevus	**Melanoma**	**Dysplastic Nevus**	**Others**	**Total**
LC-OCT	Nevus	40	1	8	0	49
	Melanoma	0	26	0	0	26
	Dysplastic nevus	2	1	5	0	8
	Others	0	0	0	1	1
	Total	42	28	13	1	84

Figure 2 shows an example of a compound nevus, Figure 3 a dysplastic nevus and Figure 4 a melanoma with all three devices compared to histology. The case diagnosed as "other" (pigmented actinic keratosis) in histology was dropped for the evaluation.

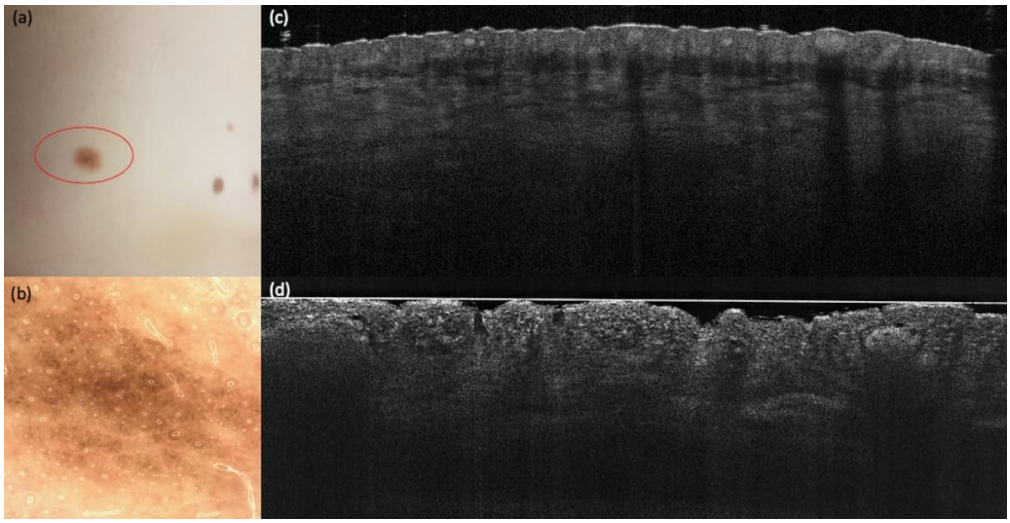

(1)

Figure 2. *Cont.*

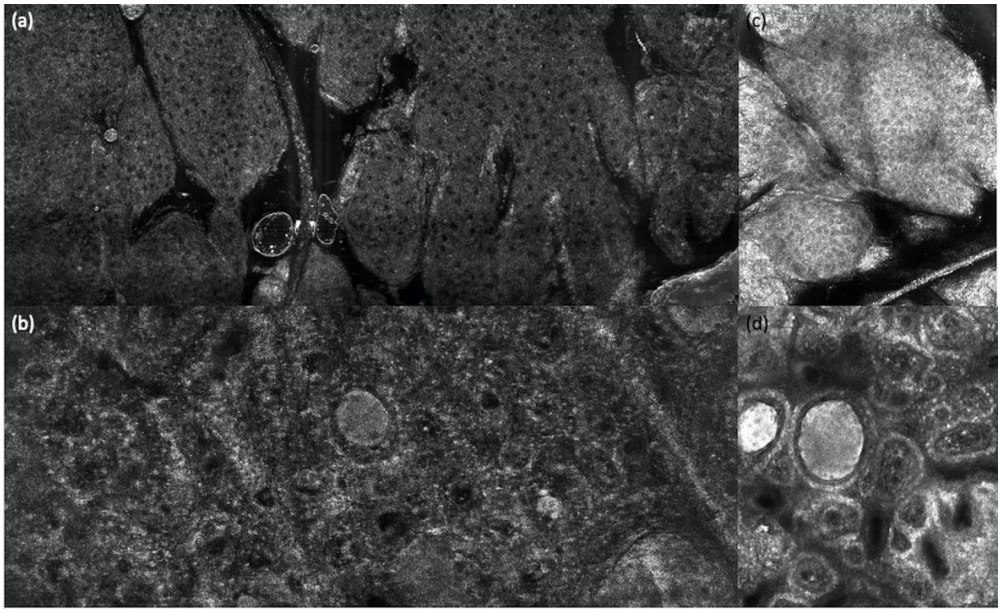

(**2**)

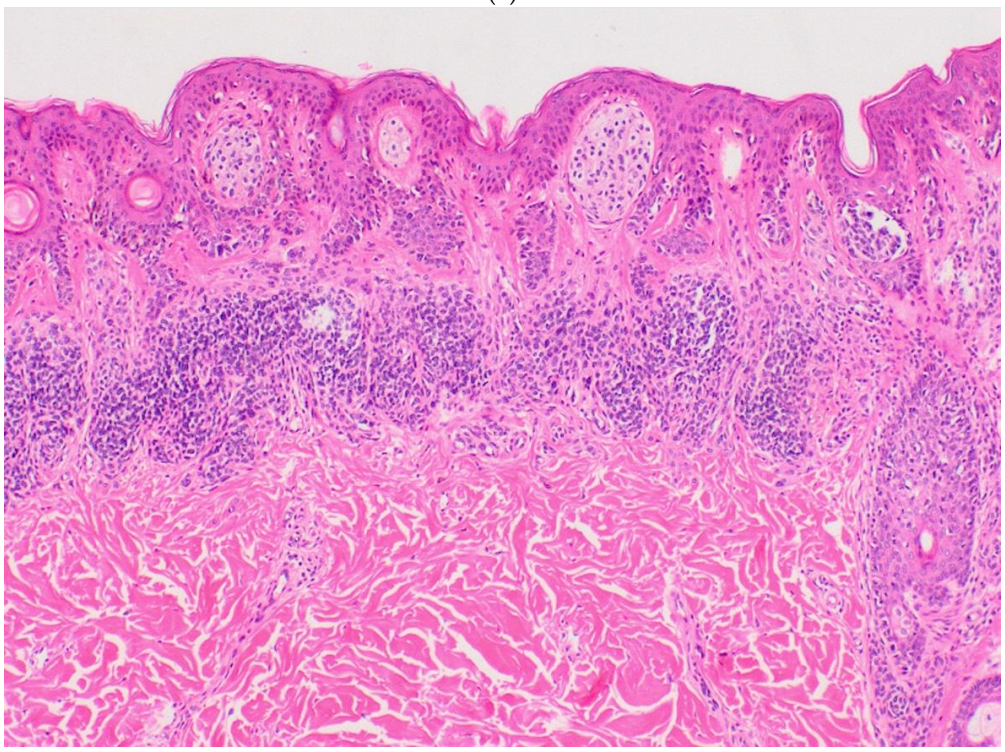

(**3**)

Figure 2. (**1**) A compound nevus in comparison with vertical LC-OCT and OCT. A compound nevus on the left lumbal trunk. (**a**) Clinical, (**b**) dermoscopical, and (**c**) optical coherence tomography (OCT; 6 mm × 2 mm) images of a representative nevus of the study. (**d**) In vertical line-field optical coherence tomography (LC-OCT; 1.2 mm × 0.5 mm) images junctional and dermal nests, a well-defined dermo-epidermal junction (DEJ), and a papillomatous surface can be seen. (**2**). A compound nevus in comparison with horizontal LC-OCT and RCM. The same compound nevus is depicted in horizontal LC-OCT (1.2 mm × 0.5 mm) with a regular honeycomb pattern (**a**), with nests in the upper dermis and regular papillae (**b**). Reflectance confocal microscopy (RCM; 500 µm × 500 µm) shows the same features. A regular honeycomb pattern (**c**) and junctional nests, as well as regular papillae, but just a little bit brighter (**d**). (**3**). A compound nevus in histology. The histology shows the same compound nevus as in (**1**) and (**2**) with 4× magnification.

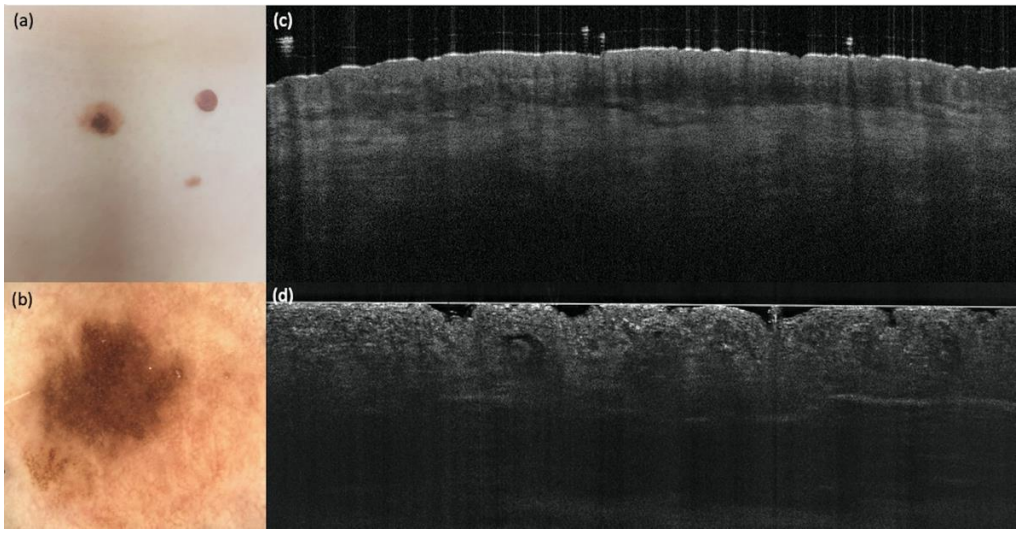

(**1**)

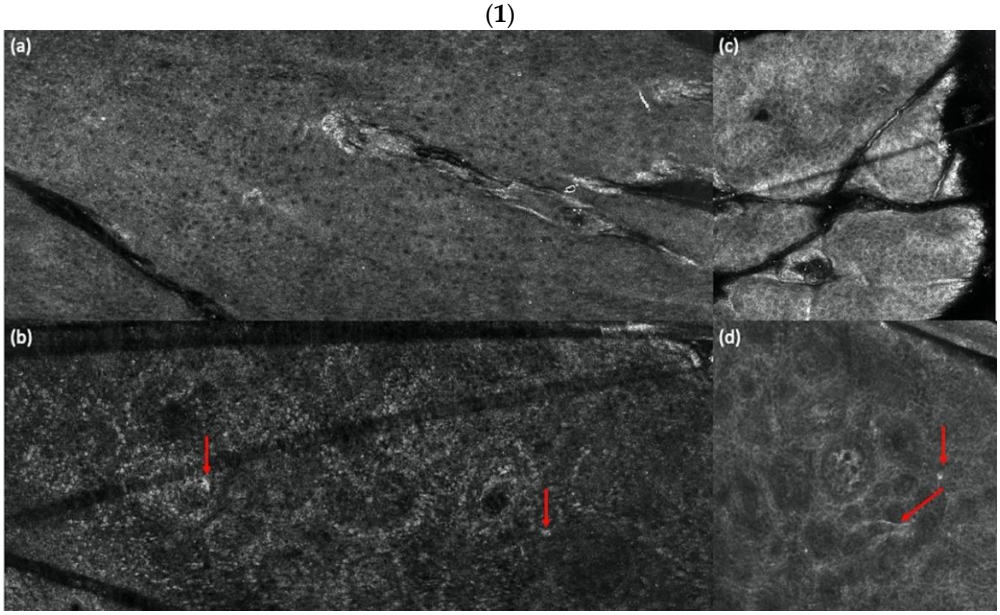

(**2**)

Figure 3. *Cont.*

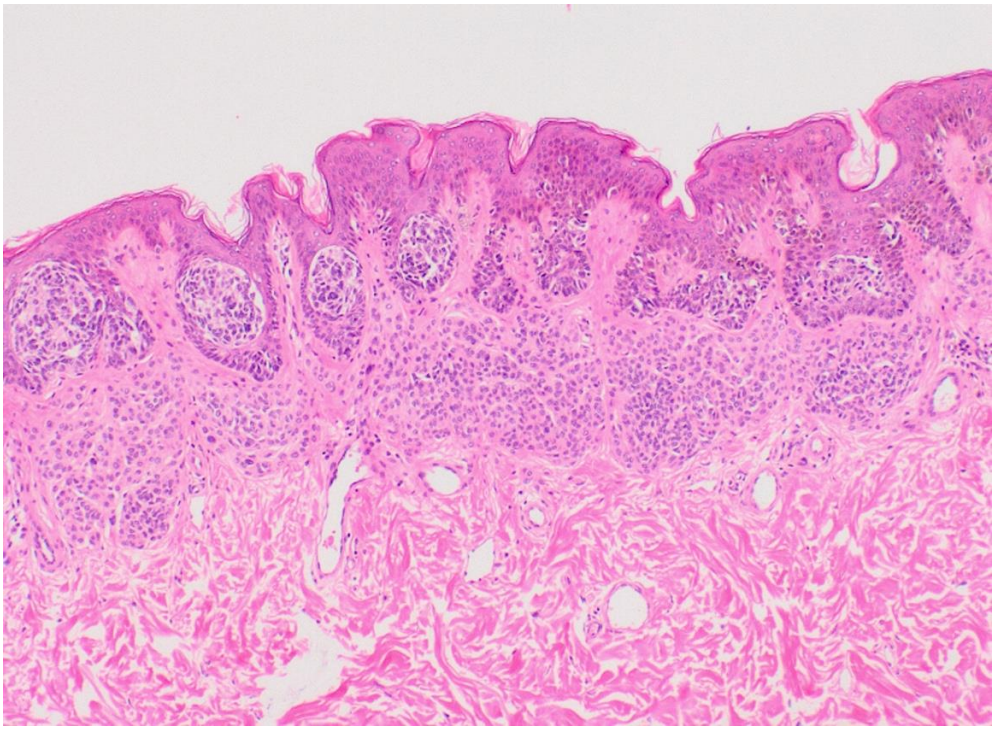

(**2**)

Figure 3. (**1**). A dysplastic compound nevus in comparison with vertical LC-OCT and OCT. A dysplastic nevus on the left lower trunk. (**a**) Clinical, (**b**) dermoscopical, and (**c**) optical coherence tomography (OCT; 6 mm × 2 mm) images of a representative dysplastic nevus of the study. (**d**) In vertical line-field optical coherence tomography (LC-OCT; 1.2 mm × 0.5 mm) images, junctional and dermal nests, a well-defined dermo-epidermal junction (DEJ), but also a few bright atypical cells are visible. (**2**) A dysplastic compound nevus in comparison with horizontal LC-OCT and RCM. The same dysplastic compound nevus is depicted in horizontal LC-OCT (1.2 mm × 0.5 mm) with a regular honeycomb pattern (**a**), with nests in the upper dermis, less regular papillae, and a few bright atypical cells (red arrows) (**b**). Reflectance confocal microscopy (RCM; 500 µm × 500 µm) shows the same features. A regular honeycomb pattern (**c**) and junctional nests, less regular papillae, and also a few bright atypical cells (red arrows) (**d**). (**3**) A dysplastic compound nevus in histology. The histology shows the same compound nevus as in (**1**) and (**2**) with 4× magnification.

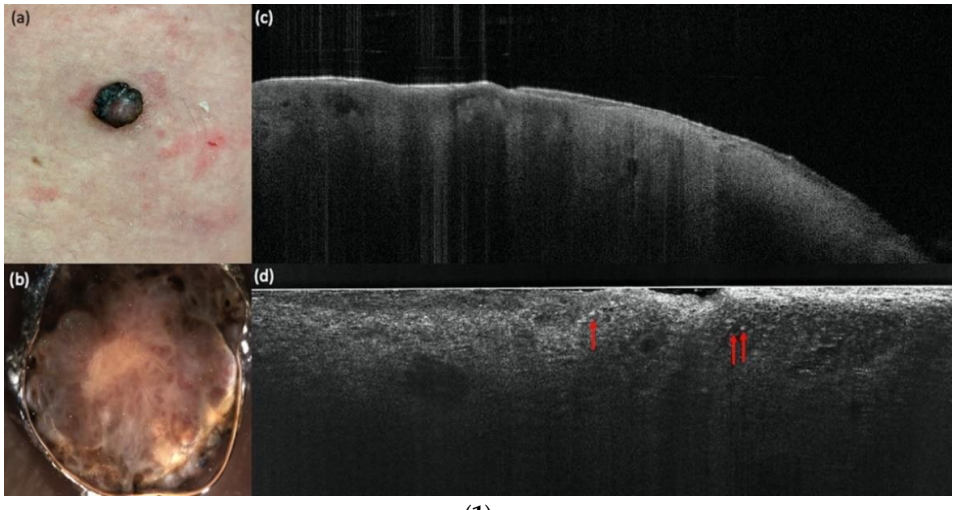

(**1**)

Figure 4. *Cont.*

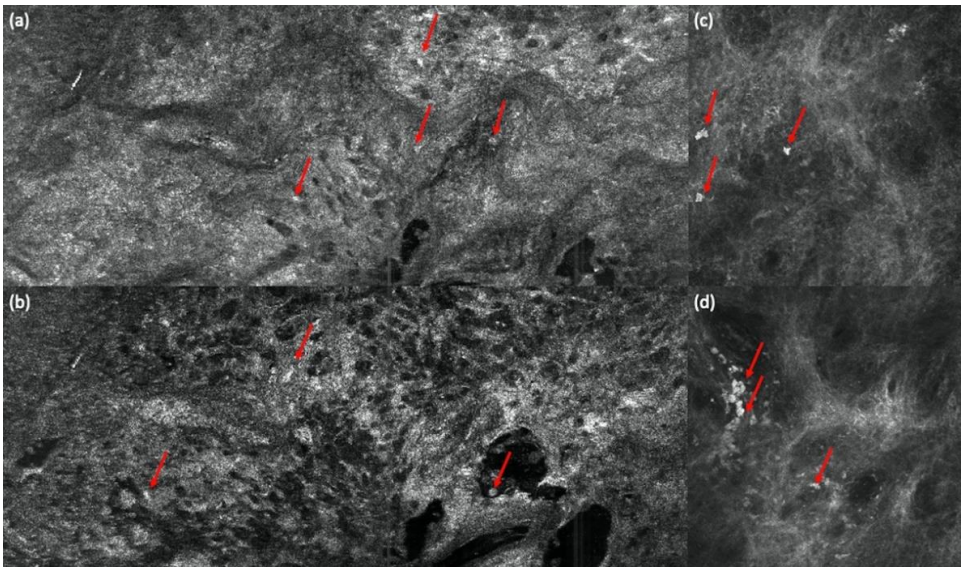

(**2**)

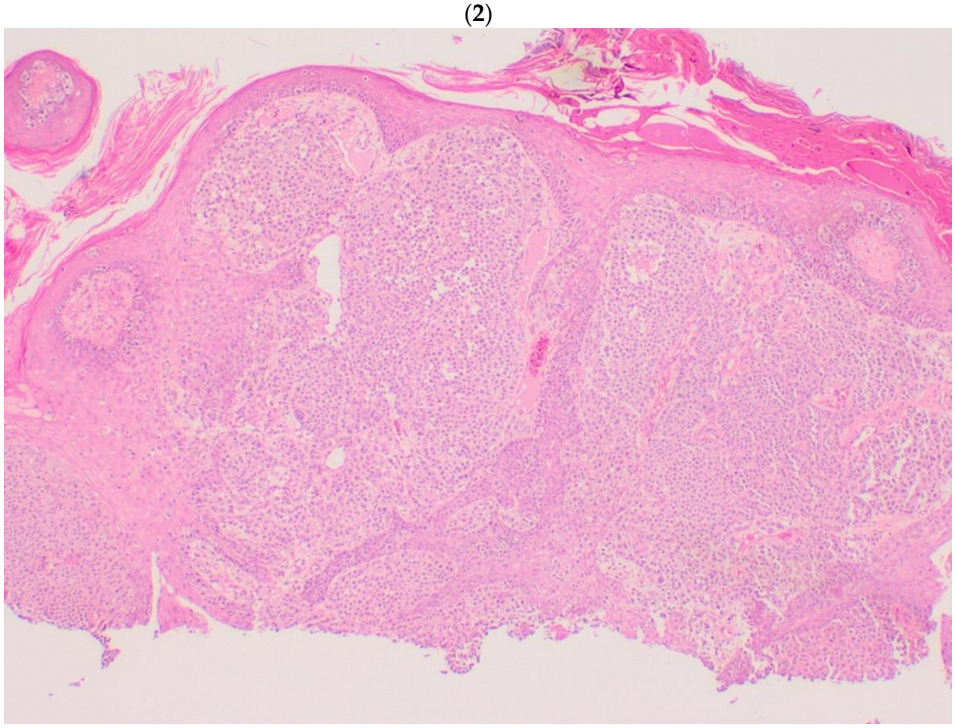

(3)

Figure 4. (**1**) A melanoma in comparison with vertical LC-OCT and OCT. An ulcerated nodular melanoma on the upper right leg. (**a**) Clinical, (**b**) dermoscopical, and (**c**) optical coherence tomography (OCT; 6 mm × 2 mm) images of a representative melanoma of the study. (**d**) In vertical line-field optical coherence tomography (LC-OCT; 1.2 mm × 0.5 mm) images, bright atypical melanocytic cells (red arrows) and a disturbed dermo-epidermal junction (DEJ) are visible. No dermal nests can be seen. (**2**) A melanoma in comparison with horizontal LC-OCT and RCM. The same melanoma is depicted in horizontal LC-OCT (1.2 mm × 0.5 mm) with an irregular honeycomb pattern with single atypical cells (red arrows) (**a**), and a pagetoid spread with atypical melanocytes (red arrows) (**b**). There were no dermal nests, a more chaotic structure, and no edged papillae visible. Reflectance confocal microscopy (RCM; 500 µm × 500 µm) shows the same features. An irregular honeycomb pattern with single atypical cells, just brighter (red arrows), (**c**) and a lighter pagetoid spread with atypical melanocytes (red arrows) (**d**). There were also no dermal nests, a more chaotic structure, and no edged papillae visible. (**3**) A melanoma in histology. The histology shows the same ulcerated nodular melanoma as in (**1**) and (**2**) with a tumor thickness of 4.8 mm and with 4× magnification.

The accuracy of all LC-OCT performances for diagnosing a melanoma vs. nevus was 97.6%, the sensitivity was 92.9%, and the specificity was 100% (see Table 5). The specificity and sensitivity of LC-OCT for diagnosing a melanoma vs. a nevus were compared with the specificity and sensitivity of histology using McNemar's test ($p = 0.48$). Two melanomas were falsely negative and were diagnosed as nevi with LC-OCT (for the analysis, see Table S5).

Table 5. LC-OCT performances for diagnosing melanomas vs. nevi (dysplastic or not).

	n	Global Accuracy	Nevus (*n* = 42)			Dysplastic Nevus (*n* = 13)			Melanoma (*n* = 28)		
			Accuracy	Sensitivity	Specificity	Accuracy	Sensitivity	Specificity	Accuracy	Sensitivity	Specificity
LC-OCT	83	86%	87%	95%	78%	87%	38%	96%	98%	93%	100%

Tables 6–8 illustrate the subgroup of 36 lesions that were imaged with LC-OCT and RCM. The accuracy of all performances with LC-OCT was 97.1% vs. 94.3% with RCM, the sensitivity for both was 92.9%, and the specificity with LC-OCT was 100% vs. 95.2% with RCM. The specificity and sensitivity of both devices for diagnosing a melanoma vs. a nevus were compared with the specificity and sensitivity of histology and with each other using McNemar's test (for all $p = 1$). One false negative was found, which was the same lesion for LC-OCT and RCM, and which had a bad image quality score in LC-OCT (3) and in RCM (2).

Table 6. LC-OCT and RCM performances for diagnosing melanomas vs. nevi (dysplastic or not) compared to histology.

n = 36		Histology			
		Melanoma	**Nevus**	**Other**	**Total**
LC-OCT	Melanoma	13	0	0	13
	Nevus	1	21	0	22
	Other	0	0	1	1
	Total	14	21	1	36
RCM	Melanoma	13	1	1	15
	Nevus	1	20	0	21
	Other	0	0	0	0
	Total	14	21	1	36

Table 7. LC-OCT and RCM performances for diagnosing melanomas vs. nevi vs. dysplastic nevi compared to histology.

n = 36		Histology				
		Nevus	**Melanoma**	**Dysplastic Nevus**	**Others**	**Total**
LC-OCT	Nevus	14	1	4	0	19
	Melanoma	0	13	0	0	13
	Dysplastic nevus	0	0	3	0	3
	Others	0	0	0	1	1
	Total	14	14	7	1	36
RCM	Nevus	13	0	3	0	16
	Melanoma	0	13	1	1	15
	Dysplastic nevus	1	1	3	0	5
	Others	0	0	0	0	0
	Total	14	14	7	1	36

Table 8. LC-OCT and RCM performances for diagnosing melanomas vs. nevi vs. dysplastic nevi.

	n	Global Accuracy	Nevus (*n* = 14)			Dysplastic Nevus (*n* = 7)			Melanoma (*n* = 14)		
			Accuracy	Sensitivity	Specificity	Accuracy	Sensitivity	Specificity	Accuracy	Sensitivity	Specificity
LC-OCT	35	86%	86%	100%	76%	89%	43%	100%	97%	93%	100%
RCM	35	83%	89%	93%	86%	83%	43%	93%	94%	93%	95%

The most significant criteria for diagnosing a melanoma with LC-OCT were irregular honeycombed pattern (92% occurrence rate; 31.7 OR), presence of pagetoid spread (89 % occurrence rate; 23.6 OR) and absence of dermal nests (23 % occurrence rate, 0.02 OR) as seen in Table 9.

Table 9. LC-OCT and RCM key criteria that were more useful in discriminating a melanoma from a nevus (dysplastic or not).

LC-OCT Parameters	OR (Univariate)	*p* Value	OR (Multivariate)	*p* Value
Horizontal parameters				
Irregular honeycombed pattern	43.64 (10.80–299.67)	<0.001	18.03 (1.50–547.32)	0.039
Pagetoid spread with atypical melanocytes in basal/suprabasal layers	41.21 (11.28–206.45)	<0.001	16.56 (1.43–435.95)	0.037
Edged papillae	0.22 (0.08–0.59)	0.003	0.43 (0.02–9.05)	0.57
Basal nests	0.23 (0.07–0.63)	0.007	0.51 (0.02–12.06)	0.67
Nests in the upper dermis	0.21 (0.06–0.61)	0.007	0.23 (0.01–3.80)	0.35
Irregular bright cells/sheets of cells in the upper dermis	5.75 (1.77–20.94)	0.005	0.51 (0.02–10.73)	0.67
Vertical parameters				
Pagetoid spread of bright cells in suprabasal/basal layers	20.36 (6.44–74.84)	<0.001	4.74 (0.35–94.88)	0.25
Junctional nests	0.31 (0.11–0.83)	0.02	1.85 (0.06–103.11)	0.73
Disturbed DEJ	10.83 (3.73–35.72)	<0.001	4.85 (0.26-144.46)	0.31
Dermal nests	0.21 (0.07–0.58)	0.004	0.08 (0.00-1.29)	0.12
Sheets of atypical bright cells	26.47 (4.50-506.78)	0.003	0.69 (0.02-29.63)	0.83
RCM parameters	**OR (univariate)**	***p* value**	**OR (multivariate)**	***p* value**
Irregular honeycombed pattern	69.67 (9.13–1553.6)	<0.001	123.91 (2.84–19309)	0.030
Pagetoid spread with atypical melanocytes in suprabasal layers	34.00 (5.91–315.56)	<0.001	0.76 (0.01–23.85)	0.88
Edged papillae	0.08 (0.01–0.44)	0.007	0.05 (0.00–0.76)	0.053

4. Discussion

Due to the high resolution and good penetration depth of LC-OCT, it is finally possible to overcome the gap between OCT and RCM. The vertical view is similar to OCT, and visualizes single cells, making the comparison with histology very intuitive. Monnier et al. already proved that LC-OCT can discriminate different skin levels and keratinocytes in healthy skin acquisitions [15–17]. Recent studies show that with single cell display, even BCC subtypes can be discriminated in vertical LC-OCT [18]. The disadvantage of LC-OCT is the lower penetration depth compared to OCT, so it is possible that deeper tumor parts may be missed [19,20]. Due to the presentation of single cells, differential diagnoses such as sebaceous hyperplasia, actinic keratoses, and squamous cell carcinomas could be differentiated, and the proliferation degree of actinic keratoses showed a 75% concordance between LC-OCT and histology [21–24].

This high single cell resolution is the reason why we assumed that even melanocytic lesions can be evaluated with LC-OCT. Regarding resolution, the horizontal LC-OCT images were very similar to RCM, which is the reference standard. With RCM it has already been shown that nevi can be discriminated from melanomas, even if there are sometimes possible false-negative and false-positive cases of melanomas [25]. Moreover, ex vivo RCM has also been successfully used for the differentiation and diagnosis of melanocytic lesions, although not all typical in vivo features could be detected since it offers a vertical view instead of horizontal as in in vivo RCM [26]. Hartmann et al. stated that ex vivo RCM might also be useful in the measurement of tumor thickness, and therefore might be of help for the presurgical definition of correct margins [27]. LC-OCT is similar to a fusion of ex vivo and in vivo RCM. It provides the vertical view of ex vivo RCM and the horizontal view of in vivo RCM on melanocytic lesions. Therefore, more information on pigmented lesions can be gained, and more typical features of both techniques can lead the clinician to the correct diagnosis. In our study, we found that image quality was responsible for the diagnostic confidence level for LC-OCT and RCM. In general, reduced image quality is mainly associated with ulceration, crusting, or image taking experience. Nevertheless, it is not recommended to measure an ulcerated or crusted pigmented lesion with non-invasive devices, and in such cases a biopsy is needed. Clearly, the diagnostic confidence for each lesion depends not only on the quality of the LC-OCT image or the difficulty of the lesion, but also on the experience of the observer. Our clinicians were all similarly experienced, and therefore we did not evaluate observer variability. Hence, further studies with clinicians of different experiences with LC-OCT need to be performed. We also conclude that for the interpretation and analysis of LC-OCT images, tele-consulting might be useful for LC-OCT beginners and for discussing difficult cases. Furthermore, the diagnostic performance of LC-OCT for melanomas (vs. all nevi) has the same sensitivity and a better specificity compared to RCM. We only had two false negative cases with LC-OCT, where two melanomas were diagnosed as nevi. We reviewed the cases, and in the first case—a nevus-associated melanoma—we detected in the integrated dermoscopic view that only the dysplastic nevus part had been imaged. Thus, it is very relevant to ensure appropriate coverage of the whole lesion, or if the lesion is too big, that more images are taken. The second case—a big in situ superficial spreading melanoma—was of a bad image quality, more in LC-OCT (score 3) than in RCM (score 2), because of an air bubble due to technical issues at that time. In big-sized lesions, multiple measurements from different parts should have been taken. Due to the lesion's large size, a biopsy or surgery would have been performed anyway. Moreover, the diagnosis of a nevus vs. a dysplastic nevus is less accurate for both techniques. This aspect needs to be reconsidered, since one limitation of our study is that the number of dysplastic nevi in the subgroup of both devices was quite small (n = 3) vs. nevi (n = 19). A larger study for the evaluation of nevi vs. dysplastic nevi is required. One should keep in mind that histology can also be erroneous, especially in biopsies, because the entire lesion cannot be assessed here. Since the vast majority of the lesions were completely excised and serial sections including immunohistologies are standard in melanomas, we assume that this possible error is negligible.

Recently Lenoir et al. published a few LC-OCT criteria for benign dermal melanocytic proliferations such as wave pattern [28]. In our study, we evaluated the most significant criteria for diagnosing a melanoma vs. nevus with LC-OCT (in comparison with RCM). We found that an irregular honeycombed pattern, the presence of pagetoid spread, and the absence of dermal nests are the most important criteria to discriminate a melanoma from a nevus in LC-OCT. These findings are very similar to studies with RCM [29–31]. We were surprised that no criteria related to the DEJ could be detected here, but this can be explained by the fact that many superficial spreading melanomas have a well-defined DEJ, which were the majority of the melanomas in our study. In the future, a study about thin versus thick melanomas should be conducted, since Rudnicka et al. showed in RCM that there might be different key criteria [32].

5. Conclusions

In conclusion, our first study with the new LC-OCT device on melanocytic lesions showed that the discrimination between melanomas and nevi is possible. The improved distinction between nevi and melanomas with LC-OCT will lead to an immediate in vivo and non-invasive diagnosis, spare unnecessary surgeries if the lesion is diagnosed as a nevus, and therefore reduce health insurance costs and free capacities for other necessary melanoma surgeries.

Supplementary Materials: The following are available online at https://www.mdpi.com/article/10.3390/cancers14051140/s1: Table S1: Most common LC-OCT parameters for melanocytic lesions; Table S2: LC-OCT key criteria more useful in discriminating a melanoma from a nevus (dysplastic or not); Table S3: Most common RCM parameters for melanocytic lesions; Table S4: RCM key criteria more useful in discriminating a melanoma from a nevus (dysplastic or not); Table S5: Analysis of the false negative cases.

Author Contributions: Conceptualization, J.W. and E.C.S.; methodology, J.W., C.R., E.C.S. and S.S; validation, J.W., C.R., E.C.S. and S.S.; formal analysis, J.W., C.R., E.C.S. and S.S.; investigation, J.W., C.R., E.C.S. and S.S.; resources, J.W., C.R., E.C.S. and S.S.; data curation, C.R., C.G., F.D. and S.S.; writing—original draft preparation, S.S.; writing—review and editing, E.C.S., J.W., S.S., C.R., C.G., F.D. and M.K.E.P.; visualization, S.S.; supervision, E.C.S. and J.W.; project administration, J.W., E.C.S., C.R. and S.S.; funding acquisition, C.R. All authors have read and agreed to the published version of the manuscript.

Funding: This study was partially funded by the FöFoLe, a Funding program for research and teaching and Research Grant of the medical faculty of the Ludwig Maximilian University of Munich (LMU Munich), protocol number 10-22.

Institutional Review Board Statement: The study was conducted according to the guidelines of the Declaration of Helsinki and approved by the Institutional Review Board of LMU Munich (Protocol Number 17-699).

Informed Consent Statement: Written informed consent was obtained from all subjects involved in the study.

Data Availability Statement: Fully anonymized data are available on request.

Acknowledgments: The authors thank DAMAE medical, together with Maxime Cazalas and Mélanie Pedrazzani for providing the device needed for this study and for their constant professional assistance.

Conflicts of Interest: The authors declare no relevant conflict of interest.

References

1. Welzel, J.; Schuh, S. Noninvasive diagnosis in dermatology. *J. Dtsch. Dermtol. Ges.* **2017**, *15*, 999–1016. [CrossRef] [PubMed]
2. Holmes, J.; von Braunmühl, T.; Berking, C.; Sattler, E.C.; Ulrich, M.; Reinhold, U.; Kurzen, H.; Dirschka, T.; Kellner, C.; Schuh, S.; et al. Optical coherence tomography of basal cell carcinoma: Influence of location, subtype, observer variability and image quality on diagnostic performance. *Br. J. Dermatol.* **2018**, *178*, 1102–1110. [CrossRef] [PubMed]
3. di Ruffano, L.F.; Dinnes, J.; Deeks, J.J.; Chuchu, N.; Bayliss, S.E.; Davenport, C.; Takwoingi, Y.; Godfrey, K.; O'Sullivan, C.; Matin, R.N.; et al. Optical coherence tomography for diagnosing skin cancer in adults. *Cochrane Database Syst. Rev.* **2018**, *12*, CD013189. [CrossRef]
4. Dinnes, J.; Deeks, J.J.; Saleh, D.; Chuchu, N.; Bayliss, S.E.; Patel, L.; Davenport, C.; Takwoingi, Y.; Godfrey, K.; Matin, R.N.; et al. Reflectance confocal microscopy for diagnosing cutaneous melanoma in adults. *Cochrane Database Syst. Rev.* **2018**, *12*, CD013190. [CrossRef]
5. Que, S.K.T.; Grant-Kels, J.M.; Longo, C.; Pellacani, G. Basics of confocal microscopy and the complexity of diagnosing skin tumors: New imaging tools in clinical practice, diagnostic workflows, cost-estimate, and new trends. *Dermatol. Clin.* **2016**, *34*, 367–375. [CrossRef]
6. Ogien, J.; Levecq, O.; Azimani, H.; Dubois, A. Dual-mode line-field confocal optical coherence tomography for ultrahigh-resolution vertical and horizontal section imaging of human skin in vivo. *Biomed. Opt. Express* **2020**, *11*, 1327–1335. [CrossRef]
7. Davis, A.; Levecq, O.; Azimani, H.; Siret, D.; Dubois, A. Simultaneous dual-band line-field confocal optical coherence tomography: Application to skin imaging. *Biomed. Opt. Express* **2019**, *10*, 694–706. [CrossRef]

8. Dubois, A.; Levecq, O.; Azimani, H.; Siret, D.; Barut, A.; Suppa, M.; Del Marmol, V.; Malvehy, J.; Cinotti, E.; Rubegni, P.; et al. Line-field confocal optical coherence tomography for high-resolution noninvasive imaging of skin tumors. *J. Biomed. Opt.* **2018**, *23*, 106007. [CrossRef]
9. Dubois, A.; Levecq, O.; Azimani, H.; Davis, A.; Ogien, J.; Siret, D.; Barut, A. Line-field confocal time-domain optical coherence tomography with dynamic focusing. *Opt. Express* **2018**, *26*, 33534–33542. [CrossRef]
10. Ogien, J.; Daures, A.; Cazalas, M.; Perrot, J.L.; Dubois, A. Line-field confocal optical coherence tomography for three-dimensional skin imaging. *Front. Optoelectron.* **2020**, *13*, 381–392. [CrossRef]
11. Pedrazzani, M.; Breugnot, J.; Rouaud-Tinguely, P.; Cazalas, M.; Davis, A.; Bordes, S.; Dubois, A.; Closs, B. Comparison of line-field confocal optical coherence tomography images with histological sections: Validation of a new method for in vivo and non-invasive quantification of superficial dermis thickness. *Skin Res. Technol.* **2020**, *26*, 398–404. [CrossRef] [PubMed]
12. Rajadhyaksha, M.; Grossman, M.; Esterowitz, D.; Webb, R.H.; Anderson, R.R. In vivo confocal scanning laser microscopy of human skin: Melanin provides strong contrast. *J. Invest Dermatol.* **1995**, *104*, 946–952. [CrossRef] [PubMed]
13. Gambichler, T.; Plura, I.; Schmid-Wendtner, M.; Valavanis, K.; Kulichova, D.; Stücker, M.; Pljakic, A.; Berking, C.; Maier, T. High-definition optical coherence tomography of melanocytic skin lesions. *J. Biophotonics* **2015**, *8*, 681–686. [CrossRef] [PubMed]
14. Gambichler, T.; Schmid-Wendtner, M.H.; Plura, I.; Kampilafkos, P.; Stücker, M.; Berking, C.; Maier, T. A multicentre pilot study investigating high-definition optical coherence tomography in the differentiation of cutaneous melanoma and melanocytic naevi. *J. Eur. Acad. Dermatol. Venereol.* **2015**, *29*, 537–541. [CrossRef]
15. Monnier, J.; Tognetti, L.; Miyamoto, M.; Suppa, M.; Cinotti, E.; Fontaine, M.; Perez, J.; Cano, C.O.; Yélamos, O.; Puig, S.; et al. In vivo characterization of healthy human skin with a novel, non-invasive imaging technique: Line-field confocal optical coherence tomography. *J. Eur. Acad. Dermatol. Venereol.* **2020**, *34*, 2914–2921. [CrossRef]
16. Ruini, C.; Schuh, S.; Sattler, E.; Welzel, J. Line-field confocal optical coherence tomography—Practical applications in dermatology and comparison with established imaging methods. *Skin Res. Technol.* **2021**, *27*, 340–352. [CrossRef]
17. Schuh, S.; Ruini, C.; Sattler, E.; Welzel, J. Confocal line-field OCT. *Hautarzt* **2021**, *72*, 1039–1047. [CrossRef]
18. Gust, C.; Schuh, S.; Welzel, J.; Daxenberger, F.; Hartmann, D.; French, L.E.; Ruini, C.; Sattler, E. Line-field confocal optical coherence tomography increases the diagnostic accuracy and confidence for basal cell carcinoma in equivocal lesions: A prospective study. *Cancers* **2022**, *14*, 1082. [CrossRef]
19. Suppa, M.; Fontaine, M.; Dejonckheere, G.; Cinotti, E.; Yélamos, O.; Diet, G.; Tognetti, L.; Miyamoto, M.; Cano, C.O.; Perez-Anker, J.; et al. Line-field confocal optical coherence tomography of basal cell carcinoma: A descriptive study. *J. Eur. Acad. Dermatol. Venereol.* **2021**, *35*, 1099–1110. [CrossRef]
20. Ruini, C.; Schuh, S.; Gust, C.; Kendziora, B.; Frommherz, L.; French, L.E.; Hartmann, D.; Welzel, J.; Sattler, E.C. Line-field optical coherence tomography: In vivo diagnosis of basal cell carcinoma subtypes compared to histopathology. *Clin. Exp. Dermatol.* **2021**, *46*, 1471–1481. [CrossRef]
21. Lenoir, C.; Diet, G.; Cinotti, E.; Tognetti, L.; Cano, C.O.; Rocq, L.; Trepant, A.L.; Monnier, J.; Perez-Anker, J.; Rubegni, P.; et al. Line-field confocal optical coherence tomography of sebaceous hyperplasia: A case series. *J. Eur. Acad. Dermatol. Venereol.* **2021**, *35*, e509–e511. [CrossRef]
22. Ruini, C.; Schuh, S.; Gust, C.; Hartmann, D.; French, L.E.; Sattler, E.C.; Welzel, J. In-vivo LC-OCT evaluation of the downward proliferation pattern of keratinocytes in actinic keratosis in comparison with histology: First impressions from a pilot study. *Cancers* **2021**, *13*, 2856. [CrossRef] [PubMed]
23. Cinotti, E.; Tognetti, L.; Cartocci, A.; Lamberti, A.; Gherbassi, S.; Cano, C.O.; Lenoir, C.; Dejonckheere, G.; Diet, G.; Fontaine, M.; et al. Line-field confocal optical coherence tomography for actinic keratosis and squamous cell carcinoma: A descriptive study. *Clin. Exp. Dermatol.* **2021**, *46*, 1530–1541. [CrossRef] [PubMed]
24. Ruini, C.; Schuh, S.; Gust, C.; Kendziora, B.; Frommherz, L.; French, L.E.; Hartmann, D.; Welzel, J.; Sattler, E.C. Line-field confocal optical coherence tomography for the in-vivo real-time diagnosis of different stages of keratinocyte skin cancer: A preliminary study. *J. Eur. Acad. Dermatol. Venereol.* **2021**, *35*, 2388–2397. [CrossRef] [PubMed]
25. Carrera, C.; Marghoob, A.A. Discriminating nevi from melanomas: Clues and pitfalls. *Dermatol. Clin.* **2016**, *34*, 395–409. [CrossRef] [PubMed]
26. Hartmann, D.; Ruini, C.; Mathemeier, L.; Bachmann, M.R.; Dietrich, A.; Ruzicka, T.; von Braunmühl, T. Identification of ex-vivo confocal laser scanning microscopic features of melanocytic lesions and their histological correlates. *J. Biophotonics* **2017**, *10*, 128–142. [CrossRef]
27. Hartmann, D.; Krammer, S.; Ruini, C.; Ruzicka, T.; von Braunmühl, T. Correlation of histological and ex-vivo confocal tumor thickness in malignant melanoma. *Lasers Med. Sci.* **2016**, *31*, 921–927. [CrossRef]
28. Lenoir, C.; Perez-Anker, J.; Diet, G.; Tognetti, L.; Cinotti, E.; Trepant, A.L.; Rubegni, P.; Puig, S.; Perrot, J.L.; Malvehy, J.; et al. Line-field confocal optical coherence tomography of benign dermal melanocytic proliferations: A case series. *J. Eur. Acad. Dermatol. Venereol.* **2021**, *35*, e399–e401. [CrossRef]
29. Fraga-Braghiroli, N.; Grant-Kels, J.M.; Oliviero, M.; Rabinovitz, H.; Ferenci, K.; Scope, A. The role of reflectance confocal microscopy in differentiating melanoma in situ from dysplastic nevi with severe atypia: A cross-sectional study. *J. Am. Acad. Dermatol.* **2020**, *83*, 1035–1043. [CrossRef]
30. Carrera, C.; Puig, S.; Malvehy, J. In vivo confocal reflectance microscopy in melanoma. *Dermatol. Ther.* **2012**, *25*, 410–422. [CrossRef]

31. Pellacani, G.; Cesinaro, A.M.; Seidenari, S. Reflectance-mode confocal microscopy of pigmented skin lesions—Improvement in melanoma diagnostic specificity. *J. Am. Acad. Dermatol.* **2005**, *53*, 979–985. [CrossRef] [PubMed]
32. Kardynal, A.; Olszewska, M.; de Carvalho, N.; Walecka, I.; Pellacani, G.; Rudnicka, L. Reflectance confocal microscopy features of thin versus thick melanomas. *G. Ital. Dermatol. Venereol.* **2019**, *154*, 379–385. [CrossRef] [PubMed]

Note of Thanks

I extend my deepest gratitude towards my mentors, Prof. Dr. med. Elke Sattler and Prof. Dr. med. Daniela Hartmann for their unwavering support and guidance, not only in my clinical research, but also my personal growth during the last four years.

Furthermore, I would like to thank PD. Dr. med. Cristel Ruini for her mentorship and assistance during my first research years in the field of Dermatology.

Additionally, I would like to express appreciation to my head of department, Prof. Dr med. Lars E. French, for his continuous support in my current and upcoming research projects.

Finally, I am profoundly grateful for my parents, for their infinite help and guidance and being there for me every step along the way. Special thanks go out to Henni g for her endless support and of course Maxus.

Table of References

Aggarwal, I., Puyana, C., Chandan, N., Jetter, N., & Tsoukas, M. (2024). Field Cancerization Therapies for the Management of Actinic Keratosis: An Updated Review. *Am J Clin Dermatol*. doi:10.1007/s40257-023-00839-8

Carr, S., Smith, C., & Wernberg, J. (2020). Epidemiology and Risk Factors of Melanoma. *Surg Clin North Am, 100*(1), 1-12. doi:10.1016/j.suc.2019.09.005

Dinnes, J., Deeks, J. J., Chuchu, N., Matin, R. N., Wong, K. Y., Aldridge, R. B., . . . Williams, H. C. (2018). Visual inspection and dermoscopy, alone or in combination, for diagnosing keratinocyte skin cancers in adults. *Cochrane Database Syst Rev, 12*(12), Cd011901. doi:10.1002/14651858.CD011901.pub2

Ferrante di Ruffano, L., Dinnes, J., Deeks, J. J., Chuchu, N., Bayliss, S. E., Davenport, C., . . . Cochrane Skin Cancer Diagnostic Test Accuracy, G. (2018). Optical coherence tomography for diagnosing skin cancer in adults. *Cochrane Database Syst Rev, 12*(12), CD013189. doi:10.1002/14651858.CD013189

Frost, C., Williams, G., & Green, A. (2000). High incidence and regression rates of solar keratoses in a queensland community. *J Invest Dermatol, 115*(2), 273-277. doi:10.1046/j.1523-1747.2000.00048.x

Guitera, P., Menzies, S. W., Longo, C., Cesinaro, A. M., Scolyer, R. A., & Pellacani, G. (2012). In vivo confocal microscopy for diagnosis of melanoma and basal cell carcinoma using a two-step method: analysis of 710 consecutive clinically equivocal cases. *J Invest Dermatol, 132*(10), 2386-2394. doi:10.1038/jid.2012.172

Guitera, P., Pellacani, G., Longo, C., Seidenari, S., Avramidis, M., & Menzies, S. W. (2009). In vivo reflectance confocal microscopy enhances secondary evaluation of melanocytic lesions. *J Invest Dermatol, 129*(1), 131-138. doi:10.1038/jid.2008.193

Gust, C., Schuh, S., Welzel, J., Daxenberger, F., Hartmann, D., French, L. E., . . . Sattler, E. C. (2022). Line-Field Confocal Optical Coherence Tomography Increases the Diagnostic Accuracy and Confidence for Basal Cell Carcinoma in Equivocal Lesions: A Prospective Study. *Cancers (Basel), 14*(4). doi:10.3390/cancers14041082

Holmes, J., von Braunmuhl, T., Berking, C., Sattler, E., Ulrich, M., Reinhold, U., . . . Welzel, J. (2018). Optical coherence tomography of basal cell carcinoma: influence of location, subtype, observer variability and image quality on diagnostic performance. *Br J Dermatol, 178*(5), 1102-1110. doi:10.1111/bjd.16154

Leiter, U., Keim, U., & Garbe, C. (2020). Epidemiology of Skin Cancer: Update 2019. *Adv Exp Med Biol, 1268*, 123-139. doi:10.1007/978-3-030-46227-7_6

Lomas, A., Leonardi-Bee, J., & Bath-Hextall, F. (2012). A systematic review of worldwide incidence of nonmelanoma skin cancer. *Br J Dermatol, 166*(5), 1069-1080. doi:10.1111/j.1365-2133.2012.10830.x

Manfredini, M., Liberati, S., Ciardo, S., Bonzano, L., Guanti, M., Chester, J., . . . Pellacani, G. (2020). Microscopic and functional changes observed with dynamic optical coherence tomography for severe refractory atopic dermatitis treated with dupilumab. *Skin Res Technol, 26*(6), 779-787. doi:10.1111/srt.12868

Mitsaki, K. S., Apalla, Z., Lazaridou, E., Lallas, K., & Lallas, A. (2024). Risk factors of lentigo maligna as compared to other melanoma subtypes. *Int J Dermatol*. doi:10.1111/ijd.17112

Ogien, J., Tavernier, C., Fischman, S., & Dubois, A. (2023). Line-field confocal optical coherence tomography (LC-OCT): principles and practical use. *Ital J Dermatol Venerol, 158*(3), 171-179. doi:10.23736/S2784-8671.23.07613-2

Olsen, J., Gaetti, G., Grandahl, K., & Jemec, G. B. E. (2022). Optical coherence tomography quantifying photo aging: skin microvasculature depth, epidermal thickness and UV exposure. *Arch Dermatol Res, 314*(5), 469-476. doi:10.1007/s00403-021-02245-8

Pellacani, G., Guitera, P., Longo, C., Avramidis, M., Seidenari, S., & Menzies, S. (2007). The impact of in vivo reflectance confocal microscopy for the diagnostic accuracy of melanoma and equivocal melanocytic lesions. *J Invest Dermatol, 127*(12), 2759-2765. doi:10.1038/sj.jid.5700993

Pellacani, G., Ulrich, M., Casari, A., Prow, T. W., Cannillo, F., Benati, E., . . . Soyer, H. P. (2015). Grading keratinocyte atypia in actinic keratosis: a correlation of reflectance confocal microscopy and histopathology. *J Eur Acad Dermatol Venereol, 29*(11), 2216-2221. doi:10.1111/jdv.13215

Ruini, C., Schuh, S., Gust, C., Hartmann, D., French, L. E., Sattler, E. C., & Welzel, J. (2021). In-Vivo LC-OCT Evaluation of the Downward Proliferation Pattern of Keratinocytes in Actinic Keratosis in Comparison with Histology: First Impressions from a Pilot Study. *Cancers (Basel), 13*(12). doi:10.3390/cancers13122856

Ruini, C., Schuh, S., Hartmann, D., French, L., Welzel, J., & Sattler, E. (2021). Noninvasive real-time imaging of mite skin infestations with line-field confocal optical coherence tomography. *Br J Dermatol, 184*(1), e3. doi:10.1111/bjd.19318

Ruini, C., Witkowski, A. M., Cesinaro, A., Teixeira De Carvalho, N., & Pellacani, G. (2015). From actinic keratosis to squamous cell carcinoma: evidence of morphologic and biologic progression. *J Am Acad Dermatol, 72*(1 Suppl), S8-S10. doi:10.1016/j.jaad.2014.02.046

Schmitz, L., Kahl, P., Majores, M., Bierhoff, E., Stockfleth, E., & Dirschka, T. (2016). Actinic keratosis: correlation between clinical and histological classification systems. *J Eur Acad Dermatol Venereol, 30*(8), 1303-1307. doi:10.1111/jdv.13626

Schuh, S., Ruini, C., Perwein, M. K. E., Daxenberger, F., Gust, C., Sattler, E. C., & Welzel, J. (2022). Line-Field Confocal Optical Coherence Tomography: A New Tool for the Differentiation between Nevi and Melanomas? *Cancers (Basel), 14*(5). doi:10.3390/cancers14051140

Schuh, S., Ruini, C., Sattler, E., & Welzel, J. (2021). [Confocal line-field OCT]. *Hautarzt, 72*(12), 1039-1047. doi:10.1007/s00105-021-04900-7

Sinx, K. A. E., van Loo, E., Tonk, E. H. J., Kelleners-Smeets, N. W. J., Winnepenninckx, V. J. L., Nelemans, P. J., & Mosterd, K. (2020). Optical Coherence Tomography for Noninvasive Diagnosis and Subtyping of Basal Cell Carcinoma: A Prospective Cohort Study. *J Invest Dermatol, 140*(10), 1962-1967. doi:10.1016/j.jid.2020.01.034

Suppa, M., Palmisano, G., Tognetti, L., Lenoir, C., Cappilli, S., Fontaine, M., . . . Del Marmol, V. (2023). Line-field confocal optical coherence tomography in melanocytic and non-melanocytic skin tumors. *Ital J Dermatol Venerol, 158*(3), 180-189. doi:10.23736/S2784-8671.23.07639-9

Traianou, A., Ulrich, M., Apalla, Z., De Vries, E., Bakirtzi, K., Kalabalikis, D., . . . Group, E. (2012). Risk factors for actinic keratosis in eight European centres: a case-control study. *Br J Dermatol, 167 Suppl 2*, 36-42. doi:10.1111/j.1365-2133.2012.11085.x

Ulrich, M., Themstrup, L., de Carvalho, N., Manfredi, M., Grana, C., Ciardo, S., . . . Welzel, J. (2016). Dynamic Optical Coherence Tomography in Dermatology. *Dermatology, 232*(3), 298-311. doi:10.1159/000444706

Ulrich, M., von Braunmuehl, T., Kurzen, H., Dirschka, T., Kellner, C., Sattler, E., . . . Reinhold, U. (2015). The sensitivity and specificity of optical coherence tomography for the assisted diagnosis of nonpigmented basal cell carcinoma: an observational study. *Br J Dermatol, 173*(2), 428-435. doi:10.1111/bjd.13853

Valdés-Morales, K. L., Peralta-Pedrero, M. L., Cruz, F. J., & Morales-Sánchez, M. A. (2020). Diagnostic Accuracy of Dermoscopy of Actinic Keratosis: A Systematic Review. *Dermatol Pract Concept, 10*(4), e2020121. doi:10.5826/dpc.1004a121

Wan, B., Ganier, C., Du-Harpur, X., Harun, N., Watt, F. M., Patalay, R., & Lynch, M. D. (2021). Applications and future directions for optical coherence tomography in dermatology. *Br J Dermatol, 184*(6), 1014-1022. doi:10.1111/bjd.19553

Wassef, C., & Rao, B. K. (2013). Uses of non-invasive imaging in the diagnosis of skin cancer: an overview of the currently available modalities. *Int J Dermatol, 52*(12), 1481-1489. doi:10.1111/ijd.12159

Wei, X., Wu, D., Chen, Y., Li, H., Zhang, R., Yao, H., . . . Si, L. (2022). Prognostic value of ulceration varies across Breslow thicknesses and clinical stages in acral melanoma: a retrospective study. *Br J Dermatol, 186*(6), 977-987. doi:10.1111/bjd.21026

Welzel, J., Lankenau, E., Birngruber, R., & Engelhardt, R. (1997). Optical coherence tomography of the human skin. *J Am Acad Dermatol, 37*(6), 958-963. doi:10.1016/s0190-9622(97)70072-0

Welzel, J., & Schuh, S. (2017). Noninvasive diagnosis in dermatology. *J Dtsch Dermatol Ges, 15*(10), 999-1016. doi:10.1111/ddg.13347

Zalaudek, I., Giacomel, J., Schmid, K., Bondino, S., Rosendahl, C., Cavicchini, S., . . . Argenziano, G. (2012). Dermatoscopy of facial actinic keratosis, intraepidermal carcinoma, and invasive squamous cell carcinoma: a progression model. *J Am Acad Dermatol, 66*(4), 589-597. doi:10.1016/j.jaad.2011.02.011

Affidavit

LMU LUDWIG-MAXIMILIANS-UNIVERSITÄT MÜNCHEN

Dekanat Medizinische Fakultät
Promotionsbüro

Eidesstattliche Versicherung

Gust, Charlotte Louise

Name, Vorname

Ich erkläre hiermit an Eides statt, dass ich die vorliegende Dissertation mit dem Thema

In-vivo Evaluation von Hauttumoren und inflammatorischen Dermatosen mittels nicht invasiver Bildgebung

selbständig verfasst, mich außer der angegebenen keiner weiteren Hilfsmittel bedient und alle Erkenntnisse, die aus dem Schrifttum ganz oder annähernd übernommen sind, als solche kenntlich gemacht und nach ihrer Herkunft unter Bezeichnung der Fundstelle einzeln nachgewiesen habe.

Ich erkläre des Weiteren, dass die hier vorgelegte Dissertation nicht in gleicher oder in ähnlicher Form bei einer anderen Stelle zur Erlangung eines akademischen Grades eingereicht wurde.

München, 29.09.24
Ort, Datum

Charlotte Gust
Unterschrift Charlotte Louise Gust